

Engineering formate assimilation in *Synechocystis* sp. PCC 6803

Zur Erlangung des akademischen Grades
doctor rerum naturalium (Dr. rer. nat.)
der Mathematisch-Naturwissenschaftlichen Fakultät
der Universität Rostock

vorgelegt von

M. Sc. Shanshan Song
geb. am 18.02.1991 in P. R. China

Rostock, Mai 2019

Die vorliegende Arbeit wurde im Zeitraum von Oktober 2015 bis April 2019 an der Universität Rostock im Arbeitskreis von Herrn Prof. Dr. Martin Hagemann angefertigt.

1. Gutachter: Prof. Dr. Martin Hagemann

2. Gutachter: Prof. Dr. Andreas P.M. Weber

Tag der Einreichung: 24th May, 2019

Tag der Verteidigung: 25th Oct, 2019

Abstract

The needed increase of crop productivity is relying on the improvement of photosynthetic efficiency, which is mainly limited by the carbon fixation pathway Calvin-Benson-Bassham cycle (CBBC) due to its insufficient carboxylase Rubisco. This enzyme is not completely discriminating between CO₂ and O₂, hence, the oxygenase reaction leads to the appearance of toxic 2-phosphoglycolate requiring CO₂-releasing photorespiration to detoxify and to recycle it into the CBBC intermediate 3-phosphoglycerate. Here, we aim to introduce a synthetic formate assimilation (FA) pathway to improve carbon fixation due to its function as an additional carbon-fixing route, which possibly also reduces the photorespiratory loss of CO₂ via decreased glycine decarboxylation. To establish FA, genes encoding the proteins 10-formyl-THF ligase (FTL), 5,10-methylene-THF dehydrogenase (MtdA), and 5,10-methenyl-THF cyclohydrolase (FchA) from *Methylobacterium extorquens* AM1 were stepwise transferred into the model cyanobacterium *Synechocystis* sp. PCC 6803 leading to the transgenic strain exF-C-M. The action of the three enzymes should permit assimilation of externally added formate. Expression of the transgenes clearly stimulated the growth of strain exF-C-M in the presence of formate, along with increased glutamate/glutamine ratio. These data indicated that FA might have been established in exF-C-M, where it assists cell growth and might reduce the loss of ammonia via glycine decarboxylation. In addition to wild-type, the high CO₂-requiring *Synechocystis* mutant $\Delta ccmM$ was selected as promising platform, because it directly permits to observe the efficiency of FA pathway via reduction of its CO₂ dependence. The addition of formate enhanced the growth of $\Delta ccmM$ /exF-C-M at decreased CO₂ supplementation, although no obvious stimulation in growth was found compared to $\Delta ccmM$. The further improvement of FA should be done with $\Delta ccmM$, since this strain allows the easiest validation of improved carbon fixation via FA. Finally, a segregated *Synechocystis* mutant $\Delta folD$ could be generated due to the expression of FTL and MtdA. The addition of formate rescued its retarded growth which can be used in future attempts to screen for suitable formate dehydrogenases. Collectively, the work reported first results to establish a synthetic FA pathway for the assimilation of organic carbon from formate in the photoautotrophic model cyanobacterium *Synechocystis*, which paves the way to introduce such a pathway subsequently in crop plants.

Die benötigte Steigerung von Ernteerträgen verlangt eine Verbesserung der Photosyntheseeffizienz, die hauptsächlich durch die Kohlenstofffixierung im Calvin-Benson-Bassham-Zyklus (CBBC) und die Effizienz dessen Carboxylase Rubisco begrenzt wird. Dieses Enzym akzeptiert neben CO₂ auch O₂ als Substrat, wobei die Oxygenasereaktion zum Auftreten des toxischen 2-Phosphoglykolat führt. Zu dessen Entgiftung benötigt es die Photorespiration, die 2-Phosphoglykolat zum CBBC-Zwischenprodukt 3-Phosphoglycerat regeneriert, aber auch CO₂ freisetzt. In der vorliegenden soll einen Syntheseweg für die Formiatassimilation (FA) etabliert werden, um die Photosynthese mit einem zusätzlichen Kohlenstoff-Fixierungsweg zu verbessern. Möglicherweise kann dieser auch den photorespiratorischen CO₂-Verlust durch verminderte Glycinecarboxylierung verringern. Um die FA zu etablieren, wurden Gene, die für die Enzyme 10-Formyl-THF-Ligase (FTL), 5,10-Methylen-THF-Dehydrogenase (MtdA) und 5,10-Methenyl-THF-Cyclohydrolase (FchA) kodieren, schrittweise aus *M. extorquens* AM1 in das Modell-Cyanobakterium *Synechocystis* sp. PCC 6803 transferiert, was zum transgenen Stamm exF-C-M führte. Die Wirkung der drei Enzyme sollte die Assimilation von extern zugesetztem Formiat ermöglichen. Die Expression der Transgene stimulierte eindeutig das Wachstum des Stammes exF-C-M in Gegenwart von Formiat und zeigte ein verringertes Verhältnis von Glutamat zu Glutamin. Diese Daten deuten darauf hin, dass die FA in exF-C-M etabliert wurde und sie hier das Zellwachstum unterstützt und den Ammoniakverlust durch Glycinecarboxylierung verringert. Zusätzlich zum Wildtyp wurde die *Synechocystis*-Mutante $\Delta ccmM$ mit hohem CO₂-Bedarf als vielversprechende Plattform ausgewählt, da sie die direkte Beobachtung der Effizienz des FA-Signalwegs durch Reduzierung ihrer CO₂-Abhängigkeit erlaubt. Die Zugabe von Formiat verstärkte das Wachstum von $\Delta ccmM$ /exF-C-M bei verminderter CO₂-Supplementierung, wobei im Vergleich zur parentalen $\Delta ccmM$ -Mutante keine offensichtliche Wachstumsstimulation erfolgte. Die weitere Optimierung der FA sollte in $\Delta ccmM$ erfolgen, da dieser Stamm die einfachste Validierung einer verbesserten Kohlenstofffixierung über FA ermöglicht. Schließlich konnte durch die Expression von FTL und MtdA eine segregierte $\Delta foID$ -Mutante erzeugt werden, die in zukünftigen Versuchen zum Screening für geeignete Formiatdehydrogenasen verwendet werden kann. Zusammenfassend berichtet die Arbeiten über die ersten Ergebnisse, einen synthetischen FA-Weg für die Assimilation organischen Kohlenstoffs aus Formiat im photoautotrophen Modell-Cyanobakterium *Synechocystis* zu etablieren. Diese Ergebnisse ebnen den Weg für die spätere Einführung eines solchen Stoffwechselweges in Kulturpflanzen.

Table of content

Abstract.....	II
Table of content	IV
Figure index.....	VII
Table index.....	VIII
Abbreviations.....	IX
1 Introduction.....	1
1.1 The necessity to improve photosynthesis.....	1
1.1.1 Improving carbon fixation via optimization of Rubisco	2
1.1.2 Improving carbon fixation via optimization of RuBP regeneration	3
1.1.3 Improving carbon fixation via optimization of photorespiration	4
1.1.4 Improving carbon fixation via engineering carbon concentrating mechanism.....	8
1.1.5 Improving carbon fixation via engineering synthetic carbon fixation pathway.....	9
1.2 The reductive acetyl-CoA pathway (rAcCoA pathway)	10
1.3 Folate-dependent one-carbon metabolism interacting with photorespiration.....	13
1.4 Introduction of formate assimilating pathway into cyanobacterial model strain <i>Synechocystis</i> sp. PCC 6803	14
1.4.1 <i>Synechocystis</i> sp. PCC 6803	14
1.4.2 Formate assimilation pathway.....	14
2 Materials.....	18
2.1 Chemicals and enzymes	18
2.1.1 Chemicals	18
2.1.2 Enzymes	18
2.2 Kits.....	18
2.3 Media.....	18
2.4 Oligonucleotides.....	18
2.5 Bacterial Strains	19
2.6 Bioinformatics tools	20
3 Methods.....	21
3.1 Growth conditions.....	21
3.2 DNA manipulation.....	21
3.3 Generation of <i>Synechocystis</i> mutants	21
3.4 Construction of expression plasmids	22
3.5 Drop-dilution assay	22
3.6 Protein expression and purification <i>in E. coli</i>	22

3.7	Protein extraction and quantification from <i>Synechocystis</i>	23
3.8	FTL activity assay	24
3.9	Formate oxidizing activity	24
3.10	Western blotting	24
3.11	Quantification of internal amino acids and organic acids	25
3.12	Carbon labeling	25
4	Results.....	26
4.1	Impact of external formate on <i>Synechocystis</i> wild-type.....	26
4.1.1	Growth effect of formate on wild-type.....	26
4.1.2	Investigation of candidate gene <i>sl1359</i> potentially encoding FDH	28
4.2	Establishing FA pathway in <i>Synechocystis</i> wild-type.....	30
4.2.1	Introduction of FTL in <i>Synechocystis</i> wild-type	31
4.2.2	Phenotype and metabolome analysis of FTL-expressing strain exFTL.....	32
4.2.3	Enhanced growth of exFTL with glycine.....	35
4.2.4	Introduction of FTL in the photorespiratory mutant	36
4.2.5	Attempt to improve formate assimilation by expression of <i>SGAT</i>	39
4.2.6	Labeling pattern of proteinogenic amino acids.....	40
4.2.7	Attempt to improve FA pathway by overexpression of <i>FoID</i> in wild-type	41
4.3	Establishing FA pathway in $\Delta ccmM$ mutant	47
4.3.1	Introduction of FTL in $\Delta ccmM$	47
4.3.2	Introduction of FTL and <i>MtdA</i> in $\Delta ccmM$	50
4.4	Formate-dependent C1-auxotrophy reporter strain	54
4.4.1	Characterization of enzyme <i>FoID</i>	54
4.4.2	Attempts to generate mutant $\Delta foID$ in wild-type	55
4.4.3	Attempts to generate mutant $\Delta foID$ in the presence of exogenous enzyme FTL	57
4.4.4	Attempts to generate mutant $\Delta foID$ using nutritional supplements	57
4.4.5	The deletion of <i>foID</i> in the presence of exogenous enzymes FTL and <i>MtdA</i>	60
5	Discussion	61
5.1	Impact of external formate on <i>Synechocystis</i>	61
5.2	Investigation of candidate gene <i>sl1359</i> encoding FDH	63
5.3	Expression of FTL in wild-type	64
5.4	Attempts to enhance FA rate by increasing glycine level	68
5.5	Labeling pattern of proteinogenic amino acid	70
5.6	Attempts to improve FA rate by overexpression of an alternative <i>FoID</i> in wild-type	72
5.7	Establishing the FA pathway in $\Delta ccmM$ mutant.....	75
5.8	Attempts to generate a formate-dependent strain on the basis of $\Delta foID$	77
5.9	Future perspectives.....	79

6	Reference.....	80
	Acknowledgement.....	i
	Curriculum vitae.....	iii
	Eidesstattliche versicherung.....	iv

Figure index

Figure 1: CBBC (Reproduced from Raines 2003).	3
Figure 2: Alternative photorespiratory pathways (reproduced from South et al. 2019).	7
Figure 3: The acetyl-CoA pathway of acetogenic bacteria (reproduced from Schuchmann & Müller 2016).	12
Figure 4: A scheme displaying synthetic FA pathway established in <i>Synechocystis</i> sp. PCC 6803.	15
Figure 5: Effect of sodium formate on the <i>Synechocystis</i> wild-type.	27
Figure 6: Genotypic and phenotypic characterization of the $\Delta sll1359$ mutant.	29
Figure 7: Schematic presentation of the FTL-expression construct and genotypic characterization of the FTL-expressing <i>Synechocystis</i> strain exFTL.	31
Figure 8: Growth rates and selected metabolites in the strains wild-type and exFTL.	33
Figure 9: Growth rates of wild-type and exFTL supplied with glycine and formate.	36
Figure 10: Genotypic and phenotypic characterization of the strain exFTL/ $\Delta 3pr$	37
Figure 11: Serine and glycine were compared between wild-type, photorespiratory mutant and FTL-expressing strains.	38
Figure 12: Schematic presentation and phenotypic characterization of the strain exFTL-SGAT. .	39
Figure 13: Labeling pattern of proteinogenic glycine, serine, methionine and histidine were compared between wild-type and exFTL.	41
Figure 14: Schematic presentation of the FchA-MtdA-expression construct and genotypic characterization of the <i>Synechocystis</i> strain exF-C-M.	42
Figure 15: Theophylline sensitivity and protein expression of wild-type, exFTL and exF-C-M.	43
Figure 16: Phenotype characterization of wild-type, exFTL and exF-C-M.	44
Figure 17: Growth of exFTL and exF-C-M strain under CO ₂ -limiting condition.	45
Figure 18: Genotypic and phenotypic characterization of the strain $\Delta ccmM$ /exFTL.	48
Figure 19: Genotypic and phenotypic characterization of the strain $\Delta ccmM$ /exF-C-M.	51
Figure 20: Amino acid sequence alignment of FOLD highlighting the conserved residues.	55
Figure 21: Attempts to delete gene <i>sll0753</i> in <i>Synechocystis</i> wild-type.	56
Figure 22: Attempts to delete gene <i>sll0753</i> in the presence of exogenous FTL.	58
Figure 23: Attempts to delete gene <i>sll0753</i> after supplementation with IMP or inosine.	59
Figure 24: The completely deletion of <i>sll0753</i>	60
Figure 25: Formate uptake assay.	62
Figure 26: Changes of metabolites related to AABA metabolism.	67
Figure 27: A Scheme displaying the probable interaction of photorespiration and one-carbon metabolism in <i>Synechocystis</i>	72
Figure 28: Growth of wild-type feed with different concentration of serine.	75
Figure 29: Growth of exF-C-M/ $\Delta folD$ in the presence or in the absence of external formate.	78

Table index

Table 1: Oligonucleotides used in this study.	19
Table 2: Strains used in this study and their respective genotype.	20
Table 3: Growth rates of <i>Synechocystis</i> wild-type cells under different growth conditions in the presence and absence of formate, respectively.	28
Table 4: Metabolome analysis of strain exFTL compared to wild-type.	34
Table 5: Metabolome analysis of strain exF-C-M compared to exFTL.	46
Table 6: Metabolome analysis of strain $\Delta ccmM$ /exFTL and $\Delta ccmM$	49
Table 7: Metabolome analysis of strain $\Delta ccmM$ /exFTL and $\Delta ccmM$ /exF-C-M at day 5.	52
Table 8: Metabolome analysis of strain $\Delta ccmM$ /exFTL and $\Delta ccmM$ /exF-C-M at day 7.	53

Abbreviations

ATP	Adenosine triphosphate
ADP	Adenosine diphosphate
Pi	Inorganic phosphate
NADPH	Reduced nicotinamide adenine dinucleotide phosphate
NADP ⁺	Nicotinamide adenine dinucleotide phosphate
NADH	Reduced nicotinamide adenine dinucleotide
NAD ⁺	Nicotinamide adenine dinucleotide
EDTA	Ethylenediaminetetraacetic acid
IPTG	Isopropyl β -D-1-thiogalactopyranoside
SDS	Sodium dodecyl sulphate
PAGE	Polyacrylamide gel electrophoresis
PVDF	Polyvinylidene difluoride
PSII	Photosystem II
PCR	Polymerase chain reaction
Ni-NTA	Nickel nitrilotriacetic acid
PMSF	Phenylmethylsulfonyl fluoride
BSA	Bovine serum albumin

1 Introduction

1.1 The necessity to improve photosynthesis

Recent reports show that global crop yield needs to double during the next 30 years to meet the requirements of the rising human population, changed diet and biofuel consumption (Ray et al., 2013; Bar-Even, 2018; Weber and Bar-Even, 2019). Numerous specialists suggested that, compared to having more cropland areas, enhancing crop production per unit area land is more sustainable for worldwide environmental protection (Tilman et al., 2011; Fan et al., 2012; Pete, 2018). In the mid of 20th-century, crop yield increased remarkably even in the absence of more arable area, called “Green Revolution”, which benefited from plant breeding development, utilization of fertilizer and improved cultivation management (Evans 1997). Now, the utilization of fertilizers and other agrochemicals like herbicides are reaching their maximum, and thus a new “Green Revolution” is needed (Fischer & Edmeades 2010, Caemmerer & Evans 2010). Long et al. (2006) clearly discussed that the leaf photosynthesis is closely associated with crop production. Hence, to further improve crop yield in the future and start the second green revolution, it is essential to improve photosynthetic efficiency.

Photosynthesis is a biological process used by photosynthetic organisms such as plants, algae and cyanobacteria to convert light energy into chemical energy and produce organic compounds from CO₂. It can be divided into three phases: light absorption and energy delivery through antenna systems; primary electron transfer in reaction centers and finally carbon fixation. In the first process, sunlight is collected by diverse pigments associated in antenna systems and transferred to reaction center chlorophylls. It is subsequently able to initiate the transport of electrons from water in the electron transport chain to acceptors, which then serve as energy for the reduction of CO₂ to triose-phosphate (Orr et al., 2017). As the light capturing efficiency in modern crop plants is near its theoretical maximum, the basic and applied researches are now mostly focus on the improvement of carbon fixation (Zhu et al., 2010; Weber and Bar-Even, 2019) described within the next chapters.

Introduction

1.1.1 Improving carbon fixation via optimization of Rubisco

Ribulose-1,5-bisphosphate carboxylase/oxygenase (Rubisco) is the predominant carbon-fixing enzyme on earth catalyzing the carboxylation of ribulose-1,5-bisphosphate (RuBP) to produce 3-phosphoglycerate (3-PGA) in the Calvin-Benson-Bassham cycle (CBBC) (Fig. 1). It is a slow catalyst with an average turnover between 1-10 s⁻¹ compared to 50-100 s⁻¹ of other enzymes in the central carbon metabolism (Erb and Zarzycki, 2016; Orr et al., 2017). Hence Rubisco contributes 30-50% of the soluble leaf protein to maintain the sufficient carbon fixing rate, which results in a huge nitrogen investment met by fertilizers (Feller et al., 2008; Sharwood, 2017). In addition, Rubisco contains both carboxylase and oxygenase activity, i.e. it can only partly discriminate between CO₂ and O₂. Thus when the carbon fixation acceptor RuBP is activated via the enolase activity of Rubisco, it also can react with O₂ forming toxic 2-phosphoglycolate (2-PG). This intermediate must be detoxified by the energetically costly photorespiratory pathway leading to the release of fixed carbon, nitrogen, and chemical energy. These features make Rubisco the key target for improving carbon fixing efficiency.

Plant Rubisco forms a large hexadecameric complex assembled by eight large subunits arranged as dimers and eight small subunits (L₈S₈). The large subunit is encoded by the chloroplast DNA and the small subunit is encoded in the nucleus and imported into the stromal compartment of chloroplast from the cytosol by crossing the chloroplast membranes (Chatterjee and Basu, 2011). Until now, re-engineering Rubisco to increase its CO₂ specificity and catalytic efficiency only achieved limited success. Tcherkez and coworkers proposed that all Rubiscos might be already perfectly adapted to the natural gaseous and thermal environments during long-term evolution (Tcherkez et al., 2006). So instead of working on to create a “super Rubisco”, replacing the endogenous Rubisco in crop plants with better natural variants could be another option. It has been reported that Rubisco from cyanobacteria have higher catalytic rate accompanied by their lower CO₂ specificity compared to plant enzymes, whereas Rubisco from red algae has the best specificity for CO₂ (Whitney et al., 2011). Transgenic tobacco lines with functional Rubisco from the cyanobacterium *Synechococcus*

Introduction

elongatus PCC 7942 with or without assembly chaperon or carboxysomal protein were successfully constructed, whilst they can only grow under elevated CO₂ condition (Lin et al., 2014; Occhialini et al., 2016). However, these efforts lay a good foundation for further research on the expression of a foreign Rubisco with or without accompanying carbon concentrating mechanisms.

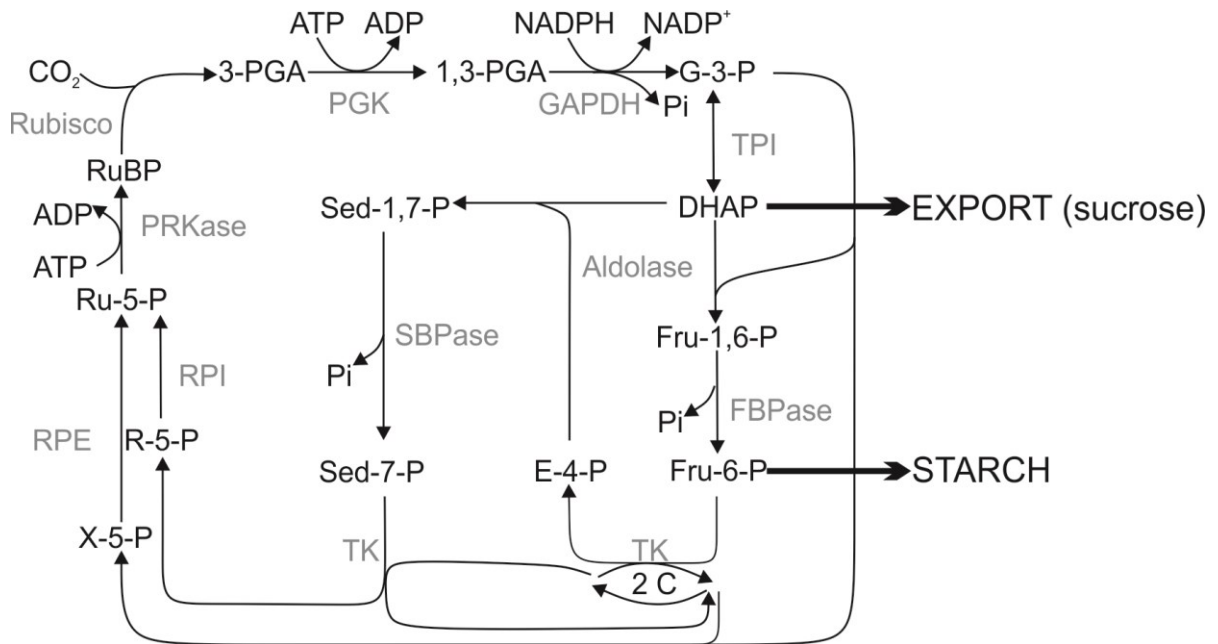


Figure 1: CBB (Reproduced from Raines 2003).

1,3-PGA, 1,3-bisphosphoglycerate; G-3-P, glyceraldehyde-3-phosphate; DHAP, dihydroxyacetone phosphate; Fru-1,6-P, fructose-1,6- bisphosphate; Fru-6-P, fructose-6-phosphate; E-4-P, erythrose-4 phosphate; Sed-1,7-P, sedoheptulose-1,7-bisphosphate; Sed-7-P, sedoheptulose-7-phosphate; X-5-P, xylulose-5-phosphate; R-5-P, ribose-5- phosphate; Ru-5-P, ribulose-5-phosphate; RuBP, ribulose-1,5- biphosphate; PGK, 3-phosphoglycerate kinase; GAPDH, glyceraldehyde-3-phosphate dehydrogenase; TPI, triose-phosphate isomerase; FBPase, fructose-1,6-bisphosphatase; TK, transketolase; SBPase, sedoheptulose-1,7-bisphosphatase; RPI, phosphopentose isomerase; RPE, phosphopentose epimerase; PRKase, ribulose-5-phosphate kinase.

1.1.2 Improving carbon fixation via optimization of RuBP regeneration

The established biochemical model of C₃ photosynthesis predicted that under sufficient CO₂ amounts, the ability of RuBP regeneration can also limit CO₂ assimilation (von Caemmerer and Farquhar, 1981). This view was supported by the analysis of transgenic tobacco plants with nearly 40% less Rubisco, which performed the same photosynthetic rate as wild-type (Stitt &

Introduction

Schulze, 1994). Investigations on CBBC enzymes (Fig. 1) responsible for RuBP regeneration indicated that reduction of the SBPase (Harrison et al., 1998; Olcer, 2001), TK (Henkes, 2001), and aldolase (Haake et al., 1999) resulted in strong reduction of photosynthesis. These results led to the assumption that overexpression of these three enzymes may lead to enhanced photosynthetic rate and growth.

In support of this hypothesis, overexpression of either bifunctional FBP/SBPase from cyanobacteria (Miyagawa et al. 2001) or SBPase from *Arabidopsis thaliana* (Lefebvre, 2005; Rosenthal et al., 2011) or *Chlamydomonas* (Tamoi et al., 2006) in tobacco enhanced photosynthetic efficiency and RuBP regenerating capability in controlled environments or field trials at atmospheric or saturating CO₂ conditions. The transgenic rice plant overexpressing SBPase showed also an enhanced tolerance of photosynthesis and growth to high temperature stress (Feng et al., 2007). In addition, similar results were observed in transgenic tobacco and *Anabaena* sp. PCC 7120 after overexpression of Fru-1,6-P aldolase (FBA) (Uematsu et al., 2012), TPI and FBPase (Kang et al., 2005; Ma et al., 2008), respectively. The transgenic tobacco with higher FBA activity exhibited higher biomass and faster photosynthetic rate under elevated CO₂ condition, while no enhanced photosynthesis occurred at ambient air. These results indicated that the photosynthetic rate limiting step is transferred from Rubisco activity to the ability of RuBP regeneration under high CO₂ concentration. However, an unexpected effect was observed in transgenic tobacco overexpressing plastidial TK from *Arabidopsis*. These plants exhibited slow growth and a chlorotic phenotype, which could be rescued by the supply of TPP or thiamine (Khozaei et al., 2015). Similarly, TK-overexpressing rice did not change its CO₂ assimilation rate (Suzuki et al., 2017). These results probably indicated that TK activity is controlled by a complex regulatory mechanism.

1.1.3 Improving carbon fixation via optimization of photorespiration

1.1.3.1 Introduction of the photorespiratory pathway

Photorespiratory pathway (Fig. 2) initiates with the oxygenation of RuBP catalyzed by the

Introduction

oxygenase activity of Rubisco producing one molecule of each 3-PGA and toxic 2-PG in the chloroplast. The photorespiratory pathway salvages the majority of organic carbon from the produced 2-PG, but around 30% of the fixed carbon in C₃ photosynthesis is lost under ambient conditions (Zhu et al., 2010). It comprises multiple enzymes and transporters localized in four compartments of plant cells (Hagemann and Bauwe, 2016). 2-PG phosphatase catalyzes in chloroplasts the 2-PG dephosphorylation to glycolate, which is transported to the peroxisome. There, glycolate is oxidized to glyoxylate by glycolate oxidase (GO) releasing H₂O₂, which is degraded by catalase (CAT). Glutamate: glyoxylate aminotransferase (GGAT) transaminates glyoxylate into glycine. The glycine is then transported into mitochondria, where glycine is decarboxylated by glycine decarboxylase complex (GDC) to 5, 10-methylene-THF with the release of NADH, CO₂ and ammonia. One molecule of glycine and 5, 10-methylene-THF are reversibly converted to serine and THF catalyzed by serine hydroxymethyltransferase (SHMT). Serine returns back into peroxisomes and reacts with glyoxylate to produce glycine and hydroxypyruvate under the catalysis of serine: glyoxylate aminotransferase (SGAT). Hydroxypyruvate is reduced to glycerate by hydroxypyruvate reductase (HPR). Finally, hydroxypyruvate is transported into chloroplast and recycled into 3-PGA by glycerate 3-kinase (GLYK). In summary, during the conversion of two molecules 2-PG one molecule of 3-PGA is produced, which returns into CBC cycle. However, one molecule each of CO₂ and of ammonia are released, which need to be re-fixed through high energy consuming reactions.

Hence the hypothesis was proposed that the reduction of costly photorespiration could improve photosynthesis (Zelitch and Day, 1973). Later on this idea was changed, because it was found that the deletion or down-regulation of enzymes to inhibit photorespiration caused a conditional lethal phenotype (high CO₂-requiring) in all oxygenic phototrophs including algae (Nakamura et al., 2005), cyanobacteria (Eisenhut et al., 2008b) and C₄ plants (Zelitch et al., 2009), which perform carbon concentration mechanisms. Therefore, researches' focus changes towards introducing bypasses to reduce photorespiratory carbon loss.

Introduction

1.1.3.2 Photorespiratory bypasses

Several strategies were proposed as photorespiratory bypasses (Fig.2) and engineered into C_3 plants attempting to improve photosynthesis. The bacterial glycolate catabolic pathway was firstly introduced into the chloroplast of *Arabidopsis* (Kebeish et al. 2007). In this bypass, glycolate is directly converted into glycerate in chloroplast reducing the photorespiratory flux through peroxisome and mitochondria and shifting CO_2 release from mitochondria to chloroplast. In this approach, five genes from *E. coli* were expressed, which encode glycolate dehydrogenase (GDH) oxidizing glycolate to glyoxylate, glyoxylate carboligase (GCL) converting two molecules of glyoxylate into one molecule tartronic semialdehyde inherent with the release of one CO_2 , and tartronic semialdehyde reductase (TSR) producing glycerate. The transgenic *Arabidopsis* plants expressing all the five genes performed reduced photorespiration and increased growth under the controlled condition (8 h light/16 h dark, short days) (Kebeish et al. 2007). The same approach was applied into biofuel crop *Camelina sativa* with similar results exhibiting reduced photorespiration, enhanced photosynthesis and increased seed yield (Dalal et al., 2015). However, the introduction of GDH alone in potato also increased its photosynthetic efficiency (Nölke et al., 2014). This result implies that glyoxylate produced by GDH maybe oxidized to CO_2 via pyruvate dehydrogenase in chloroplast (Blume et al., 2013). So, it is still a matter of discussion whether the enhanced photosynthesis results from the bypass of photorespiration or the increased CO_2 concentration in the chloroplast. The second bypass-route oxidizes glycolate completely to CO_2 in the chloroplast catalyzed by a series of endogenous and introduced enzymes including GO, CAT, and malate synthase (MS), which seemingly enable the plant to grow faster and contain higher photosynthetic rate (Maier et al., 2012). But the introduction of the second bypass into tobacco only showed limited enhancement in the productivity and around 24% of the transgenic lines exhibited yellowish leaves and stunted growth (South et al., 2019). The third bypass was designed to replace GO with GDH to avoid H_2O_2 production and keep MS. This route increased the biomass of tobacco by 18% in the greenhouse (South et al., 2019). Additionally, the establishment of bypass 3 along with the suppression of PLGG1 reducing the glycolate flux into peroxisome, further

Introduction

enhanced biomass by 24% in tobacco. The fourth strategy was to import bacterial genes encoding GCL and hydroxypyruvate isomerase (HYI) respectively targeted to the peroxisome (Carvalho et al., 2011). This bypass converted glyoxylate directly to hydroxypyruvate in the peroxisome aiming to eliminate the release of ammonia. The bypass was only partly active, since the transgenic lines generated only expressed GCL but not HYI. And they clearly exhibited signs of a stress response under ambient air condition (Carvalho et al., 2011).

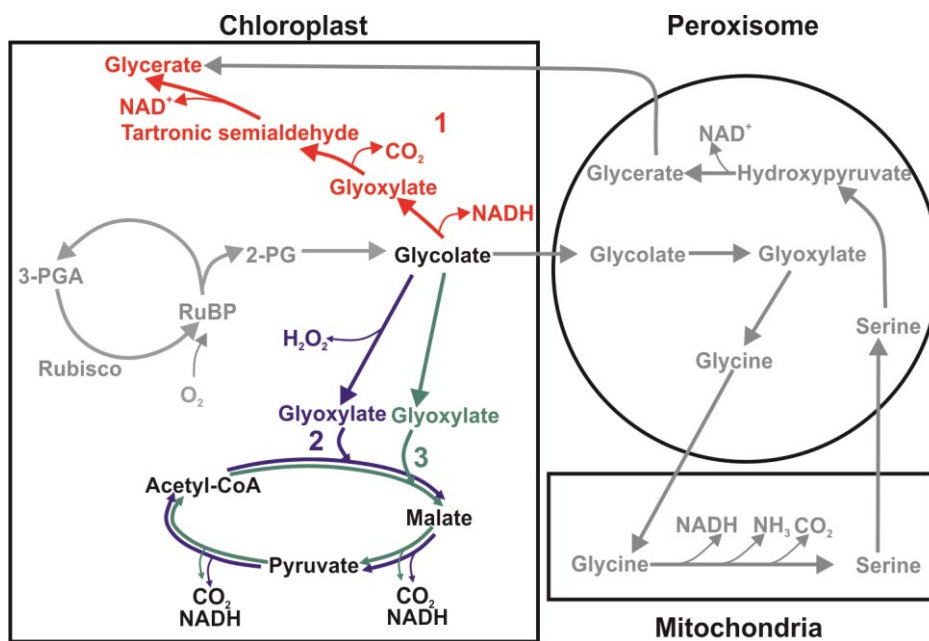


Figure 2: Alternative photorespiratory pathways (reproduced from South et al. 2019).

Bypass1 (red line) converts glycolate to glycerate with GDH, GCL and TSR. Bypass 2 (purple line) degrades glycolate to CO₂ by GO, MS and CAT. Bypass 3 (green line) relies on two introduced enzymes GDH and MS.

In recent years, with the development of synthetic biology, synthetic photorespiratory bypasses are proposed as another promising strategy to improve carbon assimilation (Blankenship et al., 2011). The oxygen-insensitive alternative carbon fixation pathway the hydroxypropionate cycle found in filamentous anoxygenic phototrophs (Berg et al., 2007; Zarzycki et al., 2009) was redesigned and introduced into *Synechococcus elongatus* PCC 7942 to recycle the toxic glyoxylate preventing the loss of ammonia and coupling to the addition fixation of bicarbonate (Shih et al., 2014). Although no obvious benefits from this novel bypass were observed, this approach opens a new gate for improving photosynthesis.

1.1.4 Improving carbon fixation via engineering carbon concentrating mechanism

Another promising method is to improve CO₂ concentration around Rubisco, thereby increasing its carboxylase activity and suppressing its side-reaction oxygenation and subsequent photorespiration. Cyanobacteria, algae and some plants (C₄ plants, CAM plants and C₃-C₄ intermediate species) have polyphyletically evolved carbon concentrating mechanisms (CCMs). CCMs act to actively accumulate inorganic carbon (i.e. bicarbonate and CO₂) inside cells and accumulate the CO₂ concentration at the site of Rubisco. It has been discussed that engineering them into C₃ species will improve biomass production (Hibberd et al., 2008; von Caemmerer and Evans, 2010; Peterhansel et al., 2013; McGrath and Long, 2014).

Bioengineering approaches to establish the best understood cyanobacterial CCM have made the most distinct progress. The cyanobacterial CCM is composed of multiple inorganic carbon uptake systems and the Rubisco-including micro-compartment carboxysomes (Raven et al., 2008; Kerfeld & Melnicki, 2016). The kinetic model proposed by McGrath and Long (2014) predicted that the introduction of cyanobacterial CCM into the chloroplast of C₃ crop plants could increase net leaf CO₂ uptake by nearly 60%, thereby resulting in a 36% to 60% enhancement of yield (McGrath and Long, 2014). Moreover, it is predicted that even the single addition of bicarbonate transporter BicA could enhance photosynthesis by 9%, whilst 16% stimulation will be achieved when multiple transporters were expressed (McGrath and Long, 2014). The overexpression of the endogenous bicarbonate transporter BicA alone stimulated cells of *Synechocystis* sp. PCC 6803 to grow faster and to accelerate biomass production (Kamennaya et al., 2015). Meanwhile, studies to select suitable transit peptides that direct the cyanobacterial bicarbonate transporter to the inner envelope membrane of chloroplasts in plants have made significant progress (Pengelly et al., 2014; Nielsen et al., 2016; Rolland et al., 2016). A lot of effort was also made to understand the principles of carboxysome assembly (Cameron et al., 2013; Kerfeld and Melnicki, 2016). The attempts to establish functional carboxysome were already tested in the heterologous host *E. coli* (Bonacci et al., 2012; Cai et

Introduction

al., 2016). A simplified α -carboxysome encapsulating with Form 1A-Rubisco from *Cyanobium* was produced within tobacco chloroplast and enabled it to grow autotrophically under high CO_2 condition (Long et al., 2018).

To achieve the goal of introducing C_4 photosynthesis in C_3 crop plants, the international C_4 rice consortium has been established (Hibberd et al., 2008; von Caemmerer et al., 2012). The major challenges in this task are the alterations of the anatomy and complex biochemistry in leaves (Häusler et al., 2002). C_4 photosynthesis starts by the carboxylation of phosphoenolpyruvate (PEP) through PEP carboxylase (PEPC) yielding oxaloacetate (OAA) in the mesophyll cells. OAA is then reduced to malate by malate dehydrogenase (MDH), which is transported into the low gas permeable bundle sheath cells, where CO_2 is released from malate through decarboxylase malic enzyme (ME). This results in an enrichment of CO_2 in the proximity of Rubisco (Häusler et al., 2002). The ME reaction product pyruvate is returned back to mesophyll cells and is then used for the regeneration of the CO_2 acceptor PEP by pyruvate orthophosphate dikinase (PPDK). However, overexpression of the single or all C_4 -specific major enzymes caused aberrant chloroplasts or did not significantly affect the photosynthetic assimilation rate (Ku et al., 1999; Takeuchi et al., 2000; Häusler et al., 2001; Taniguchi et al., 2008). Hence, in addition to the main catalytic enzymes, the metabolite transporters between different subcellular compartments and their regulation also need to be identified (Denton et al., 2013). With the advanced development of next generation sequencing, a list of key factors including the regulatory proteins, putative transcriptional proteins and transporters was obtained to establish C_4 biochemistry in C_3 plants (Majeran et al., 2005; Bräutigam et al., 2008; Majeran and van Wijk, 2009; Li et al., 2010; Gowik et al., 2011; Schuler et al., 2016; Wang et al., 2016, 2017; Sedelnikova et al., 2018). These studies lay a good foundation for the understanding C_4 photosynthesis and may help to produce a C_4 rice prototype in the future.

1.1.5 Improving carbon fixation via engineering synthetic carbon fixation pathway

Instead of engineering the natural carbon assimilation pathways, the design and import a

Introduction

complete novel pathway supporting or replacing CBBC are more ambitious. A computational approach was developed to investigate all the feasible and effective synthetic pathways basing on roughly 5000 enzymes from KEGG database. According to the final calculation, the malonyl-CoA-oxaloacetate-glyoxylate (MOG) pathway using the most effective carboxylase PEPC was determined as the most promising one (Bar-Even et al., 2010). Implementation of a partial MOG pathway in *Synechococcus elongates* PCC 7942 increased approximately 2 fold in bicarbonate assimilation (Yu et al., 2018). Another synthetic pathway, called CETCH was generated, which is supposed to be more energy efficient than CBBC and other natural existing oxygen-insensitive carbon fixation pathways (Schwander et al., 2016). The CETCH pathway is based on enoyl-CoA carboxylase/reductase to fix CO₂ and was firstly constructed *in vitro*. This pathway is conducted by 17 enzymes originated from 9 different organisms and optimized by enzymes engineering and metabolic proofreading (Schwander et al., 2016). Subsequent attempts to establish such complicated novel pathways in plants are challenging, since plants contain a more complex background. Thus, the compatibility between the introduced synthetic pathways and endogenous metabolism should be analyzed before the real implementation (Erb et al., 2017).

A recent comparison of carboxylation and CO₂ reduction modules showed that pathways combining carboxylation with reduction are the most efficient way, providing us a new horizon to improve photosynthesis (Cotton et al., 2018). The reductive acetyl-CoA pathway (rAcCoA pathway) is the only known pathway initiated with CO₂ reduction and its subsequent steps overlap with one-carbon metabolism in most organisms. Based on this, novel formate assimilating pathway (named FA pathway hereafter) supporting CBBC was proposed and tested in *E. coli* (Yishai et al., 2017). All the necessary components are naturally existing and are integrated from different living organisms to build this synthetic alternative carbon fixing pathway.

1.2 The reductive acetyl-CoA pathway (rAcCoA pathway)

The rAcCoA pathway (Fig. 3) was elucidated in the mid-to-late 1980s as a pathway used by

Introduction

anaerobic, acetogenic bacteria to synthesize acetyl-CoA from CO₂. This pathway is also referred to as Wood-Ljungdahl pathway in recognition of the two biochemists H.G. Wood and L.G. Ljungdahl, who together with their co-workers described this pathway (Ljungdahl, 1986; Wood, 1991; Drake et al., 2008; Fuchs, 2011). Compared to other carbon fixation pathways, it is a linear pathway separated in methyl and carbonyl branches that catalyzes the reduction and merging of two molecules of CO₂ producing one molecule of acetyl-CoA (Drake et al., 2008). The methyl branch starts with the reduction of one molecule of CO₂ to formate through formate dehydrogenase (FDH) (Ljungdahl, 1986). Formate is then activated with tetrahydrofolate (THF) into 10-formyl-THF catalyzed by 10-formyl-THF ligase (FTL). This step is an ATP-consuming reaction (Lovell et al., 1988). 10-formyl-THF is further reduced to 5,10-methenyl-THF via 5,10-methenyl-THF cyclohydrolase (Fch) and subsequently 5,10-methylene-THF by 5,10-methylene-THF dehydrogenase (Mtd) (Ljungdahl et al., 1980). The enzyme 5,10-methylene-THF reductase (Clark and Ljungdahl, 1984; Ragsdale, 2008) converts stepwise 5,10-methylene-THF to more stable 5-methyl-THF. The methyl group of 5-methyl-THF, serving as the precursor of the methyl group of acetyl-CoA, is transferred to the cobalt site of the heterodimeric corrinoid iron-sulfur protein (CoFeSP) catalyzed by 5-methyl-THF bounded corrinoid iron-sulfur protein methyltransferase (Svetlitchnaia et al., 2006; Ragsdale, 2008). The following reaction transfers the methyl group from methyl-CoFeSP to the reduced NiFeS active site cluster A of acetyl-CoA synthase (ACS). In the carbonyl branch, the second molecule of CO₂ is reduced to enzyme-bound CO by the NiFe clusters of CO dehydrogenase (CODH) (Lindahl et al., 1990). CODH is normally forming a complex with ACS that accepts the methyl group from methyl-CoFeSP and produces acetyl-CoA from CO, CoA and the methyl group (Fuchs, 2011). The product acetyl-CoA is then incorporated into acetate by acetate kinase or biomass.

The reactions of CO₂ reduction to 5,10-methylene-THF are most essential in the THF-dependent one-carbon metabolism, which is present from bacteria to human (Hanson and Roje, 2001) with the exception of the first two steps, the production of formate and its activation to 10-formyl-THF. In photosynthetic organisms, one carbon metabolism closely connects with

Introduction

serine-glycine interconversion in the photorespiratory process (Bauwe et al., 2010), which makes the establishment of synthetic FA bypass feasible and easier compared with other complex synthetic carbon fixing pathways.

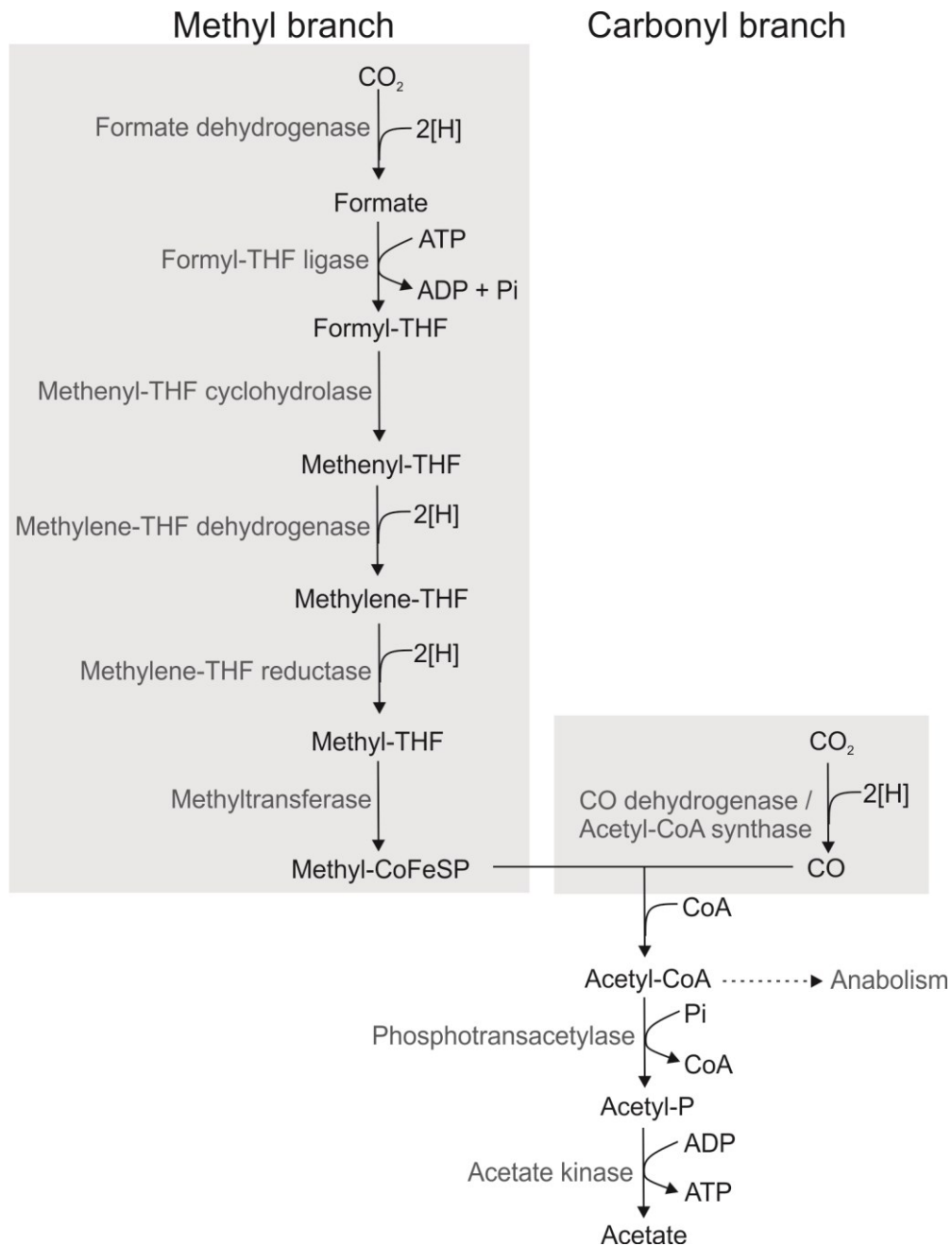


Figure 3: The acetyl-CoA pathway of acetogenic bacteria (reproduced from Schuchmann & Müller 2016).

[H], redox equivalent (one electron+one proton); THF, tetrahydrofolate; CoFeSP, corrinoid iron-sulfur protein; CoA, Coenzyme A. The left reaction line represents the methyl branch and the right one shows the carbonyl branch.

1.3 Folate-dependent one-carbon metabolism interacting with photorespiration

One-carbon metabolism plays a pivotal role in all living organisms, supplying C1 units for the synthesis of many intermediates and the regulation of metabolic processes (Jabrin et al., 2003). The most reduced THF-derivative 5-methyl-THF is utilized by methionine synthase (MS) to convert homocysteine to methionine (Ferla and Patrick, 2014). As a proteinogenic amino acid, methionine is broadly known as its function in the initiation of translation (Zou et al., 2017). In addition, it is the precursor for the synthesis of S-adenosyl methionine (SAM), which is an essential molecule involved in important metabolic processes such as transmethylation, transsulfuration and polyamine synthesis (Lu, 2000). 5,10-methylene-THF serves as both, C1 donor and cofactor in the production of thymidylate catalyzed by thymidylate synthase (TS) (Carreras and Santi, 1995). 10-formyl-THF is required for the formation of purine rings in the *de novo* purine biosynthesis (Christensen and MacKenzie, 2006; Murta et al., 2009). In addition, 10-formyl-THF supplies its formyl group to synthesize formylmethionyl-tRNA (Dartois et al., 2003; Ravel, 2011).

Serine and glycine are the most important cellular sources for one carbon units (Hanson and Roje, 2001). As mentioned before, SHMT catalyzes the reversible reaction from glycine and 5,10-methylene-THF to produce serine and free THF. On the other hand, glycine is oxidized by GDC with the formation of 5,10-methylene-THF and the release of CO₂ and ammonia. In photosynthetic organisms, SHMT and GDC activities are coupled to maintain a steady state equilibrium of 5,10-methylene-THF and THF during photorespiration. 5,10-methylene-THF could be further reduced to 5-methyl-THF by 5,10-methylene-THF reductase (Sheppard et al., 1999) or it can be oxidized to 5,10-methenyl-THF and subsequent hydrolyzed to form 10-formyl-THF through Mtd and Fch activity, respectively. Besides, formate could also be incorporated to THF to produce 10-formyl-THF by FTL (Hanson and Roje, 2001). In humans and yeast, the FTL, Fch and Mtd activities are most associated together with a trifunctional protein named C1-THF synthase (Vickers et al., 2009). In addition, these activities are usually separated into a mono-functional FTL and a bifunctional enzyme FOLD in plants and

prokaryotes (Vickers et al., 2009) or three mono-functional proteins in methylobacteria (Vorholt et al., 1998).

1.4 Introduction of formate assimilating pathway into cyanobacterial model strain *Synechocystis* sp. PCC 6803

1.4.1 *Synechocystis* sp. PCC 6803

Considering the complexity of novel carbon fixation pathways, it has been suggested to initially test them in algae or cyanobacteria benefiting from their faster growth and easier genetic manipulation compared to higher plants (Ort et al., 2015). The cyanobacterial model strain *Synechocystis* sp. PCC 6803 (hereafter referred to as *Synechocystis*) was chosen and used as wild-type in this study. *Synechocystis* is a unicellular phototrophic cyanobacterium, using Rubisco as the main carboxylase and performing similar photosynthesis as higher plants (Durall and Lindblad, 2015). Furthermore, it was the first fully sequenced phototrophic organism (Kaneko et al. 1996). The genome information is now displayed in the manually curated database CyanoBase, which provides useful information about gene sequences and functions (Ikeuchi and Tabata, 2001). *Synechocystis* is also naturally competent and able to integrate foreign DNA into its genome via homologous recombination allowing easy mutation but also expression of foreign genes (Zang et al., 2007). Finally, its metabolic network is also relatively well understood. The photorespiration process in *Synechocystis* (Fig. 4) unlike in the compartmented plant cell occurs only in cytosol, which also could make the introduction of the FA pathway easier and feasible.

1.4.2 Formate assimilation pathway

In this study, the alternative synthetic FA pathway (Fig. 4) supporting CBBC will be introduced into the photosynthetic model organism *Synechocystis*. It is assumed that it will not only reduce the net loss of fixed carbon and nitrogen during the photorespiratory cycle but can also result in the additional carbon fixation via the CO₂ reduction to formate. Furthermore, the FA pathway should not disrupt photorespiration, which is essential to oxygenic phototrophs.

Introduction

The FA bypass begins with CO₂ reduction to formate by FDH. Formate is then converted to 10-formyl-THF through FTL similarly as in the rAcCOA pathway. 10-formyl-THF will be further reduced to 5,10-methylene-THF via Fch and Mtd activity. *Synechocystis* expresses the bifunctional FoID, which can naturally catalyze the reversible conversion between 10-formyl-THF and 5,10-methylene-THF. Then the product 5,10-methylene-THF condenses with glycine to produce serine under the catalysis of native SHMT, which thereby is assumed to considerably reduce glycine decarboxylation via GDC.

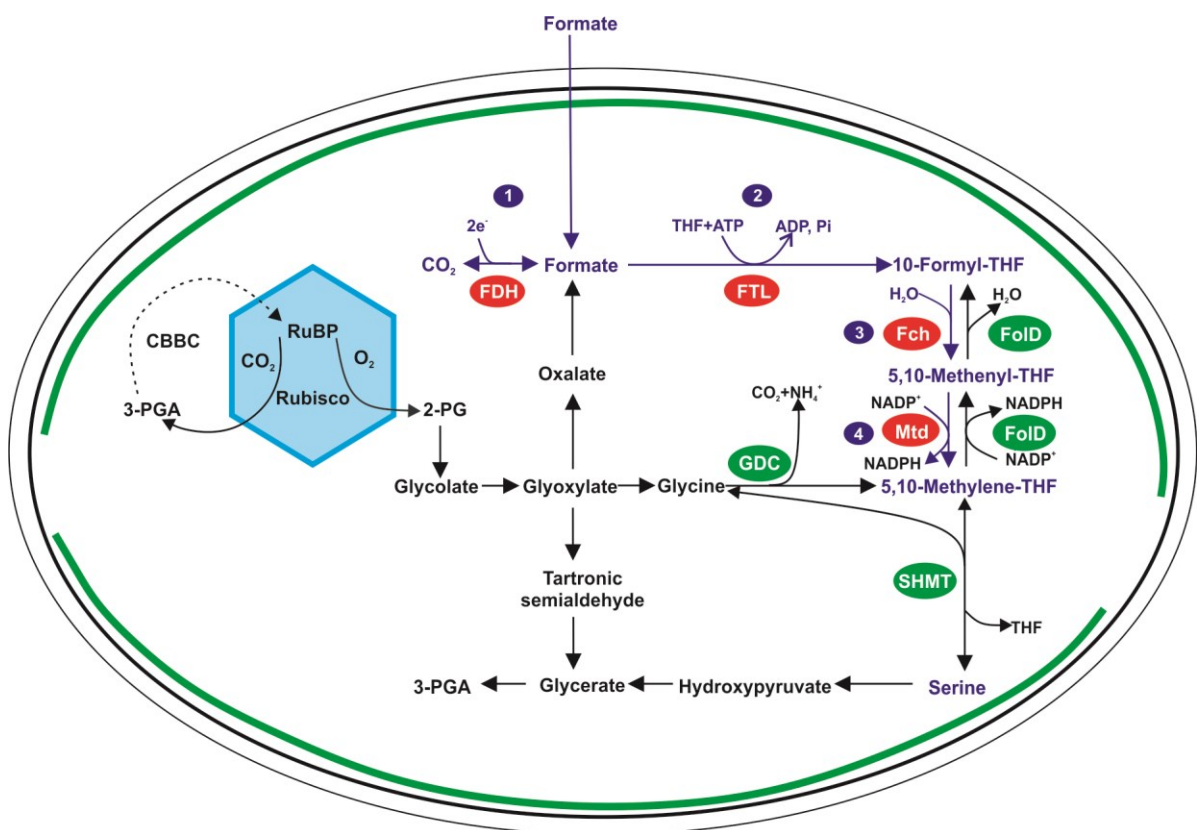


Figure 4: A scheme displaying synthetic FA pathway established in *Synechocystis* sp. PCC 6803.

Purple arrows indicate FA pathway and black arrows indicate the native photorespiratory pathways and CBBC. The establishment of FA pathway in *Synechocystis* requires the following four steps. ①: FDH catalyzes the reduction of CO₂ to formate. ②: FTL catalyzes formate and THF to form 10-formyl-THF. ③: 10-Formyl-THF is converted to 5,10-methenyl-THF via Fch activity. ④ 5,10-Methenyl-THF is further reduced to 5,10-methylene-THF through Mtd activity.

For the initial reaction, the pathway depends on a suitable FDH, which is not present in cyanobacteria. FDHs (EC 1.17.1.9) comprise a heterogeneous group of proteins broadly discovered in eukaryotes and prokaryotes (Jormakka et al., 2003; Yu et al., 2014). They can

Introduction

be divided into two major classes, based on their metal content and the subsequent chemical strategy followed by the active site to carry out the formate oxidation (Maia et al., 2017). One class, metal-independent FDHs that contain no metal ion are composed of the NAD⁺-dependent FDHs, and belong to the superfamily of D-specific dehydrogenases of 2-hydroxy acids (Tishkov and Popov, 2006; Maia et al., 2017). FDHs from this class usually catalyze formate oxidation coupled with the reduction of NAD⁺ to NADH. The other class of metal-dependent FDHs are NAD⁺-independent, contain a complex inventory of redox active centers and are sensitive to oxygen (Maia et al., 2015). These proteins hold molybdenum, tungsten or other transition metals in their active sites coordinated with their pyranopterin cofactors to mediate the formate oxidation or CO₂ reduction. An excellent candidate is the NAD-dependent FDH from acetogenic *Clostridium carboxidivorcans*. The ccFDH with a low binding affinity for formate was reported preferentially to reduce CO₂ to formate with a catalytic rate 0.08 s⁻¹ (Alissandratos et al., 2013). Besides, several reports showed that certain FDHs were able to catalyze CO₂ to produce formate (Maia et al., 2017), but this enzyme class is still difficult to use in application because of their slower rates (lower than Rubisco) and usual oxygen sensitivity.

Thus, we first aimed to introduce the other enzymes necessary for the designed formate assimilating pathway except FDH into *Synechocystis*. This engineering attempt should result in a *Synechocystis* strain that can metabolize external formate. It will then be analyzed whether this new pathway increases cellular carbon fixation and possibly biomass production. The similar strategy was already applied to *E. coli* by three independent groups. Their studies successfully showed that external formate can be utilized to produce serine, which was supported by performing ¹³C isotope analysis (Yishai et al., 2017; Bang and Lee, 2018; Tashiro et al., 2018). However, to establish and verify formate assimilation, specific mutant combinations were generated which made *E. coli* completely dependent on the new pathways. Especially, in the background of the serine auxotrophy mutant of *E. coli* the serine synthesis from formate and formate assimilation flux was enhanced (Bang and Lee, 2018). Nevertheless, these studies verified that the formate assimilation pathways can be functional in an

Introduction

engineered organism and provides many information which enzymes are suitable for further attempts.

Our study is the first trial in a photoautotrophic organism, here *Synechocystis*. In contrast to the studies with *E. coli*, which is not performing photosynthesis and photorespiration, we aim to establish FA pathway in *Synechocystis* working supplementary to the CBBC. The presence of an intact CCM probably supplies enough organic carbon and energy for cells, which might make it more difficult to see the advantage of the additional formate assimilation. In order to improve the contribution of FA pathway to carbon assimilation and to make the cyanobacterial model more plant like, we also used a CCM-defective *Synechocystis* mutant $\Delta ccmM$. Mutant $\Delta ccmM$ exhibited high CO₂-requiring phenotype along with a significant increase in 2-PG and a decrease in 3-PGA content after a shift to low carbon conditions (Hackenberg et al., 2012). These features resulted from enhanced oxygenase activity and declined carboxylase activity of Rubisco in $\Delta ccmM$, making it a suitable background for the test of FA pathway. In addition, *Synechocystis* produces high amounts of NADPH and ATP through photosynthetic electron transport chain under light, supporting enough energy and reducing equivalents for formate assimilation with only small effects on the endogenous carbon fixing pathways.

In summary, we present here experiments to establish an alternative carbon fixation route via the FA pathway to improve photosynthesis based on simplified sets of enzymes. Although lots of effort should be putting on engineering a better FDH to efficiently reduce CO₂ to formate to complete the FA pathway in the future, our study serves as a platform for improving photosynthesis according to the biological C1 unit conversion in cyanobacteria.

2 Materials

2.1 Chemicals and enzymes

2.1.1 Chemicals

¹³C-Formate, ¹⁴C-Formate and tetrahydrofolic acid (THF) were purchased from Sigma Aldrich (USA). Tag-PCR Master Mix was bought from Qiagen (Germany). And all the other chemicals used in this project were obtained from Carl Roth (Karlsruhe, Germany).

2.1.2 Enzymes

Restriction endonucleases for DNA modification were purchased from New England Biolabs (USA). All the other enzymes used in this study, such as T4 DNA ligase for DNA ligation were obtained from Thermo Fischer Scientific (USA).

2.2 Kits

Kits for DNA extraction from standard agarose gels and mini-plasmid isolation were purchased from Macherey-Nagel (Düren, Germany).

2.3 Media

LB broth and LB agar for *E. coil* cultivation were bought from Carl Roth. BG11 for *Synechocystis* cultivation was prepared according to Rippka et al. (1979).

2.4 Oligonucleotides

All oligonucleotides used in this study were ordered from Eurofins Genomics (Ebersberg, Germany) and Microsynth (Switzerland) and stored as 100 µM stock solution. Oligonucleotides and respective sequences are listed in table 1.

Materials

Table 1: Oligonucleotides used in this study.

Name	Sequence	Company
sII0753-rev	GAATTCTTAAATACCTAACCGTTGCCG	Eurofins
sII0753-fw	AACATATGACTGCCGTACCCCATCCTG	Eurofins
sII0753-de-fw	GATGTCTGCTTGCCGGTGATATCG	Microsynth
sII1359-rev	GGTAAAGCCAGCGTTAGTC	Eurofins
sII1359-fw	CGGCAGAGAAACCGATAAG	Eurofins
sII1359-Ecoli-fw	AACATATGAAAATAGGAAGAATTACGG	Eurofins
sII1359-Ecoli-rev	GGATCCTCAATTCTGGCGTGATCCGG	Eurofins
ftI-fw	AGATCTATGCATCATCACCATCAC	Eurofins
ftI-rev	CAATTGTTAGAACAGACCGTTCGAT	Eurofins
ftI-Ecoli-fw	GAGCTCATGCATGCATCATCACCATCAC	Eurofins
ftI-Ecoli-rev	GGTACCTTAGAACAGACCGTTCGAT	Eurofins
ConII-fw	GAGCTGCAGGAGCTCACCGGTTTCGAATTG	Microsynth
Fch-fw	GCGACTAGTATGCATCATCACCATCACCACG	Microsynth
MtdA-rev	GCGCTCGAGTTAAGCCATTTCTTTAGCCAG	Microsynth
<i>ccmM</i> (sII1031)-fw	CCATCATCCGCCGTTAAT	Eurofins
<i>ccmM</i> (sII1031)-rev	ACCGAGACAAGCTGTTGC	Eurofins
<i>odc</i> (sII1358)-fw	TCATAGCGCACACATTG	Eurofins
<i>odc</i> (sII1358)-rev	GTCATGGAAGGCAGAACC	Eurofins
<i>tsr</i> (sII0229)-fw	ATAAGTCAGAGAAGTGAA	Eurofins
<i>tsr</i> (sII0229)-rev	CCATGTTTACTCCAGTAA	Eurofins
<i>gcvT</i> (sII0171)-fw	AGACCTGAAGGAAGCTGTAG	Eurofins
<i>gcvT</i> (sII0171)-rev	GAGGAAGTGGTGACAGGTT	Eurofins
SGAT-fw	CATATGATGGACTATATGTATGGACCAGGG	Microsynth
SGAT-rev	AGATCTTTAGATTCTAGAGGGAATGAGAGG	Microsynth

Underlines present restriction enzyme sites: CATATG (*Nde*I), GGATCC (*Bam*HI), AGATCT (*Bgl*II), CAATTG (*Mun*I), GAGCTC (*Sac*I), GTACC (*Kpn*I), CTGCAG (*Pst*I), ACTAGT (*Spe*I), CTCGAG (*Xho*I).

2.5 Bacterial Strains

Cloning and amplification of plasmids were performed in *E. coli* DH5 α . A glucose-tolerant derivative of *Synechocystis* sp. strain PCC 6803 was used in all the experiments and served as the wild-type. *Synechocystis* sp. PCC 6803 and mutants used in this study are listed in table 2 with their respective genotypes.

Materials

Table 2: Strains used in this study and their respective genotype.

Strain	Genotype	Reference
<i>Synechocystis</i> strains		
Wild-type	PCC 6803	
$\Delta sll1359$	PCC 6803 <i>sll1359::Gm</i>	This work
$\Delta folD$	PCC 6803 <i>sll0753::Km</i>	This work
exFTL/ $\Delta folD$	PCC 6803 <i>exftl//sll0753::Km</i>	This work
exF-C-M/ $\Delta folD$	PCC 6803 <i>exftl//exfchA//exmtdA //sll0753::Km</i>	This work
exFTL	PCC 6803 <i>exftl</i>	This work
exFTL-SGAT	PCC 6803 <i>exftl//exSGAT</i>	This work
exFTL/ $\Delta 3pr$	PCC 6803 <i>exftl/sll0171::Sp//slr0229::Km//slr1358::Cm</i>	This Work
$\Delta 3pr$	PCC 6803 <i>sll0171::Sp//slr0229::Km//slr1358::Cm</i>	(Eisenhut et al., 2008b)
exF-C-M	PCC 6803 <i>exftl//exfchA//exmtdA</i>	This work
$\Delta ccmM$ /exFTL	PCC 6803 <i>exftl//sll1031::Km</i>	This work
$\Delta ccmM$ /exF-C-M	PCC 6803 <i>exftl//exfchA//exmtdA //sll1031::Km</i>	This work
$\Delta ccmM$	PCC 6803 <i>sll1031::Km</i>	(Hackenberg et al., 2012)

2.6 Bioinformatics tools

Synechocystis sp. PCC 6803 nucleotide sequences were referred from the genome database CyanoBase (http://genome.microbedb.jp/cyanobase/GCA_000009725.1, (Nakamura et al., 1998)). Multiple protein sequence alignments were done via the web tool Clustal Omega (Sievers et al., 2011). Multiple nucleic acids sequence alignments were done via the software BioEdit (Hall et al., 2011).

3 Methods

3.1 Growth conditions

The cyanobacteria strains used in this work are listed in Table 2. The glucose-tolerant strain of *Synechocystis* sp. PCC 6803 served as wild-type. Cultivation of mutants and transgenic strains was performed at 50 $\mu\text{g}/\text{mL}^{-1}$ kanamycin (Km), 20 $\mu\text{g}/\text{mL}^{-1}$ spectinomycin (Sp), 10 $\mu\text{g}/\text{mL}^{-1}$ chloramphenicol (Cm), or at 50 $\mu\text{g}/\text{mL}^{-1}$ erythromycin (Ery) as required. Axenic cultures of *Synechocystis* were grown photoautotrophically in batch cultures at 30 °C under continuous illumination. Contamination by heterotrophic bacteria was checked by spreading of 0.2 mL of culture on LB plates.

The *E. coli* strain DH5 α cultured in LB medium supplemented with respective antibiotics at 37 °C was used for routine DNA manipulations.

3.2 DNA manipulation

Total DNA from *Synechocystis* was isolated according to Hagemann et al. (1997). And other DNA techniques, for example, transformation of *E. coli* cells, ligation and restriction analysis were done according to the standard methods (Sambrook and Russell 2001). PCR with specific oligonucleotides as described before was carried out using the Tag-PCR Master Mix. Plasmid isolation from *E. coli* cells was performed by mini-plasmid isolation kit.

3.3 Generation of *Synechocystis* mutants

Construction of mutants was conveniently performed by insertional mutagenesis. The targeted genes were amplified with specific primers (given in Table 1) using chromosomal *Synechocystis* wild-type DNA as template and cloned into pGEM-T vector (Promega). And the targeted genes were checked by DNA sequencing. The gene cassettes encoding different antibiotics were inserted into the coding region of target genes with around 500 bp flanking region on left and right terminals. Subsequently, the transformation (Grigorieva and Shestakov, 1982) was

followed by selection with respective antibiotics producing the desired mutants. The genotype of mutants was characterized with specific primers via PCR (Table 1).

3.4 Construction of expression plasmids

For the expression of gene *sll1359* in the *E. coli* vector pET28a (Novagen), the coding sequence was amplified through PCR using DNA of *Synechocystis* with primer pair sll1359-Ecoli-fw/rev adding *Nde*I and *Bam*HI restriction sites for cloning. The resulting fragment was first cloned into pGEM-T (Promega). And the sequence was further confirmed with DNA sequencing. After restriction, the *sll1359* fragment was inserted into pET28a vector, resulting in plasmid pET28a-sll1359.

The exogenous genes *ftl*, *fchA* and *mtdA* from *M. extorquens* AM1 were codon-optimized synthesized and kindly supplied by Dr. Arren Bar-Even. The CDS region of gene *SGAT* was amplified from cDNA of *Arabidopsis thaliana*. The construction process was described in detail in the results.

3.5 Drop-dilution assay

For drop-dilution assay on solid medium, strains were pre-cultivated in liquid BG11 supplemented with antibiotics if required. Cultures were adjusted to $OD_{750\text{ nm}} = 1$ and diluted to 1:10, 1:100, 1:1000 and 1:10000. 2 μ l of each drop was spotted onto plates (BG11, pH 8, solidified by 0.9% Kobe agar) containing given amounts of supplements and cultivated under constant illumination at 30 °C for 10 days. Each spotting assay was done at least two replicates. Representative results are shown in the thesis.

3.6 Protein expression and purification in *E. coli*

The recombinant proteins were expressed in *E. coli* BL21. The correct clones with the respective plasmid were inoculated overnight at 37 °C in 5 mL LB-medium containing the respective antibiotic for selection. The pre-culture was diluted in fresh LB-medium to an

Methods

OD_{600 nm} of 0.1 and incubated at 37 °C to OD_{600 nm} of 0.6 to 0.8 before induction with 1mM IPTG or 0.02% L-arabinose. Expression was carried out for 4 hours at 37 °C. Cells were harvested by centrifugation at 6000 g for 10 minutes and washed with lysis buffer (20 mM Tris-HCl pH 7.8, 50 mM NaCl, 10 mM imidazole). Cells were lysed in lysis buffer supplemented with 1 mg/mL lysozyme and incubated on ice for 30 minutes. The resulting suspension was subsequently sonicated for 3 x 30 s at maximal power. Lysate was cleared by centrifugation at 14000 g for 30 minutes at 4 °C.

His-tagged proteins were purified via IMAC according to the manufactures protocol (QIAexpressionist, Qiagen) in the gravity flow mode. Lysate passed the Ni-NTA three times, followed by 3 washing steps with 20 batch volumes washing buffer (20 mM Tris-HCl pH 7.8, 1 M NaCl, 40 mM imidazole). Elution was done with 1 batch volume of elution buffer (20 mM sodium phosphate pH 7.8, 500 mM NaCl, 300 mM imidazole) and repeated up to 3 times if desired.

3.7 Protein extraction and quantification from *Synechocystis*

10 – 20 mL *Synechocystis* cells were grown to a cell density of OD_{750 nm} = 1 and total protein was extracted from these cells. Cells were collected by centrifugation at 6000 g for 10 minutes and immediately frozen in liquid nitrogen and storage in – 80 °C for further protein extraction. Frozen cells were added with 200 µL homogenization buffer (75 mM Tris-HCl, 1.5 mM EDTA, pH 7.5), 10 µL PMSF (30 mM dissolved in isopropanol as stock solution), 5 µL NaHSO₃ (60 mM as stock solution), 5 µL (6 mM as stock solution) Pefablock and 0.5 mm glass beads when they are ready for proteins extraction. Samples were mixed by vortex 1 min, then frozen for 20 s in liquid nitrogen and melted under ambient air. Repeat these three steps for 5 times. Lysate was got by centrifugation at 600 g for 5 minutes.

Protein quantification was done according to the protocol (Schulz et al., 1994). The standard calibration curve was done with different concentration of BSA. 100 µL BSA reference solutions or cell lysate were mixed separately with 400 µL staining solution (90% MeOH, 10% acetic

Methods

acid and 0.01% amido black 10B) by vortex. The supernatant was removed by centrifugation at 12 000 g for 30 minutes. Then pellet was re-dissolved with 1 mL wash solution (90% MeOH, 10% acetic acid). After the second centrifugation at 12 000 g for 15 minutes, the supernatant was discarded and the pellet was dried at 37 °C for 5 minutes. Finally, the pellet was dissolved in 1 mL resolving solution (200 mM NaOH) and absorption at 615 nm was measured in a photometer. The values obtained for the BSA reference solutions created the standard calibration equation using for the determinant of *Synechocystis* cells protein.

3.8 FTL activity assay

The FTL activity was assayed via the quantitative conversion of 10-formyl-THF, which is formed from formate in the FTL enzymatic reaction, to methenyl-THF by the addition of acid as described (Marx et al., 2003). The concentration of methenyl-THF was determined spectrophotometrically by its characteristic absorption changes at 350 nm. The assay was done under anaerobic conditions since THF is sensitive to oxygen. The reaction solution included 0.1 M Tris (pH 8), 10 mM MgCl₂, 5 mM ATP, 50 mM sodium formate, 0.2 μM THF and 50 μg lysate protein. THF was firstly aliquoted in Tris buffer at 4 mg/mL as mother solution under anaerobic condition.

3.9 Formate oxidizing activity

Formate oxidizing activity was measured according to the method (Choe et al., 2014). The formate degrading activity was determined spectrophotometrically by its characteristic absorption changes at 340 nm during the reaction at room temperature. The assay was performed using a solution containing 20 mM sodium phosphate buffer pH 7, 5 mM NAD⁺ or NADP⁺, 50 mM sodium formate and different amount of *Synechocystis* lysate.

3.10 Western blotting

Protein samples were mixed with 3-fold lammi buffer and boiled at 90 °C for 10 minutes. Samples were loaded in 12% (W/V) SDS-PAGE gel, further electrophoretically transferred to

PVDF membrane and detected using antibodies raised against either His-tag or special antibody (e.g. FTL antibody). After a subsequent washing step, the membrane was incubated with the secondary antibody conjugated to enzyme peroxidase. Then protein was probed using ECL chemiluminescence detection reagent.

3.11 Quantification of internal amino acids and organic acids

Free amino acids and organic acids were extracted from the frozen *Synechocystis* cell pellets of 5 mL of cultures with $OD_{750\text{ nm}} = 1$ using 80% ethanol under 65 °C for 3 h. After centrifugation, the supernatant was dried by lyophilization and re-dissolved in 1 mL LC water. Amino acids and organic acids were separated through liquid chromatography coupled to tandem mass spectrometry (LC-MS/MS) with Discovery H5 F5 HPLC column (Sigma-Aldrich). All assays were repeated in 3 times by independent cell cultivation. Pair-wise *t* test was applied for the statistical comparison of mean values.

3.12 Carbon labeling

For stationary isotope tracing of proteinogenic amino acids, cells were pre-cultivated with air-enriched by 5% CO₂ in the BG11 medium. Then cells from wild-type and exFTL strains were shifted to ambient air starting with $OD_{750\text{ nm}}$ of 0.1 under continuous light and were cultivated fed with either ¹³C-labeled or unlabeled sodium formate. When the optical density at $OD_{750\text{ nm}}$ of cells were up to 1, cells were diluted to 0.1 and re-cultivated until 1. This step was repeated for 3 times to ensure at least 9 generation growing and enough ¹³C incorporation into proteinogenic amino acids. Furthermore, 2 mL of cells were harvested by centrifugation for 5 min at 11 000 g. The pellet was hydrolyzed by incubation with 1 mL of 6N hydrochloric acid for a duration of 24 h in 95 °C. Samples were then lyophilized and sent to Dr. Arren Bar-Even' lab for measurement. The further steps were done as described in the paper of Yishai et al. (2017).

4 Results

4.1 Impact of external formate on *Synechocystis* wild-type

Before the introduction of formate assimilation pathway into cyanobacterium model strain *Synechocystis* sp. PCC 6803, the impact of external formate on the *Synechocystis* wild-type and its ability of formate utilization were investigated. Since formate is frequently used as the bicarbonate analog for the study of the interaction of PSII and bicarbonate which can replace bicarbonate from its binding site in PSII (Stemler and Radmer, 1975; Semin et al., 1990; Shevela et al., 2007), its effect on photosynthesis was also studied and found to act as potent inhibitor. In addition, the candidate gene *sll1359* encoding FDH in the genome of *Synechocystis* was also investigated if it could interfere with the planned formate assimilation strategy. Throughout this study, I used sodium formate to provide this compound to cells, since *Synechocystis* is sensitive to pH of its growth environment (Nguyen and Rittmann, 2016).

4.1.1 Growth effect of formate on wild-type

The resistance of *Synechocystis* wild-type cells toward formate was studied on agar media supplied with formate whose concentration ranged from 0 to 200 mM (Fig. 5A). The growth of *Synechocystis* became retarded when exposed to formate above 100 mM, however, the cells survived with up to 200 mM formate in the medium. No change in growth and pigmentation was observed with formate supplementation below 50 mM to the plates.

The effect of formate on photosynthetic oxygen evolution was then tested with concentrations lower than 50 mM in the presence of different light intensities (25 μmol , 50 μmol and 100 $\mu\text{mol photons m}^{-2} \text{ s}^{-1}$). Photosynthesis of *Synechocystis* was not affected by 10 mM formate under all the tested light intensities, but it was severely inhibited by 50 mM formate at higher light intensity (Fig. 5B).

Results

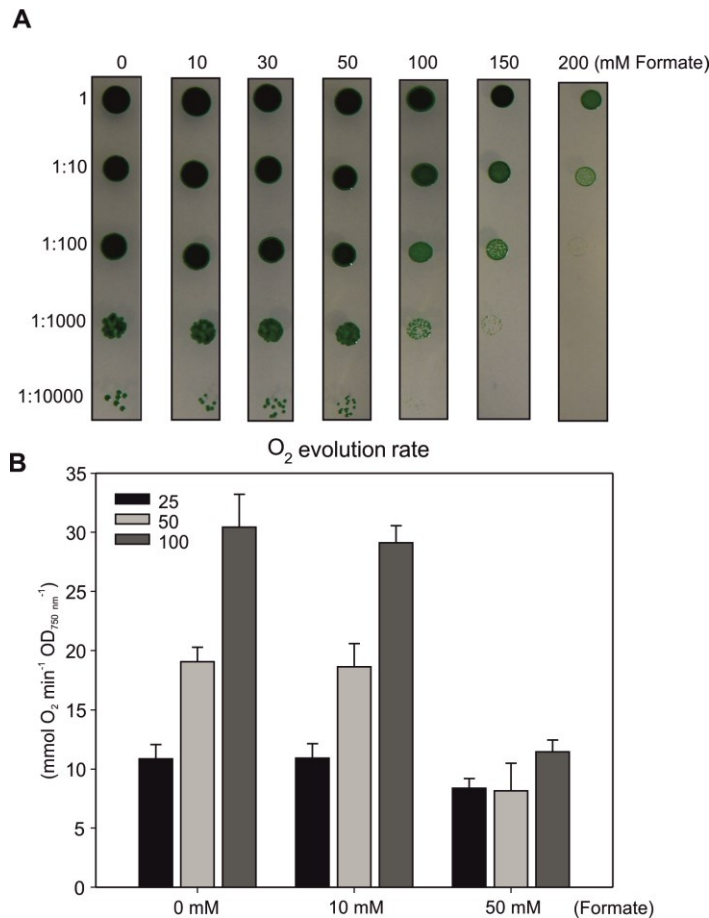


Figure 5: Effect of sodium formate on the *Synechocystis* wild-type.

A. Resistance of wild-type cells toward formate. Serial dilutions of cell suspension ($OD_{750\text{ nm}}$ was approximately 1) were dropped on BG11 agar plates, pH 8, supplemented with different concentrations of formate (0-200 mM) for 7 d. **B.** Photosynthetic O_2 evolution rates in the presence of different amounts of formate (0-50 mM). The pre-cultivated cells were grown under ambient air in flask and then inoculated at different light intensities when the O_2 evolution rate was measured (25 - 100 $\mu\text{mol photons m}^{-2} \text{s}^{-1}$).

The growth rates of wild-type were compared to detect the impact of formate below 20 mM. Cells were cultivated in the multi-cultivator with continuous illumination. No significant difference was observed between cells in the presence of formate or in the absence of formate under different light intensities (50 μmol , 100 μmol and 200 $\mu\text{mol photons m}^{-2} \text{s}^{-1}$) and different carbon concentrations (0.04% and 5% CO_2 , as shown in Table 3). To evaluate the impact of formate on wild-type cells in more detail, the steady state level of cellular metabolites was analyzed. For this purpose, cells were grown in liquid culture under ambient air and 100 $\mu\text{mol photons m}^{-2} \text{s}^{-1}$ supplied with 10 mM sodium formate or not. Samples were taken 24 h later and evaluated by LC-MS/MS. In summary, the levels of cellular metabolites showed

Results

no significant difference between cells grown with or without formate (Table 4).

Collectively, these data indicate that formate can be taken up by *Synechocystis*, but low concentrations of formate are tolerated and only concentrations higher than 20 mM start to have negative impact on photosynthesis and growth of wild-type cells. Hence, 10 mM formate was used for all growth assays in liquid medium in this study, whereas ≥ 50 mM formate were used as supplementation for medium in agar plates to test the sensitivity of transgenic clones to formate.

Table 3: Growth rates of *Synechocystis* wild-type cells under different growth conditions in the presence and absence of formate, respectively.

The values of growth rates were normalized as d^{-1} and presented as means \pm SE of three independent replicates.

Growth rate (d^{-1})	Formate concentration	Light intensity ($\mu\text{mol photons m}^{-2} \text{s}^{-1}$)		
		50	100	200
High carbon (5% CO_2)	0 mM	0.146 \pm 0.036	0.207 \pm 0.043	0.244 \pm 0.033
	10 mM	0.147 \pm 0.018	0.183 \pm 0.015	0.242 \pm 0.059
	20 mM	0.147 \pm 0.015	0.194 \pm 0.019	0.234 \pm 0.048
Low carbon (air, 0.04% CO_2)	0 mM	0.073 \pm 0.018	0.112 \pm 0.027	0.138 \pm 0.012
	10 mM	0.084 \pm 0.029	0.115 \pm 0.021	0.136 \pm 0.006
	20 mM	0.084 \pm 0.018	0.114 \pm 0.025	0.14 \pm 0.012

4.1.2 Investigation of candidate gene *sll1359* potentially encoding FDH

It has been reported that *Synechocystis* is able to degrade photorespiratory glyoxylate through the complete decarboxylation to CO_2 via oxalate and formate (Eisenhut et al., 2008b). In this decarboxylation branch, oxalate is decarboxylated to formate with the release of one molecule of CO_2 by oxalate decarboxylase (ODC) encoded by the gene *sll1358* (Eisenhut et al., 2008a; Tottey et al., 2008). It has been postulated that the intermediate formate is further oxidized to CO_2 through FDH. The gene encoding FDH in the genome of *Synechocystis* is not yet annotated. However, the ODC-encoding gene *sll1358* is co-transcribed with the downstream gene *sll1359* and both genes showed about 1.8 folds higher expression when cells were shifted

Results

from high to low CO₂ conditions, which promotes higher photorespiratory rates. The gene *sll1359* encodes a protein that contains a cytochrome-c-like domain (Eisenhut et al., 2008a). These data indicated that Sll1359 might be a candidate encoding FDH despite the missing similarity to already assigned FDH proteins.

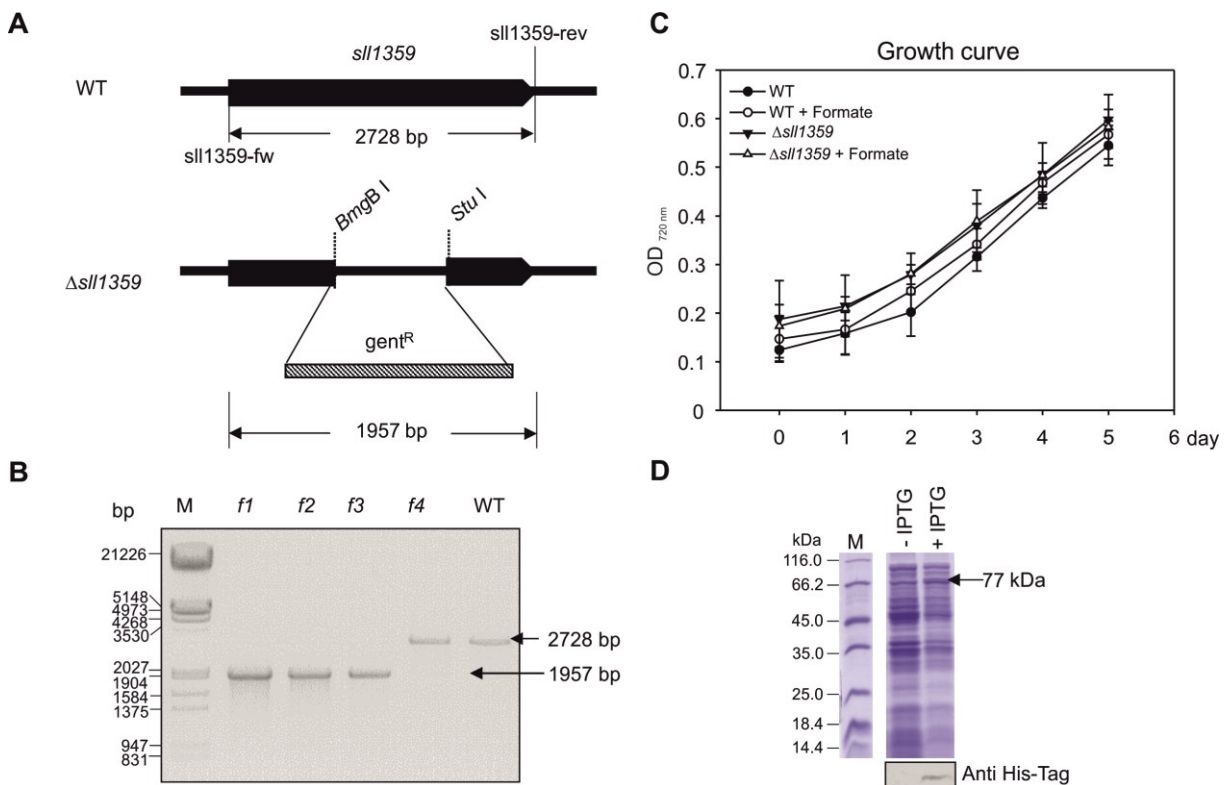


Figure 6: Genotypic and phenotypic characterization of the $\Delta sll1359$ mutant.

A. Schematic presentation of construct for deletion of gene *sll1359* in *Synechocystis*. The gene encoding gentamycin-resistance was inserted into gene *sll1359*. Oligonucleotides sll1359-fw and sll1359-rev flanking the insertion site were used to test the segregation. **B.** Complete segregation of the mutant $\Delta sll1359$ was verified with *sll1359* specific primers. M: DNA marker; f1-f4: different clones; WT: wild-type. **C.** Growth curves of $\Delta sll1359$ (triangle) and wild-type (circle) were measured either supplied with 10 mM formate (open) or not (solid) under constant light 100 $\mu\text{mol photons m}^{-2} \text{s}^{-1}$ and ambient air condition in multi-cultivator. **D.** The induction of recombinant Sll1359 protein with IPTG. *E. coli* BL21 cells containing pET-28a-sll1359 plasmid was induced with 1 mM IPTG for 4 h under 37 °C. The accumulation of His-tagged recombinant protein was verified by Western-blotting (below coomassie-stained gel).

To investigate the function of Sll1359, the gene was inactivated through interposon-mutagenesis (Fig. 6A). The gentamycin resistance gene was obtained from pUC4G after *HincII* digestion. The *sll1359* gene and its flanking sequence (2728 bp) were obtained from DNA of the *Synechocystis* wild-type (WT) via PCR using gene specific primers. The mutant plasmid

Results

was constructed, where the gentamycin resistance cassette interrupted gene *sll1359* (1957 bp) after deleting the internal part flanked by *BmgBI* and *Stul* sites. After selection of resistant colonies, the genotype of the obtained clones was checked with PCR. Clone *f1* to *f3* were completely segregated while *f4* was not (Fig. 6B). The easily achieved mutation of *sll1359* indicates that its gene product has no essential function in *Synechocystis* under laboratory condition. Clone *f1*, named $\Delta sll1359$ was used for further research. Subsequent growth experiments showed no difference in sensitivity to formate between mutant $\Delta sll1359$ and wild-type nor any growth retardation at ambient air (Fig. 6C). Additionally, the recombinant His-tagged Sll1359 protein was purified for enzyme activity analysis (Fig. 6D). No formate-oxidizing or CO₂-reducing activity was observed with recombinant Sll1359 protein in our lab. The same result was found with the total lysate of wild-type *Synechocystis* cells. These results indicate that Sll1359 is most likely not representing the FDH in *Synechocystis*. Therefore, the gene was left intact in the subsequent strains constructed with FA pathway to metabolize formate.

4.2 Establishing FA pathway in *Synechocystis* wild-type

Crucial for formate assimilation is the enzyme FTL that catalyzes the incorporation of formate into 10-formyl-THF, which can be subsequently converted into 5, 10-methenyl-THF and 5, 10-methylene-THF, hence supplying C1 units for serine synthesis and contributing biomass. There is no gene annotated to encode FTL in the *Synechocystis* genome according to the database CyanoBase. It has been reported that the overexpression of FTL from *Methylobacterium extorquens* AM1 enable *E. coli* mutant $\Delta serA\Delta gcvTHP$, in which the genes encoding SHMT and GDC were deleted, to substitute C1 units with the supply of external formate (Yishai et al., 2017).

In the following chapter, the gene encoding FTL from *M. extorquens* AM1 was chosen for the expression in *Synechocystis* attempting to efficiently utilize external formate through the FA pathway. The results we got proved that the introduction of FTL alone was insufficient for significant formate incorporation into the cyanobacterial biomass. Therefore, the further overexpression of an efficient alternative FoLD was achieved aiming to enable *Synechocystis*

Results

to assimilate external sodium formate into serine and stimulate its cell growth.

4.2.1 Introduction of FTL in *Synechocystis* wild-type

The codon-optimized gene *ftl* from *M. extorquens* AM1 was cloned under control of the strong light-induced promoter P_{psbA2} on the plasmid pA2 (Lagarde et al., 2000) carrying an erythromycin resistance marker gene (plasmid referred to pA2-FTL; Fig. 7A). After selection of erythromycin-resistant clones, the stable integration of *ftl* into the genome was verified by PCR, which showed expected DNA bands of 1704 bp using DNA from transformants but not from wild-type (Fig. 7B). The clones were named accordingly exFTL. Western-blotting analysis using a FTL-specific antibody verified that these clones expressed the FTL protein, whereas no cross-reaction was observed with wild-type extracts (Fig. 7C). Moreover, 10-formyl-THF ligase activity was detected in crude extracts of the exFTL strain, when incubated with formate and THF (Fig. 7D). The lysate of exFTL cells displayed higher production of methenyl-THF than that of wild-type. These data confirmed that an active FTL from *M. extorquens* AM1 was expressed in *Synechocystis*.

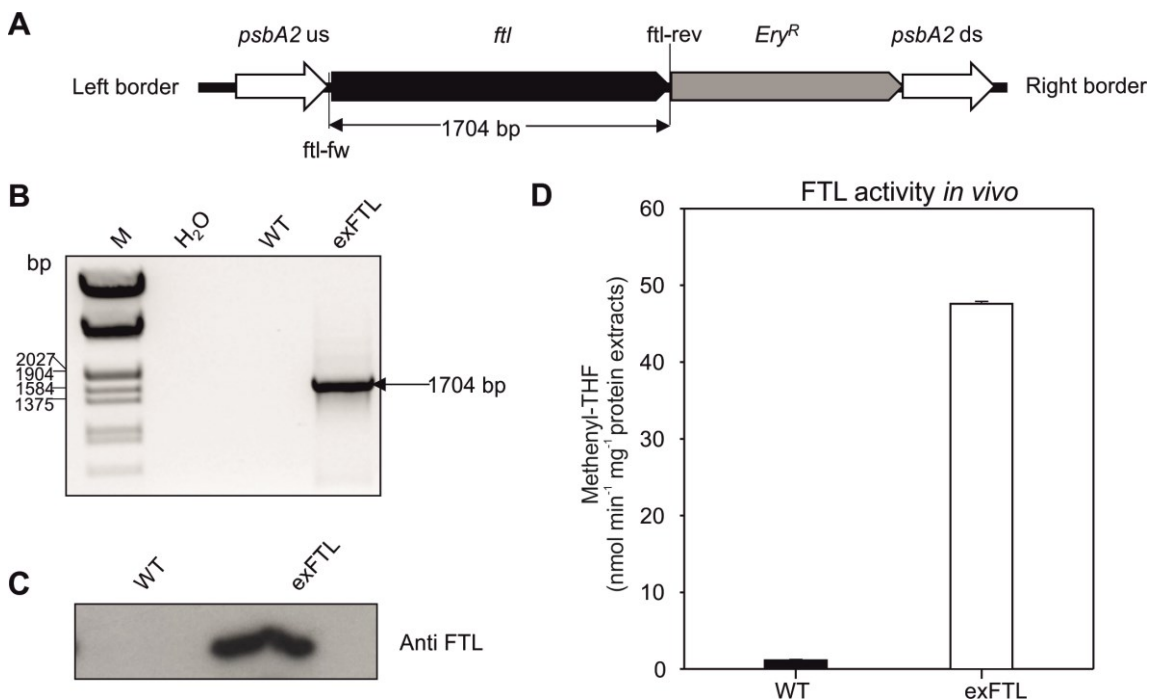


Figure 7: Schematic presentation of the FTL-expression construct and genotypic characterization of the FTL-expressing *Synechocystis* strain exFTL.

Results

A. Construct for FTL expression in *Synechocystis*. The codon-optimized gene *ftl* from *M.extorquens* AM1 was integrated into the *psbA2* site of the *Synechocystis* genome using the *psbA2* flanking sequences for homologous recombination. An erythromycin-resistance marker (Ery^R) allowed the selection of recombinant lines. **B.** Verification of the genotype by PCR using DNA from the *ftl*-expressing clone (exFTL), wild-type (WT) or not DNA (H₂O) as template and *ftl*-specific primer *ftl*-fw and *ftl*-rev. **C.** Western-blotting with an FTL-specific antibody verified the expression of FTL in exFTL but not in wild-type. 20 µg of total lysate from each strain were loaded into SDS-PAGE gel. **D.** FTL enzyme activity was compared in crude protein extracts of exFTL and WT. The activity assay is detailed described in Methods.

4.2.2 Phenotype and metabolome analysis of FTL-expressing strain exFTL

The exFTL strain showed similar growth rate after addition of 10 mM sodium formate compared to wild-type at ambient air (Fig. 8A). Interestingly, exFTL cells exhibited higher glycine tolerance in the presence of formate. This strain grew with 3 mM glycine and formate, while wild-type cannot survive on plates containing 3 mM glycine and 100 mM formate (Fig. 8D). It seems that formate and glycine have an additive toxic effect on *Synechocystis* cells, which is relieved after *ftl* expression indicating that FTL could probably alleviate the toxicity of excess formate via formate assimilation.

When the liquid BG11 medium was supplemented with formate, we observed marked difference in the metabolome of exFTL compared to wild-type cells. As expected, particularly serine and glycine levels changed. The incubation of formate resulted in nearly 3 folds higher serine levels in exFTL strain compared to wild-type, while in the absence of formate only slightly increased serine levels were found (Fig. 8B). In contrast, glycine contents were approximately 3 folds lower in exFTL with formate supplementation, whereas without formate addition only small differences appeared (Fig. 8C). The reduction of glycine in exFTL cells is consistent with its higher resistance to glycine. These results indicated that formate might be as expected incorporated into serine via FA pathway in exFTL strain resulting in the decreased pool of the precursor glycine.

Results

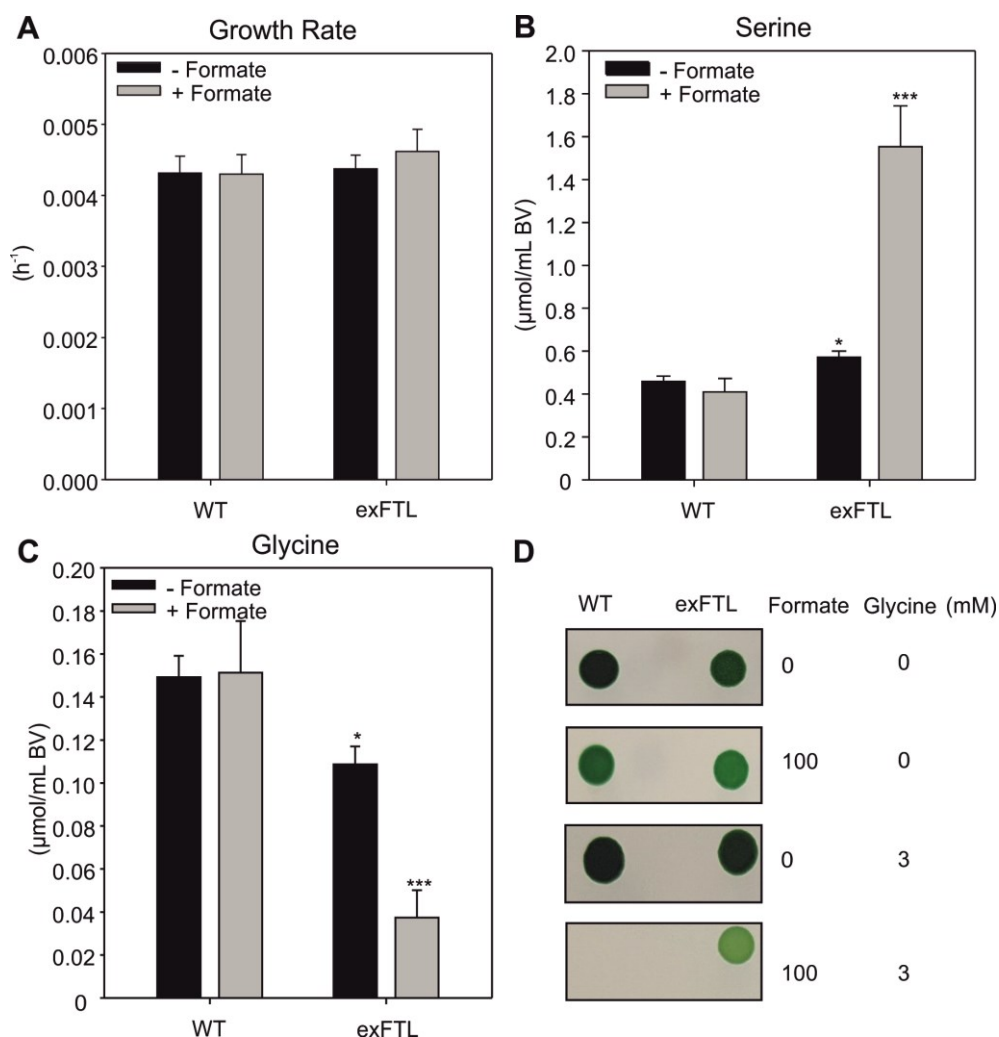


Figure 8: Growth rates and selected metabolites in the strains wild-type and exFTL.

A. Growth rates of exFTL and wild-type (WT) incubated with or without formate were compared. **B.** Resistance of WT and exFTL toward formate and glycine. The content of serine (**C**) and glycine (**D**), in WT and exFTL were measured by LC-MS/MS. Cells were cultivated under ambient air at $100 \mu\text{mol photons m}^{-2} \text{s}^{-1}$. Samples were collected 24 h after sodium formate or not incubation, respectively. Given are mean values and SE of at least three independent replicates. *: $P < 0.05$; **: $P < 0.01$; ***: $P < 0.001$.

The relative fold changes of other metabolites in cells of exFTL compared to wild-type are listed in Table 4. The samples from exFTL contained significant less 2-OG and other intermediates of the tricarboxylic acid (TCA) cycle than wild-type. Consistently, glutamate also decreased. In addition, amino acids leucine, proline and phenylalanine showed quite low level, while asparagine was higher in exFTL. With the supply of formate, histidine and methionine whose one carbon origins from 10-formyl-THF and 5, 10-methylene-THF respectively in exFTL performed marginal enhanced level. Aspartate and its derived amino acids lysine, threonine

Results

and isoleucine exhibited increase. Leucine, proline and phenylalanine also performed higher level although they were still lower than those from wild-type. Interestingly, the exFTL strain showed slight increase in the carboxylation product 3-PGA, while the oxygenase product 2-PG was slightly decreased upon incubation with formate. The highest accumulation was detected for 2-aminobutyric acid (AABA) that rose 9-fold in the presence of formate. Collectively, these metabolic changes show that FTL activity has broad impact on cellular metabolism after addition of formate.

Table 4: Metabolome analysis of strain exFTL compared to wild-type.

Relative folds	WT+F / WT	exFTL+F / exFTL	exFTL / WT	exFTL+F / WT+F
Asn	0.96±0.05	0.95±0.11	1.67±0.38	1.63±0.19
Asp	0.84±0.12	1.33±0.22	1.15±0.19	1.88±0.7
Ser	0.89±0.05	2.74±0.53	1.25±0.21	3.81±0.65
Ala	0.96±0.09	1.41±0.14	0.91±0.06	1.34±0.23
Gly	1.02±0.22	0.34±0.09	0.73±0.02	0.26±0.13
Gln	0.8±0.09	1.55±0.29	1.11±0.17	2.12±0.31
Thr	0.94±0.02	2.35±0.58	1.18±0.27	2.89±0.61
Met	1.04±0.06	1.3±0.14	0.87±0.23	1.09±0.36
Cys	0.97±0.36	1.85±0.6	1.09±0.29	2.24±1.12
Glu	0.98±0.19	0.68±0.14	0.78±0.12	0.55±0.14
Pro	1.15±0.08	1.84±0.24	0.4±0.11	0.64±0.16
Lys	0.81±0.08	1.45±0.44	1.1±0.14	1.95±0.55
His	1.3±0.25	2.54±0.66	0.76±0.19	1.47±0.32
Arg	0.8±0.17	1±0.44	1.16±0.22	1.37±0.24
Val	0.79±0.19	1.58±0.21	0.72±0.06	1.46±0.04
Ile	1.09±0.38	1.1±0.14	1.74±0.13	1.83±0.29
Leu	1.05±0.24	1.96±0.33	0.24±0.04	0.45±0.01
Phe	1.3±0.26	1.67±0.24	0.54±0.06	0.63±0.06
AABA	0.79±0.1	9.12±2.38	0.89±0.03	10.22±1.72
2-PG	1.04±0.17	0.83±0.07	1.03±0.22	0.83±0.09
3-PGA	0.97±0.19	1.32±0.21	1.08±0.12	1.48±0.3
2-OG	1.08±0.21	0.98±0.29	0.64±0.04	0.59±0.14
Malate	1.21±0.2	0.8±0.12	0.43±0.07	0.28±0.03
Isocitrate	0.86±0.1	0.71±0.11	0.65±0.01	0.54±0.08
Lactate	0.93±0.19	0.85±0.16	0.71±0.21	0.64±0.14
Citrate	0.86±0.09	0.73±0.14	0.63±0.01	0.53±0.07
Succinate	1.07±0.18	0.64±0.08	0.18±0.01	0.11±0.02

Results



Samples were collected 24 h later after either added with or without 10 mM formate. The values are normalized as relative folds and presented as means±SE from three independent biological replicates. The heatmap displays the log₂ (relative folds) on a color-scale.

4.2.3 Enhanced growth of exFTL with glycine

As mentioned above, external formate did not stimulate the growth of FTL-expressing strain exFTL. Moreover, the serine levels increased while glycine dropped by nearly 70%. These data implied that glycine might be the limiting factor for higher formate incorporation rate. Therefore, growth experiments were performed, in which the medium was supplemented with glycine together with formate to verify our hypothesis. The questions are: can glycine be efficiently taken up by *Synechocystis* and how much glycine is suitable? Amino acids uptake of cyanobacteria are proposed to be manipulated by ATP-binding cassette (ABC)-type transporters (Quintero et al., 2001; Eisenhut et al., 2007; Bualuang and Incharoensakdi, 2015). Besides, it is reported that the supply of glycine up to 10 mM significantly increased cell growth of *Aphanothece halophytica* whereas higher than 40 mM glycine caused severe growth retardation (Bualuang et al., 2015). An increase in the growth inhibition corresponded with an increase of the externally supplied glycine in the range of 0-50 mM was observed in *Synechocystis* and the application of 20 mM MgCl₂ relieved the toxicity of external glycine below 10 mM (Eisenhut et al., 2007). Furthermore, as we observed, glycine at 3 mM was found no obvious influence on wild-type and exFTL cells on the plates, whereas it was toxic to wild-type when incubated with excess formate (Fig. 8D). Hence, glycine could be taken up directly by cyanobacteria and different species have different capability to resist glycine. In our case, growth experiments of exFTL and wild-type were monitored with the addition of 3 mM glycine. In addition, 20 mM MgCl₂ was added to alleviate the toxicity of glycine to *Synechocystis* (Eisenhut et al., 2007). Consistent with our assumption, strain exFTL showed significantly higher growth rate than wild-type in the presence of both formate and glycine, whereas there was no marked growth difference when only glycine or formate was added (Fig. 9).

Results

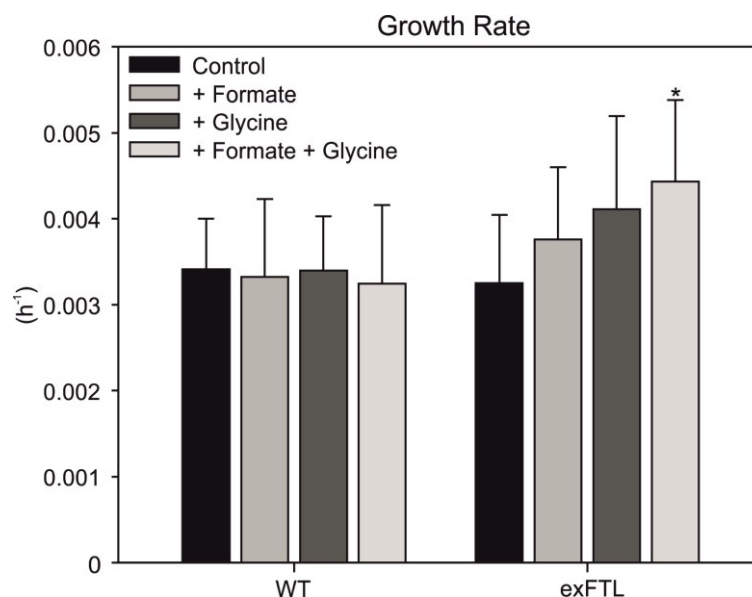


Figure 9: Growth rates of wild-type and exFTL supplied with glycine and formate.

Cells were cultivated and monitored in multi-cultivator under ambient air at $100 \mu\text{mol photons m}^{-2} \text{s}^{-1}$ in BG11 medium supplemented with formate (10 mM), glycine (3 mM) or glycine and formate. 20 mM MgCl_2 was added together to relieve the toxicity of glycine.

4.2.4 Introduction of FTL in the photorespiratory mutant

The aforementioned results indicated that glycine may limit the utilization of externally supplied formate. Therefore, strains that accumulate higher glycine levels were henceforth used for FTL expression. Glycine was accumulated by the photorespiratory triple mutant named $\Delta gcvT/\Delta tsr/\Delta odc$ (Eisenhut et al., 2008b). The mutant $\Delta gcvT/\Delta tsr/\Delta odc$ (named $\Delta 3pr$ in this thesis hereafter) is defective in all the three routes metabolizing 2-PG, which is realized by the inactivation of *odc* encoding the oxalate decarboxylase involved in the decarboxylation branch, *gcvT* encoding the T-protein of glycine decarboxylase in the plant-like C2 cycle, and *tsr* encoding the tartronic semialdehyde reductase in the glycerate pathway.

4.2.4.1 Generation of exFTL/ $\Delta 3pr$ strain and phenotype characterization

Plasmid pA2-FTL was transformed into the photorespiratory triple mutant $\Delta 3pr$. PCR analysis verified that the gene *ftl* was integrated into genome of the strain exFTL/ $\Delta 3pr$ and all the wild-type copies of the *gcvT*, *tsr* and *odc* genes were still inactivated (Fig. 10A). Western-blotting analysis confirmed that strain exFTL/ $\Delta 3pr$ expressed protein FTL successfully (Fig. 10B). $\Delta 3pr$

Results

exhibited higher sensitive to formate probably because of its higher glycine content, since the previous result already implied that glycine and formate had an additive toxic effect on cells (Fig. 8D). The exFTL/ $\Delta 3pr$ cells grew in the medium supplied with 150 mM formate, while mutant $\Delta 3pr$ cannot survive under the same condition (Fig. 10C). This result implied that higher content of formate was detoxified due to the expression of FTL in the new strain exFTL/ $\Delta 3pr$. The strain exFTL/ $\Delta 3pr$ cells showed significantly faster growth than mutant $\Delta 3pr$, however this enhancement did not depend on the addition of external formate (Fig. 10D).

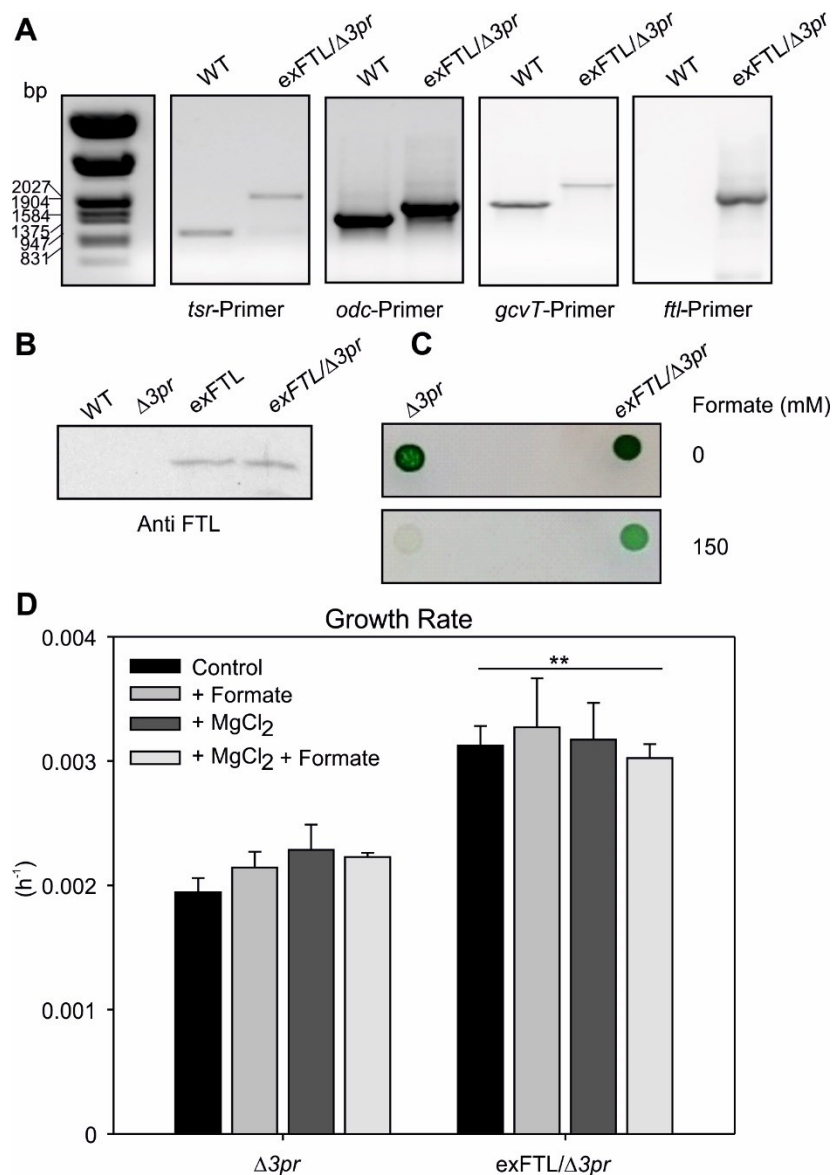


Figure 10: Genotypic and phenotypic characterization of the strain exFTL/ $\Delta 3pr$.

A. Verification of the genotype by PCR using DNA from WT and strain exFTL/ $\Delta 3pr$ with specific primers described in materials and methods. **B.** Western-blotting with the FTL-specific antibody verified the

Results

expression of FTL in the strain *exFTL/Δ3pr*. **C.** Resistance of $\Delta 3pr$ and *exFTL/Δ3pr* toward formate. Strains were plated on BG11 agar plates, pH 8, supplied with different amounts of formate incubated under continuous illumination of $30 \mu\text{mol}$ of photons $\text{m}^{-2} \text{s}^{-1}$ at $30 \text{ }^\circ\text{C}$ and ambient air for 7 d. **D.** Growth rates of $\Delta 3pr$ and *exFTL/Δ3pr* were monitored as an increase of $\text{OD}_{720 \text{ nm}}$ in BG11 medium supplied with either 10 mM formate, 20 mM MgCl_2 or both over time. Cells were cultivated in the multi-cultivator under $100 \mu\text{mol}$ of photons $\text{m}^{-2} \text{s}^{-1}$, $30 \text{ }^\circ\text{C}$ bubbling with ambient air.

4.2.4.2 Metabolites analysis with *exFTL/Δ3pr* strain

Serine and glycine concentration were further analyzed. The supply of formate did not change serine level in *exFTL/Δ3pr*, which remained significantly lowered (approximately 80%) than that of wild-type (Fig. 11A). Additionally, *exFTL/Δ3pr* showed similar content of serine with $\Delta 3pr$ mutant. Glycine showed a slight decrease in *exFTL/Δ3pr* after incubation with formate, but it still presented at quite high levels pointing at almost not stimulated consumption of glycine (Fig. 11B). Other amino acids and TCA cycle associated organic acids did not show significant changes (data not shown). These results supposed that formate did not contribute to larger extent toward the production of serine in *exFTL/Δ3pr* strain, which is contrary to the previous accumulation of serine observed in *exFTL* strain.

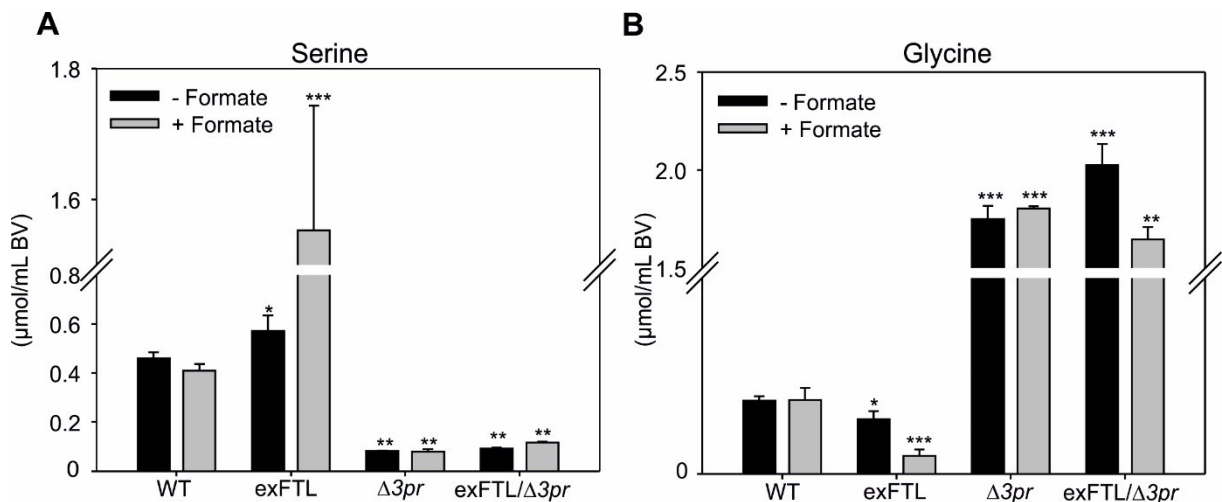


Figure 11: Serine and glycine were compared between wild-type, photorespiratory mutant and FTL-expressing strains.

The content of serine (A) and glycine (B), in WT, *exFTL*, $\Delta 3pr$ and *exFTL/Δ3pr* were evaluated. Cells were cultivated under ambient air at $100 \mu\text{mol}$ photons $\text{m}^{-2} \text{s}^{-1}$. Samples were collected 24 h either with or without 10 mM formate, respectively. Given are mean values and SE of at least three replicates. *: $P < 0.05$; **: $P < 0.01$; ***: $P < 0.001$.

Results

4.2.5 Attempt to improve formate assimilation by expression of SGAT

In addition to enhance the glycine pool, another bottleneck to achieve higher growth in exFTL might be limited serine utilization. To this end, we aimed to increase its conversion rate to hydroxypyruvate via the enzyme SGAT that converts serine and glyoxylate to glycine and hydroxypyruvate. Hence, a new strain exFTL-SGAT was built attempting to improve the formate assimilation flux via serine into 3-PGA.

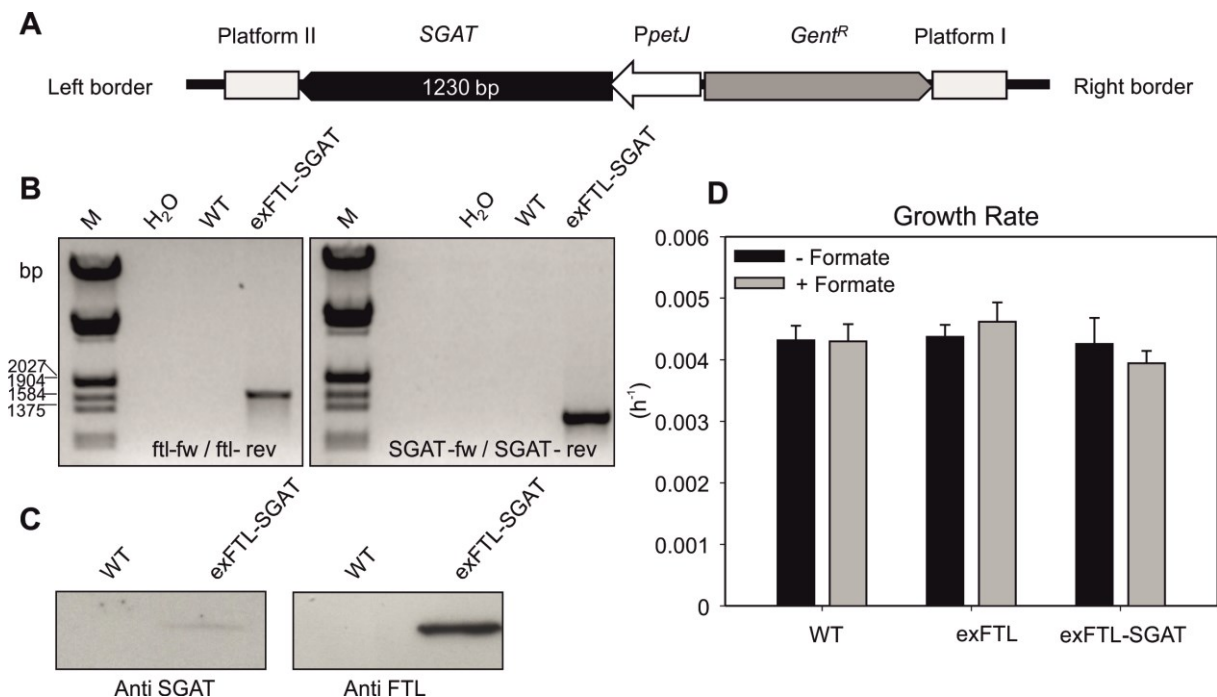


Figure 12: Schematic presentation and phenotypic characterization of the strain exFTL-SGAT.

A. Construct for SGAT expression in *Synechocystis*. The codon-optimized gene *SGAT* from *Arabidopsis thaliana* was integrated into the neutral site of the *Synechocystis* genome. A gentamycin-resistance marker (*Gent^R*) was allowed for the selection of recombinant lines. **B.** Verification of the genotype by PCR using DNA from the *ftl* and *SGAT*-expressing clone (exFTL-SGAT), wild-type (WT) or no DNA (H₂O) as template and *ftl*-specific primer and *SGAT*-specific primer. M: DNA marker; WT: wild-type. **C.** Western blotting with *SGAT*-specific or *FTL*-specific antibodies verified the protein expression in the strain exFTL-SGAT. Cells were cultivated in the copper-free BG11. 20 μ g of total lysate from each strain were loaded into SDS-PAGE gel. The blotting membrane was probed firstly with *SGAT*-specific antibody to detect *SGAT*. After stripping, *FTL*-specific antibody was used to detect *FTL*. **D.** Growth rates of WT, exFTL and exFTL-SGAT were monitored as increase in OD_{720 nm} over time in BG11 medium free of copper supplied with or without 10 mM formate. Cells were cultivated in the multi-cultivator at 100 μ mol photons m⁻² s⁻¹ and bubbling with ambient air.

Results

The coding region of gene *SGAT* (AT2G13360) from *Arabidopsis thaliana* was cloned into the cyanobacterial expression vector pSK9 under the control of promoter *PpetJ* and integrated into the neutral site of the genome in *Synechocystis* (Fig. 12A). The recombinant strains were verified by PCR, which displayed the expected DNA fragment of 1230 bp (Fig. 12B). The *petJ* promoter is suppressed by copper in the medium. Hence, cells of exFTL-SGAT were cultivated in copper-free medium to achieve high expression of protein SGAT (44 kDa), which was confirmed by Western-blotting analysis (Fig. 12C). However, we did not observe any stimulation on the growth of strain exFTL-SGAT by formate (Fig. 12D).

4.2.6 Labeling pattern of proteinogenic amino acids

To verify whether externally supplied formate is incorporated into cellular biomass, the ¹³C-labeling pattern of proteinogenic amino acids was evaluated in cells grown in the presence of ¹³C-labeled formate. The amino acids methionine, histidine, glycine and serine were particularly analyzed to elucidate whether the C1-dependent building blocks produced from formate in exFTL strain can be traced in these target amino acids. We speculated that most methionine in exFTL will be labeled once because its methyl group comes from 5-methyl-THF. 5-Methyl-THF serves its methyl group for the methylation of homocysteine to produce methionine, which can be adenylated to form S-adenosyl-methionine (Ferla and Patrick, 2014). The same result was expected with histidine, since one carbon of it is originated from 10-formyl-THF. In addition, a small portion of serine will be labeled when it is produced from glycine and formate converted 5, 10-methylene-THF, while glycine was not expected to be labeled. Samples were harvested 5 days after incubated either with 10 mM unlabeled or ¹³C-labeled formate. Protein was hydrolyzed and used for labeling pattern analysis. As Fig. 13A shows, glycine was unlabeled, which was in consistence with our assumption. Serine was also completely unlabeled in wild-type and exFTL cells pointing against incorporation of formate into this expected amino acid (Fig. 13B). Methionine was only slightly labeled, around 1.5% of methionine in exFTL was labeled than wild-type (Fig. 13C). Histidine presented the same nominal labeled pattern as methionine in exFTL (Fig. 13D).

Results

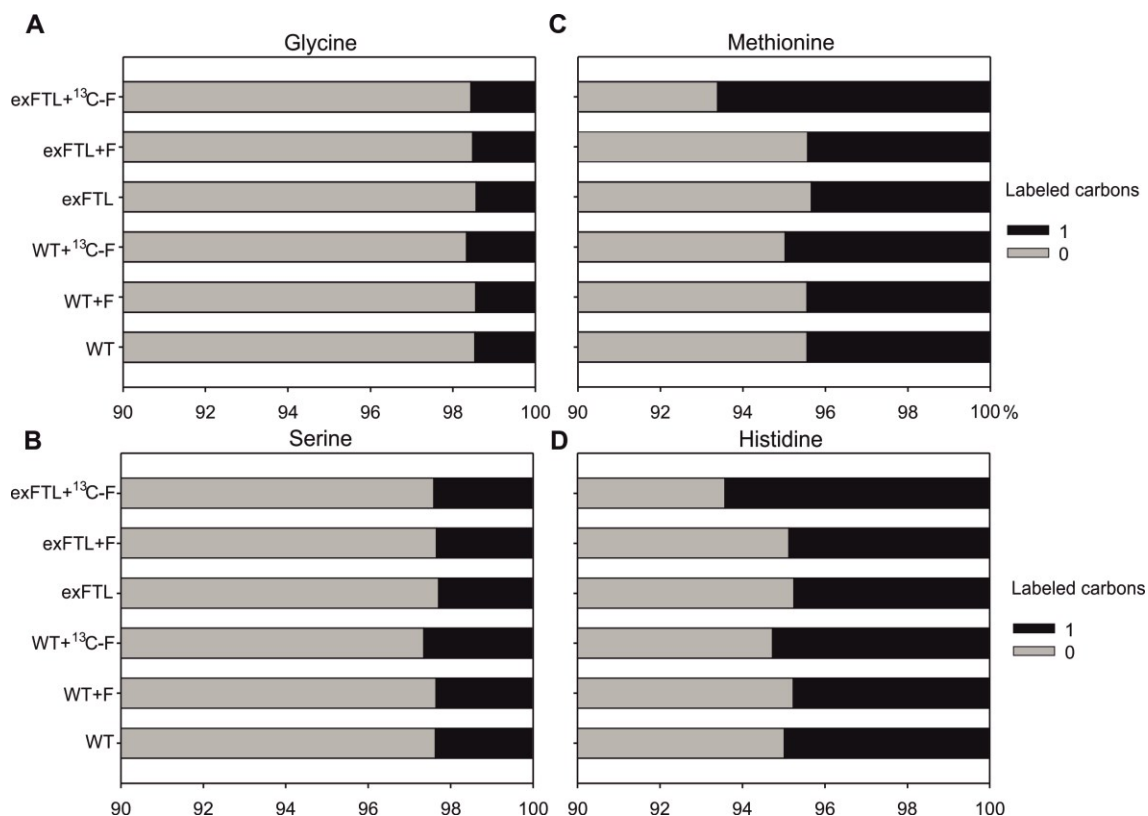


Figure 13: Labeling pattern of proteinogenic glycine, serine, methionine and histidine were compared between wild-type and exFTL.

Wild-type (WT) and exFTL cells were fed without, with either unlabeled or ^{13}C -labeled formate for 5 d under ambient air at $100 \mu\text{mol photons m}^{-2} \text{s}^{-1}$.

4.2.7 Attempt to improve FA pathway by overexpression of FOLD in wild-type

These ^{13}C -formate-labeling results indicated that a rather small amount of C1 units derived from formate was used for methionine and histidine synthesis, but it was not at all used for serine synthesis. These results indicated that the endogenous FOLD might be the limiting factor for the assimilation of formate to serine. It is reported that FOLD protein activity is often inhibited by 10-formyl-THF (Dev and Harvey, 1978). To overcome this problem, another FOLD protein from *M. extorquens* AM1 was expressed in *Synechocystis*. In *M. extorquens* AM1 the FOLD enzyme is separated on the two proteins FchA and MtdA, which catalyze the conversion from 10-formyl-THF to 5, 10-methenyl-THF and 5, 10-methenyl-THF reduced to 5, 10-methylene-THF, respectively. Furthermore, these enzymes are known to work preferentially in the direction of methylene-THF synthesis. Correspondingly, the expression of proteins FTL, FchA

Results

and MtdA from *M. extorquens* AM1 enabled *E. coli* to supply all its glycine and serine from formate and CO₂ through the reductive glycine pathway and the synthesized C1 compounds were able to provide 10% of the biomass carbon (Yishai et al., 2018). Hence the overexpression of this efficient FOLD from *M. extorquens* AM1 should pave the way for formate assimilation through FA pathway.

4.2.7.1 Construction of the FchA-MtdA expressing vector allowing regulation of their translation

Codon-optimized versions of the two genes *fchA* (UniProt Q49135) and *mtdA* (UniProt P55818) were synthesized. Each gene was fused with a ribosome-binding site and the two genes were put in one operon under the control of the constitutive promoter P_{conII} . Furthermore, an engineered theophylline-dependent riboswitch (Ma et al., 2014) was introduced to control the translation initiation of FchA, which will allow to switch protein expression on and off by adding or removing theophylline. His-extensions (His-tag) were added to the N-terminal of both FchA and MtdA protein for easier characterization of protein expression. The entire construct was cloned into the autonomous plasmid pVZ322 leading to the recombinant plasmid pVZ-fchA-mtdA (Fig.14A). The plasmid was transferred via conjugation into the strains exFTL. The genotype of transformants were characterized with specific primers as shown in Fig. 14B and 14C. The correct clone was named exF-C-M.

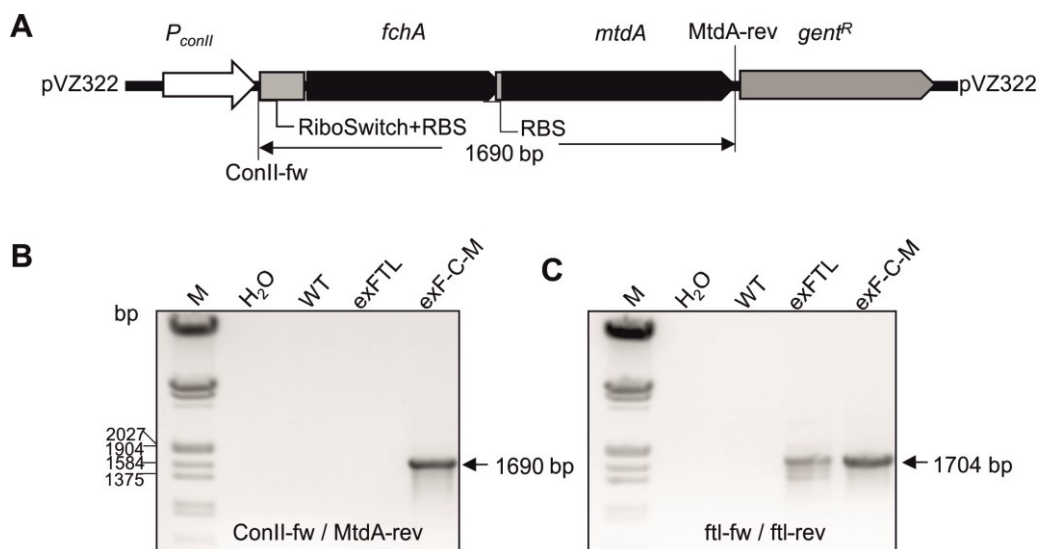


Figure 14: Schematic presentation of the FchA-MtdA-expression construct and genotypic characterization of the *Synechocystis* strain exF-C-M.

Results

A. Construct for Fch-MtdA expression in *Synechocystis*. The codon-optimized genes *fchA* and *mtdA* from *M. extorquens* AM1 were cloned in the autonomous plasmid pVZ322. **B** and **C.** Verification of the genotype by PCR using DNA from the *ftl*-expressing clone (exFTL), wild-type (WT) and transformant exF-C-M as template with *mtdA*-specific primer and *ftl*-specific primer, respectively.

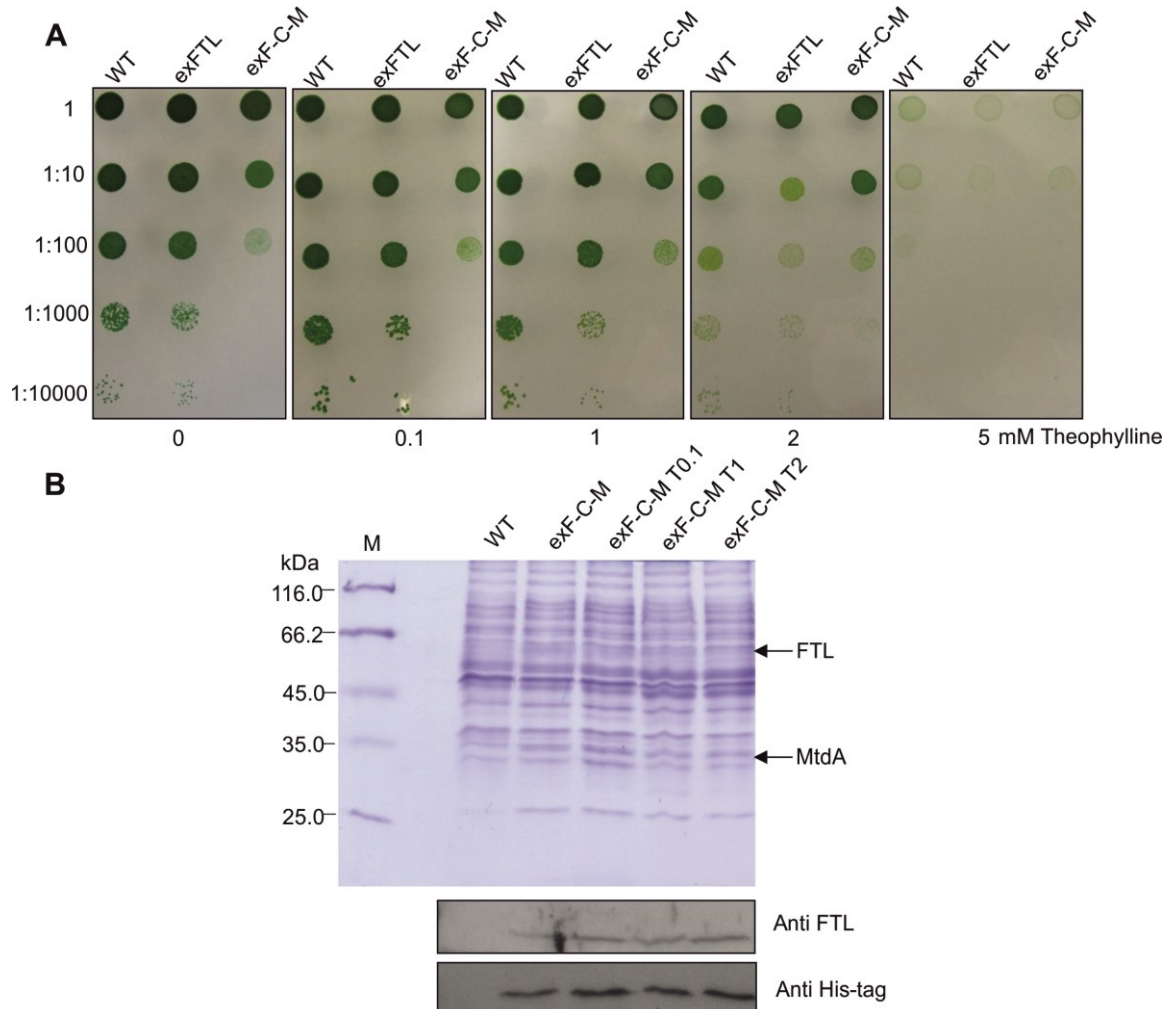


Figure 15: Theophylline sensitivity and protein expression of wild-type, exFTL and exF-C-M.

A. Serial dilution of cells ($OD_{750\text{ nm}} = 1$) were dropped on BG11 agar plates, pH 8, supplemented with various concentrations of theophylline (0-5 mM) for 7 d at ambient air condition. **B.** Western-blotting with FTL-specific antibody and His-tag antibody verified the expression of FTL and MtdA in exF-C-M but not in WT. Strain exF-C-M was induced with different concentrations of theophylline: T0.1, 0.1 mM; T1, 1 mM; T2, 2 mM.

The translation of FchA was induced by addition of different concentrations of theophylline in the medium. To determine the applicable range of theophylline concentration in *Synechocystis*, we examined the tolerance of cells to various concentrations of theophylline (Fig. 15A). We observed significant growth retardation of *Synechocystis* on the plates supplemented with

Results

≥ 2 mM theophylline. The expression of introduced proteins was analyzed by Western-blotting. FTL proteins were successfully expressed in exF-C-M strain using FTL-specific antibody and the expression of MtdA with size of approximately 30 kDa was confirmed with His-tag antibody (Fig. 15B), while no evidence of expression of FchA protein with size of about 21 kDa was obtained under the induction of different concentrations of theophylline (0-2 mM) (data not shown). Considering the toxicity of high content of theophylline to *Synechocystis* cells and similar expression level of FTL and MtdA under different induced conditions (Fig. 15B), 0.1 mM theophylline was chosen as the concentration used in the further experiments in this study.

4.2.7.2 Phenotype and metabolome analysis of exF-C-M

The overexpression of MtdA, was obviously harmful to cells, which is concluded from the retarded growth of the strain exF-C-M strain compared to only FTL-expressing strain exFTL when spotted on agar plates (Fig. 16A) or cultivated in liquid media (Fig. 16B). As shown, the supplement of formate to the media clearly rescued the growth of exF-C-M strain indicating that the rewiring of one-carbon metabolism made *Synechocystis* more dependent on formate.

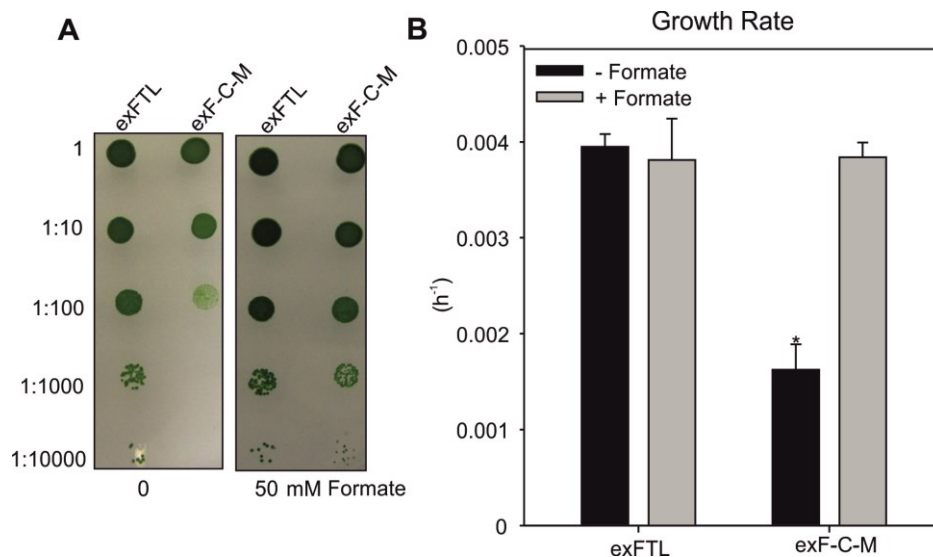


Figure 16: Phenotype characterization of wild-type, exFTL and exF-C-M.

A. Resistance of exFTL and exF-C-M toward formate. Serial dilution of cells ($OD_{750\text{ nm}} = 1$) were dropped on BG11 agar plates, pH 8, supplemented with 0.1 mM theophylline and formate (0 and 50 mM) for 7 d. **B.** Growth rate of cells was measured supplied either with or without 10 mM sodium formate. The medium of exF-C-M was added with 0.1 mM theophylline. Cells were grown in liquid BG11 in the multi-cultivator at ambient air under $100\ \mu\text{mol photons m}^{-2}\ \text{s}^{-1}$.

Results

Considering CO₂ is preferred than formate as the inorganic carbon source, a CO₂ limiting environment was built to examine whether external formate had an additive stimulation on the growth in exF-C-M strain. The CO₂ in the air was removed through the irreversible reaction with barium hydroxide to produce insoluble barium carbonate. The left air with less CO₂ was used to bubble cells. Cells grew much slower under this condition, however, the supply of formate did not enhance their growth (Fig. 17).

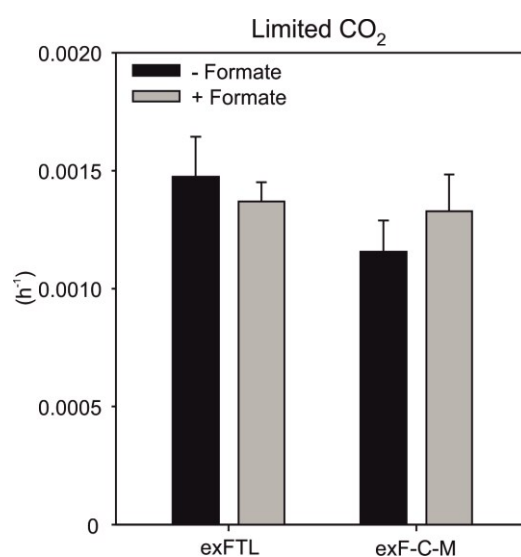


Figure 17: Growth of exFTL and exF-C-M strain under CO₂-limiting condition.

Growth rate of cells was measured supplied either with or without 10 mM formate. The medium of exF-C-M contained 0.1 mM theophylline. Cells were grown in liquid BG11 in the multi-cultivator with CO₂-depleted air and 100 μmol photons m⁻² s⁻¹ condition.

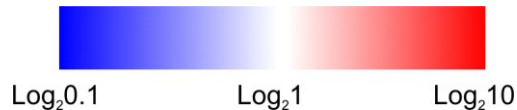
The relative fold changes of internal metabolites in cells of exF-C-M compared to exFTL are listed in Table 5. The samples from exF-C-M contained relative higher amino acids except glutamate and histidine. Among them, lysine and arginine enhanced around 4-fold. Less malate, lactate and succinate were also detected. When supplemented with formate, most amino acids including serine and glycine showed declined level in exF-C-M. On the contrary, glutamate rose to approximately 2-fold and TCA cycle related organic acids increased to some extent. The content of 2-PG decreased and 3-PGA increased in formate inoculated exF-C-M. Intriguingly, citrate and isocitrate in exF-C-M displayed more than 3-fold higher than exFTL after incubation with formate. Additionally, when formate was supplied, the unexpected higher content of AABA observed in exFTL was not found in exF-C-M. Oppositely, the level of AABA

Results

decreased in the latter strain added with formate.

Table 5: Metabolome analysis of strain exF-C-M compared to exFTL.

Relative folds	exF-C-M / exFTL	(exF-C-M+F) / exF-C-M	(exF-C-M+F) / (exFTL+F)
Asn	1.53±0.16	0.85±0.1	0.85±0.1
Asp	1.77±0.17	0.52±0.08	1.3±0.03
Ser	1.24±0.07	0.62±0.05	0.62±0.05
Ala	2.12±0.24	0.84±0.17	2.18±0.07
Gly	1.38±0.17	0.84±0.3	1.87±0.14
Gln	2.13±0.07	0.67±0.1	1.43±0.05
Thr	1.26±0.07	0.77±0.06	0.9±0.05
Glu	0.44±0.03	2.02±0.06	0.98±0.13
Pro	2.07±0.35	0.87±0.15	1.61±0.08
Lys	4.58±0.28	0.62±0.22	2.78±0.05
His	0.66±0.05	0.73±0.08	0.53±0.11
Arg	3.81±0.28	0.89±0.25	3.32±0.07
Val	1.59±0.11	0.75±0.13	1.79±0.06
Met	1.7±0.08	0.86±0.15	1.61±0.08
Tyr	1.43±0.14	0.78±0.12	1.09±0.08
Ile	1.86±0.18	0.69±0.11	1.42±0.05
Leu	1.27±0.04	0.97±0.08	1.42±0.06
Phe	1.53±0.18	1.03±0.09	1.44±0.07
Trp	1.91±0.23	0.74±0.16	1.47±0.08
AABA	1±0.28	0.58±0.02	0.07±0.16
2-PG	0.79±0.22	0.75±0.09	0.64±0.07
3-PGA	1.14±0.03	1.32±0.08	1.01±0.1
2-OG	1.17±0.08	1.12±0.09	1.39±0.07
Malate	0.73±0.12	1.18±0.04	0.57±0.09
Isocitrate	1.08±0.08	1.37±0.33	3.67±0.12
Lactate	0.52±0.06	1.29±0.1	0.65±0.19
Citrate	1.11±0.08	1.39±0.39	3.86±0.14
Succinate	0.67±0.06	1.15±0.06	0.52±0.13



Cells were grown in liquid BG11 in the multi-cultivator at ambient air under 100 $\mu\text{mol photons m}^{-2} \text{s}^{-1}$. Samples were collected 24 h later after either added with 10 mM formate or not. The medium of exF-C-M was added with 0.1 mM theophylline. The values are normalized as relative folds and presented as means±SE from two independent biological replicates. The heatmap displays the log₂ (relative folds) on a color-scale.

4.3 Establishing FA pathway in $\Delta ccmM$ mutant

Mutant $\Delta ccmM$ harbours a deletion of gene *sll1031*, which encodes the carboxysomal structural protein CcmM. Hence, the mutant cannot form carboxysomes, which resulted in a high CO₂-requiring phenotype, i.e. this mutant is unable to grow under ambient air conditions (Hackenberg et al., 2012). The enhanced oxygenase activity of Rubisco and the increased flux into the photorespiratory pathway in $\Delta ccmM$ make this strain more similar to the plant situation and it is hypothesized that generated formate assimilation rate could reduce its CO₂ dependence.

4.3.1 Introduction of FTL in $\Delta ccmM$

The gene *ccmM* (*sll1031*) was inactivated through interposon-mutagenesis (Fig. 18A). The kanamycin resistance gene was obtained from pUC4K after *Hinc* II digestion. The *ccmM* gene and its flanking sequence (2799 bp) were obtained from DNA of the *Synechocystis* wild-type (WT) via PCR using gene specific primers. The mutant plasmid was constructed, where the kanamycin resistance cassette interrupted gene *ccmM* (2242 bp) after deleting the internal part flanked by *Dra*I and *Hpa*I sites. After selection of resistant colonies, the genotype of the obtained clones was checked with PCR (Fig. 18B). Then the plasmid PA2-FTL was transformed into mutant $\Delta ccmM$. PCR analysis verified that the gene *ftl* was integrated into genome of the new strain $\Delta ccmM/exFTL$ (Fig. 18B). Western-blotting analysis confirmed that strain $\Delta ccmM/exFTL$ expressed protein FTL successfully (Fig. 18B). Due to the high CO₂-requiring phenotype, the cultivation of mutant $\Delta ccmM$ was always done at 5% CO₂ as standard high carbon condition. Considering our aim that the assimilation of formate will support CO₂ fixation and reduce photorespiration, we assumed that the successful expression of the FA pathway can reduce the CO₂ requirement significantly lower than 5% CO₂. Hence the strains in the $\Delta ccmM$ background were cultivated under stepwise reduced CO₂ conditions to test whether formate can support the growth of $\Delta ccmM/exFTL$ at relative carbon-limiting environment. For this purpose, the starting concentration of CO₂ was set to 0.8%. After an initial growth phase, the CO₂ concentration was stepwise reduced to 0.7%, 0.6% until 0.3%

Results

every second day. As shown in Fig. 18C, $\Delta ccmM/exFTL$ strain extended the lag phase at the beginning. However, during the stepwise reduced CO₂ condition, the FTL-expressing mutant cells still showed growth at 0.4 and even 0.3% CO₂, where the parental mutant $\Delta ccmM$ already stopped growth. Unfortunately, the supplement of formate did not stimulate the growth of $\Delta ccmM/exFTL$. An interesting phenomenon was that $\Delta ccmM$ and $\Delta ccmM/exFTL$ cells died in the growth experiments when the starting concentration of CO₂ was set to 0.6%, implying 0.8% CO₂ might be the lowest concentration for the survive of $\Delta ccmM$.

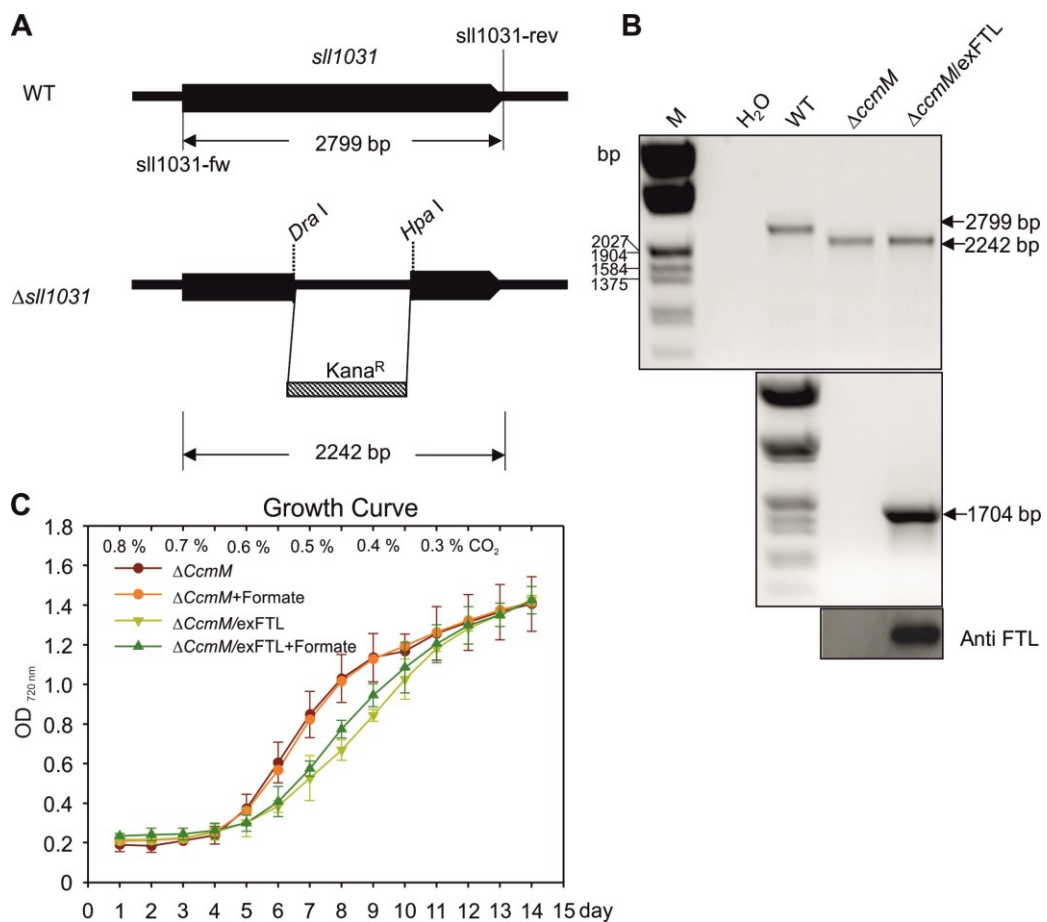


Figure 18: Genotypic and phenotypic characterization of the strain $\Delta ccmM/exFTL$.

A. Schematic presentation of construct for deletion of gene *ccmM* in *Synechocystis*. Oligonucleotides *sll1031-fw* and *sll1031-rev* flanking the insertion site were used to test the segregation. **B.** Verification of the genotype by PCR using DNA from wild-type (WT), mutant $\Delta ccmM$, and $\Delta ccmM/exFTL$ as template with *sll1031*-specific primer and *ftl*-specific primer, respectively. Western-blotting with an FTL-specific antibody verified the expression of FTL in $\Delta ccmM/exFTL$ but not in $\Delta ccmM$. **C.** Growth curves of $\Delta ccmM$ (circle) and $\Delta ccmM/exFTL$ (triangle) were monitored as an increase of OD_{720 nm} either supplied with 10 mM formate or not under constant light 100 $\mu\text{mol photons m}^{-2} \text{s}^{-1}$ and stepwise reduced CO₂ condition (0.8%-0.3% CO₂) in multi-cultivator.

Results

Table 6: Metabolome analysis of strain $\Delta ccmM$ /exFTL and $\Delta ccmM$.

Relative folds	$(\Delta ccmM+F) / \Delta ccmM$	$(\Delta ccmM / \text{exFTL}+F) / (\Delta ccmM / \text{exFTL})$	$(\Delta ccmM / \text{exFTL}) / (\Delta ccmM)$	$(\Delta ccmM/\text{exFTL}+F) / (\Delta ccmM +F)$
Asn	1.02±0.14	1.05±0.17	0.46±0.06	0.5±0.17
Asp	0.66±0.07	0.94±0.09	0.47±0.03	0.68±0.14
Ser	1.03±0.16	0.78±0.08	0.88±0.05	0.69±0.15
Ala	0.99±0.15	1.39±0.03	0.5±0.04	0.71±0.07
Gly	1.03±0.11	0.79±0.07	0.63±0.05	0.49±0.07
Gln	1.22±0.06	2.02±0.1	1.26±0.14	2.09±0.17
Thr	1.13±0.05	1.08±0.06	1.05±0.12	1±0.1
Glu	1.15±0.1	0.59±0.06	0.6±0.02	0.33±0.06
Pro	0.98±0.04	1.07±0.07	0.39±0.02	0.43±0.04
Lys	1.22±0.01	1.11±0.03	2.24±0.14	2.04±0.08
His	0.98±0.09	0.9±0.09	1.67±0.02	1.54±0.16
Arg	0.91±0.13	1.33±0.05	1.75±0.06	2.58±0.31
Val	0.89±0.26	0.92±0.05	1.52±0.07	1.66±0.42
Met	1.07±0.17	0.91±0.04	1.31±0.11	1.16±0.3
Tyr	0.73±0.22	1.12±0.04	2.76±0.33	4.47±1.12
Ile	0.85±0.2	0.93±0.05	0.24±0.02	0.27±0.06
Leu	0.76±0.27	0.95±0.04	0.92±0.08	1.26±0.36
Phe	0.92±0.09	0.93±0.1	0.43±0.05	0.43±0.03
Trp	0.93±0.06	0.96±0.06	1.52±0.16	1.57±0.19
AABA	0.72±0.07	0.99±0.05	1.05±0.14	1.29±0.24
2-PG	0.96±0.09	0.84±0.06	1.04±0.08	0.84±0.06
3-PGA	0.75±0.07	0.43±0.05	0.84±0.15	0.47±0.11
2-OG	1.07±0.29	0.71±0.09	1.44±0.16	1.04±0.38
Malate	1.3±0.19	0.89±0.14	1.22±0.11	0.84±0.18
Isocitrate	0.67±0.16	0.58±0.06	0.97±0.37	0.9±0.43
Lactate	1.07±0.08	0.92±0.17	0.88±0.12	0.76±0.21
Citrate	0.67±0.16	0.67±0.05	0.99±0.39	1.09±0.58
Succinate	1.63±0.29	0.96±0.15	0.49±0.05	0.29±0.07



Samples were collected 24 h later after either added with 10 mM formate or not. The values are normalized as relative folds and presented as means±SE from two independent biological replicates. The heatmap displays the log₂ (relative folds) on a color-scale.

Results

The internal metabolites from $\Delta ccmM$ did not display huge difference compared to those inoculated with formate (as shown in Table 6). In contrast, many cellular metabolites showed alterations in $\Delta ccmM/exFTL$ in comparison with $\Delta ccmM$. Strain $\Delta ccmM/exFTL$ displayed enhanced glutamine, lysine, histidine, arginine, valine, tyrosine and leucine to different extent, while glutamate and other amino acids and TCA cycle related organic acids presented lower level compared to $\Delta ccmM$. Among them, tyrosine exhibited the highest increase (approximately 2.5 folds), whereby isoleucine decreased about 70%. After supplemented with formate, the most intriguingly changes were the increased content of glutamine and decreased glutamate in $\Delta ccmM/exFTL$, similar with those observed with exFTL. The same changes as those in exFTL were also detected in TCA cycle related intermediates. Different with exFTL, the significant increase of serine level and decrease of glycine were not observed with formate inoculated $\Delta ccmM/exFTL$. The unexpected high content of AABA in exFTL also did not appear in $\Delta ccmM/exFTL$ when added with formate.

4.3.2 Introduction of FTL and MtdA in $\Delta ccmM$

The recombinant plasmid pVZ-fchA-mtdA was also transferred into $\Delta ccmM/exFTL$ to establish FA pathway. PCR analysis verified that the genes *fchA* and *mtdA* were transferred into the strain $\Delta ccmM/exFTL$ (Fig. 19A). The gene *ccmM* was still inactivated and gene *ftl* was still integrated into the genome of new strain $\Delta ccmM/exF-C-M$. Western-blotting analysis confirmed that strain $\Delta ccmM/exFTL$ expressed protein FTL and MtdA successfully (Fig. 19A). But as same to exF-C-M, FchA was not expressed (data not shown). To compare the growth of $\Delta ccmM/exF-C-M$ and $\Delta ccmM/exFTL$, the starting concentration of CO₂ was set to 0.8%. After an initial growth phase, the CO₂ concentration was stepwise reduced to 0.7%, 0.6% until 0.5% every second day. As Fig. 19B shows, formate did not affect the growth of $\Delta ccmM/exFTL$. Supplemented with 0.1 mM theophylline, $\Delta ccmM/exF-C-M$ without formate grew much slower, whereas the addition of formate enabled it to recover as $\Delta ccmM/exFTL$.

Results

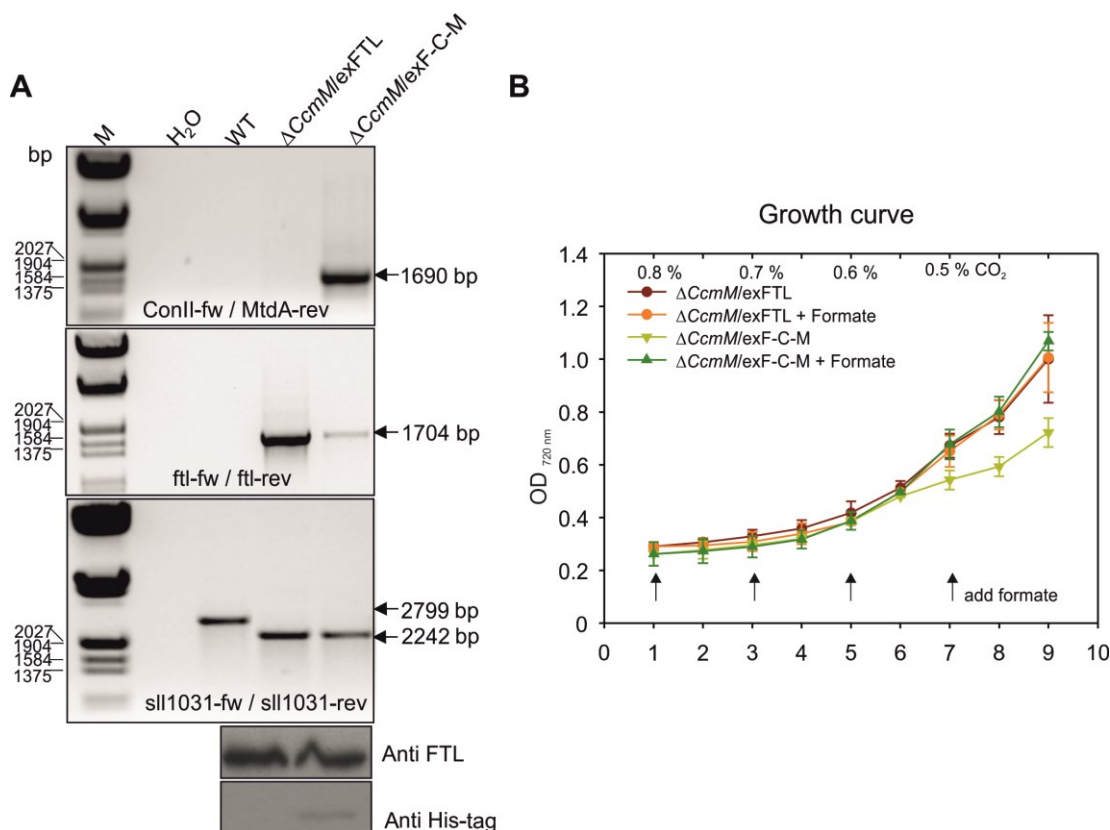


Figure 19: Genotypic and phenotypic characterization of the strain Δ *ccmM*/exF-C-M.

A. Verification of the genotype by PCR using DNA from wild-type (WT), Δ *ccmM*/exFTL and Δ *ccmM*/exF-C-M as template with *sll1031*-specific primer, *ftl*-specific primer and *mtdA*-specific primer, respectively. Western-blotting with an FTL-specific antibody verified the expression of FTL in both Δ *ccmM*/exF-C-M and Δ *ccmM*/exFTL, while MtdA was only expressed in Δ *ccmM*/exF-C-M using His-tag antibody. **B.** Growth curves of Δ *ccmM*/exFTL (circle) and Δ *ccmM*/exF-C-M (triangle) were monitored as an increase of OD_{720 nm}. Formate was added into the medium per 2 day. The medium of Δ *ccmM*/exF-C-M was supplemented with 0.1 mM theophylline. Cells were grown at stepwise decreased CO₂ conditions in liquid BG11 medium with continuous light of 100 μ mol photons m⁻² s⁻¹.

The internal metabolite pools were compared subsequently. Samples were collected at the fifth day and the seventh day, at the latter time point the cultures started to show growth differences (Fig. 19B). The intermediates with clear and interesting changes are listed in Table 7 and 8. Compared to Δ *ccmM*/exFTL, the strain Δ *ccmM*/exF-C-M showed lower contents of organic acids whereas higher levels of most amino acids were observed (Table 7). Among them, glutamine increased more significantly with time (Table 7 and 8). Under formate supplementation, the most prominent changes were measured in the glutamine and glutamate amounts in Δ *ccmM*/exF-C-M, which decreased nearly by 60% and increased around 65%, respectively, in samples collected at the fifth day (Table 7). In samples from day 7 the difference

Results

of glutamine increased to over 100% in formate-supplemented cells of $\Delta ccmM/exF-C-M$ (Table 8). Additionally, the levels of TCA cycle intermediates increased approximately 65 - 90% with time. Finally, these compounds accumulated approximately 3 times in strain $\Delta ccmM/exF-C-M$ compared to $\Delta ccmM/exFTL$. In addition, 3-PGA showed slightly increased content, while 2-PG displayed marginal decreased level in $\Delta ccmM/exF-C-M$ cells with formate.

Table 7: Metabolome analysis of strain $\Delta ccmM/exFTL$ and $\Delta ccmM/exF-C-M$ at day 5.

Day 5	$(\Delta CcmM/exFTL+F)$ / $(\Delta CcmM/exFTL)$	$(\Delta CcmM/exF-C-M+F)$ / $(\Delta CcmM/exF-C-M)$	$(\Delta CcmM/exF-C-M)$ / $(\Delta CcmM/exFTL)$	$(\Delta CcmM/exF-C-M+F)$ / $(\Delta CcmM/exFTL+F)$
Asn	0.75±0.34	1.6±0.24	1.07±0.13	2.74±0.17
Asp	1.05±0.13	1.32±0.23	1.38±0.2	1.71±0.09
Ser	0.88±0.04	1.11±0.32	1.47±0.28	1.8±0.23
Ala	1.4±0.11	0.99±0.21	1.33±0.11	0.93±0.16
Gly	0.89±0.1	0.83±0.22	1.47±0.32	1.32±0.18
Gln	1.06±0.06	0.42±0.02	1.88±0.06	0.74±0.06
Thr	0.8±0.06	0.85±0.18	1.36±0.12	1.43±0.28
Glu	0.65±0.02	1.69±0.24	1.33±0.16	3.43±0.33
Pro	0.89±0.03	0.61±0.09	0.92±0.09	0.64±0.1
Lys	1.08±0.07	0.79±0.06	0.99±0.03	0.73±0.07
His	0.79±0.14	0.96±0.14	0.87±0.17	1.05±0.08
Arg	0.84±0.08	0.59±0.03	0.85±0.01	0.61±0.09
Val	0.76±0.06	0.59±0.08	1.22±0.09	0.94±0.03
Met	0.81±0.06	1.03±0.18	1.09±0.13	1.37±0.19
Tyr	1.01±0.06	0.96±0.07	0.8±0.03	0.76±0.1
Ile	0.92±0.11	0.74±0.04	1.33±0.02	1.08±0.15
Leu	1.07±0.09	0.79±0.05	1.4±0.05	1.05±0.12
Phe	0.95±0.08	0.76±0.08	1.39±0.04	1.12±0.16
Trp	0.99±0.1	0.65±0.04	1.39±0.08	0.92±0.14
AABA	1.26±0.26	0.96±0.1	0.89±0.21	0.69±0.16
2-PG	0.87±0.09	0.9±0.13	1.1±0.12	1.1±0.12
3-PGA	0.92±0.12	1.23±0.18	0.96±0.21	1.26±0.09
2-OG	0.87±0.1	1.08±0.22	1.12±0.19	1.36±0.05
Malate	0.94±0.18	1.9±0.27	0.59±0.16	1.18±0.28
Isocitrate	0.42±0.04	1.94±0.23	0.72±0.06	3.32±0.33
Lactate	0.81±0.13	1.15±0.21	1.11±0.21	1.57±0.17
Citrate	0.43±0.04	1.9±0.26	0.72±0.07	3.19±0.26
Succinate	0.98±0.14	1.02±0.17	1.13±0.18	1.18±0.27

Results

Table 8: Metabolome analysis of strain $\Delta ccmM/exFTL$ and $\Delta ccmM/exF-C-M$ at day 7.

Day 7	$(\Delta CcmM/exFTL+F)$ / $(\Delta CcmM/exFTL)$	$(\Delta CcmM/exF-C-M+F)$ / $(\Delta CcmM/exF-C-M)$	$(\Delta CcmM/exF-C-M)$ / $(\Delta CcmM/exFTL)$	$(\Delta CcmM/exF-C-M+F)$ / $(\Delta CcmM/exFTL+F)$
Asn	0.89±0.04	1.67±0.17	0.83±0.08	1.54±0.12
Asp	0.66±0.08	2.4±0.07	0.61±0.09	2.21±0.08
Ser	0.67±0.06	1.06±0.02	1±0.06	1.57±0.06
Ala	1.32±0.09	0.95±0.02	0.89±0.06	0.64±0.01
Gly	0.78±0.05	1.18±0.21	0.92±0.21	1.36±0.03
Gln	1.06±0.01	0.49±0.01	1.74±0.04	0.81±0.02
Thr	0.91±0.04	1.19±0.03	1.07±0.01	1.41±0.1
Glu	0.86±0.02	2.15±0.08	0.77±0.02	1.93±0.07
Pro	0.87±0.09	0.67±0.02	1.14±0.05	0.88±0.05
Lys	1.06±0.01	0.49±0.01	1.77±0.05	0.83±0.03
His	1.02±0.08	0.86±0.09	1.13±0.03	0.96±0.04
Arg	1.08±0.03	0.93±0.02	0.98±0.02	0.85±0.04
Val	0.99±0.08	1.09±0.1	0.96±0.04	1.06±0.11
Met	1.02±0.11	1.27±0.11	0.92±0.1	1.16±0.09
Tyr	1.13±0.02	1.13±0.07	1.02±0.02	1.02±0.09
Ile	0.91±0.05	0.93±0.03	1.11±0.04	1.14±0.05
Leu	0.74±0.09	0.57±0.04	1.82±0.14	1.42±0.07
Phe	0.84±0.02	1.43±0.04	0.96±0.04	1.63±0.09
Trp	0.92±0.02	0.95±0.07	1.13±0.02	1.16±0.07
AABA	1.42±0.15	0.84±0.09	0.84±0.12	0.5±0.04
2-PG	0.92±0.22	0.92±0.43	1.21±0.15	1.17±0.22
3-PGA	1.2±0.13	1.34±0.1	0.9±0.06	1.02±0.11
2-OG	0.96±0.02	1.48±0.15	0.83±0.06	1.28±0.08
Malate	0.99±0.07	1.23±0.07	0.66±0.03	0.82±0.06
Isocitrate	0.53±0.08	1.66±0.11	0.95±0.03	3.03±0.3
Lactate	0.98±0.17	0.98±0.16	0.95±0.1	0.95±0.13
Citrate	0.53±0.09	1.67±0.14	0.95±0.02	3.04±0.56
Succinate	0.8±0.11	0.94±0.07	0.79±0.04	0.96±0.24



Samples were collected at day 5 and day 7, respectively, as shown in Fig. 19B. The values are normalized as relative folds and presented as means±SE from three independent biological replicates. The heatmap displays the log₂ (relative folds) on a color-scale.

4.4 Formate-dependent C1-auxotrophy reporter strain

The C1-auxotrophy and serine-auxotrophy strains relying on formate were successfully created in *E. coli* (Yishai et al., 2017). These strains served as base to confirm that it is possible to produce all the necessary C1 units via different THF-derivatives and serine, respectively, from formate. The aforementioned experiments in this study indicated that successful formate incorporation into 10-formyl-THF may allow to replace the endogenous FoID, which could result in the generation of a formate-dependent *Synechocystis* strain that can be later on applied to select efficient formate production enzymes. The following chapter describes the generation process of the formate-dependent null mutant $\Delta foID$ in *Synechocystis*.

4.4.1 Characterization of enzyme FoID

Until now, the gene for FoID has not been verified in *Synechocystis*. First, we searched possible candidate gene coding for this protein in the genome of *Synechocystis*. There was one putative gene *slI0753* annotated to encode FoID according to the database CyanoBase, which shows amino acid sequence similarities to FoID proteins from *Escherichia coli*, *Arabidopsis thaliana*, *Photobacterium phosphoreum*, *Mycobacterium tuberculosis*, *Rhodospirellula baltica* and *Streptococcus pneumoniae* (Fig. 20) with 46, 34, 38, 44, 46, and 51% identity, respectively. Bifunctional FoID consists of a N-terminal bifunctional domain (D/C) and a C-terminal domain for NADP⁺ cofactor binding (Ho Lee et al., 2011; Sah and Varshney, 2015), which are both found in *slI0753*. As reported, the highly conserved motif Y-X-X-X-K in the N-terminal is involved in the active site for the dehydrogenase/cyclohydrolase activity (as shown in Fig. 15). In addition, the C-terminal domain contains a G-X-G-X-X-X-G finger print motif forming a Rossmann fold for the location of NADP⁺ molecule (Pawelek et al., 2000; Ho Lee et al., 2011; Sah and Varshney, 2015). Hence, the protein *slI0753* was our prime candidate for further analysis of FoID in *Synechocystis*.

Results

```

Synechocystis PSCQILDGKALAQKMQGELQRDIAQLVAQGHRSPLGLAVLMVGDNPASAVYVRNKEKACEK 65
E. coli MAAKIIDGKTTIAQQVRSEVAQKVQARIAAGLRAPGLAVVLVGSNPASQIYVASKRKACEE 60
Arabidopsis QKTVVIDGNVIAEEIRTKIISEVGMKKAQVGVKVPGLAVVLVGEQRDSQTYVRNKIKACEE 120
Photobacterium MSAQIIDGKIIISQTVRQEVAAARVKARTDAGLRAPGLAVVLVGDQPASQIYVGSKRKACEE 60
Mycobacterium MGAIMLDGKATRDEIFGDLKQ RVAALD - AAGRTPGLGTILVGDPPGSQAYVRGKHADCAK 59
Rhodopirellula MPATRLDGKKIAAEIRSEVAADVETFVSGGNPPQLAAVLVGEDPASQVYVRNKERACAK 60
Streptococcus -MTQIIDGKALAAKLQGLAEKTAKLKEETALVPLVVLVGDNPASQVYVRNKERSALA 59
      **:      :  :      * * .: **. * ** *

Synechocystis LGMVS-FGKHFSADTDQETLTAASLNEDERVDGILVQLPLPDH-----LDAVKLLHT 118
E. coli VGFVRSR-YDLPETTSEAELELIDTLNADNTIDGILVQLPLPAG-----IDNVKVLER 113
Arabidopsis TGIKSVL-AELPEDCTEQIISVLRKFNEDTSHIGILVQLPLPQH-----LNESKILNM 173
Photobacterium VGFISKS-FDLPSASSEQQLLDLIDELNQDPTMDGILVQLPLPAG-----MDCRILER 113
Mycobacterium VGITSIR-RDLPADISTATLNETIDELNANPDCTGYIVQLPLPKH-----LDENAALER 112
Rhodopirellula AGIASRL-DRMPAATTQAEELAKVAELNADPAVSGILVQLPLPSKANGGTGIDERAVLDA 119
Streptococcus AGSRSEV-VRVPETITQEELLDLIAKYNQDPAWHGILVQLPLPKH-----IDEEAVLLA 112
      *      .      :      :      * :      * :*****      :      *

Synechocystis IDPSKADGLHPVNLGHLV--RGEGLRSCTPAGVMALLAEYNLDLTGKNAVVLGRSILV 176
E. coli IHPDKVDGFHPYNVGRLC--QRAPRLRCPTRGIVTLLERYNIDTFGLNAVVI GASNIV 171
Arabidopsis VRLEKVDGFHPLNVGNLAMRGREPLFVSCPKGCVELLIRTGVEIAGKNAVVI GRSNIV 233
Photobacterium IDPEKVDGFHPYNVGRLS--QRIPKLRSCTPKGIITLLERYNIEVRGKHAVIV GASNIV 171
Mycobacterium VDPKADADGLHPTNLGRLV--LGTPAPLPCPTRGIVHLLRRYDISIAGAHVVVIGRGVTV 170
Rhodopirellula IDPIKVDAFSPVNVGLLM--QGRPRFLPCTPHGIVQLLHRTGIETSGKHVVVVGRSDIV 177
Streptococcus IDPEKVDGFHPLNMGRWL--SGHPVMI PSTPAGIMEMFHEYGIDLEGKNAVVI GRSNIV 170
      :      **.*.: * ** *      .** * : : . .: * .*:.* . *

Synechocystis GKPLALMLLEKN-----CTVTIAHSRTQNLADITRQADILVAAIGKPEFVTADMVK 227
E. coli GRPMSMELLLAG-----CTTTVTHRFKTLNRHHVENADLLIVAVGKPGFIPGDWIK 222
Arabidopsis GLPMSLLQRHD-----ATVSTVHAFKDPHEITRKADIVIAAAGIPNLVRSWLK 284
Photobacterium GRPMTLELLLAG-----ATTTTCHRFQDLEGHIRQADILVVAVGKPNFIPGGWIK 222
Mycobacterium GRPLGLLLTRRS-----ENATVTLCHTGTDRDLPALTRQADIVVAAVGVAHLLTADMVR 223
Rhodopirellula GKPMAMMLAQKDSTCGPAVANATVTIAHSRTSNLAEICRQADILIAAVGRPEMITAEMIQ 237
Streptococcus GKPMQQLLAKN-----ATVTLTHSRTHNLAKVAADILVVAIGRAKFVTADFVK 221
      * *:      * .      .*. * * :      *:::.* *      :. . :.

Synechocystis PGAVVDVGINRLDLGE--GKSTLVGDVDFAGVAPVASYLTPVPPGGIGPMTVTL LLANTV 285
E. coli EGAVIDVGINRLE-----NGKVVDVVFEDAARASYITPVPPGGVGPMTVATLIEN TL 276
Arabidopsis PGAVVIDVGTTPVEDSSCEFGYRLVGDVCYEEALGVASAITPVPPGGVGPMTITMLLCNTL 344
Photobacterium EGATVIDVGINRLE-----NGKLCGDVEFDVACQRAKYITPVPPGGVGPMTVASLIEN TL 276
Mycobacterium PGAAVIDVGVSR TD-----DGLVGDVHP-DVWELAGHVSPNPPGGVGPLTRAFLLTNVV 275
Rhodopirellula PGAVVIDVGINRVG-----DKLVGDVAFDEAEAVASAITPVPPGGVGPLTIAMLLHNTL 290
Streptococcus PGAVVIDVGMNRDE-----NGKLCGDVDYEAVALASHITPVPPGGVGPMTITMLMEQTY 275
      ** *.*** .      : ***      . * :.* * *.*:* : * : .
  
```

Figure 20: Amino acid sequence alignment of FoID highlighting the conserved residues.

The amino acid sequence (residues 5–285) of *Sll0753* from *Synechocystis* is aligned with the FoID sequences from *Escherichia coli*, *Arabidopsis thaliana*, *Photobacterium phosphoreum*, *Mycobacterium tuberculosis*, *Rhodopirellula baltica* and *Streptococcus pneumoniae* by Clustal Omega. The completely conserved residues are denoted with asterisks below the sequence. The NADP⁺ binding motif with its interacting residue is indicated in blue box and the active sites for D/C activity are shown in red box.

4.4.2 Attempts to generate mutant ΔfoD in wild-type

Gene *sll0753* was inactivated by standard interposon-mutagenesis. The mutant plasmid in

Results

which a kanamycin resistance cassette interrupted gene *sll0753* was constructed (Fig. 21A). The kanamycin resistance gene *aphII* was obtained from pUC4K after *HincII* digestion. The *sll0753* gene and its flanking sequence (1257 bp) were amplified from DNA of the *Synechocystis* wild-type via PCR using gene-specific primers. The DNA fragment was cut by *EcoRV* and *BmgBI*, leading to the deletion of an internal fragment of 147 bp (Fig. 21A), which encode for amino acid residues 204-252 involved in the NADP⁺ binding (Fig. 20). The completed plasmid pT-0753-k was characterized with specific primers (Fig. 21B) and transformed into *Synechocystis* wild-type cells. Genotypic analysis of 50 recombinant clones showed that all were showed non-segregated genomes, i.e. they contained both the wild-type and the mutant gene copies (Fig. 21C and D, data not shown). The non-segregated genotype of these clones confirmed the essential function of protein FOLD and verified our assumption that *Synechocystis* requires another pathway to synthesize 10-formyl-THF to replace FOLD.

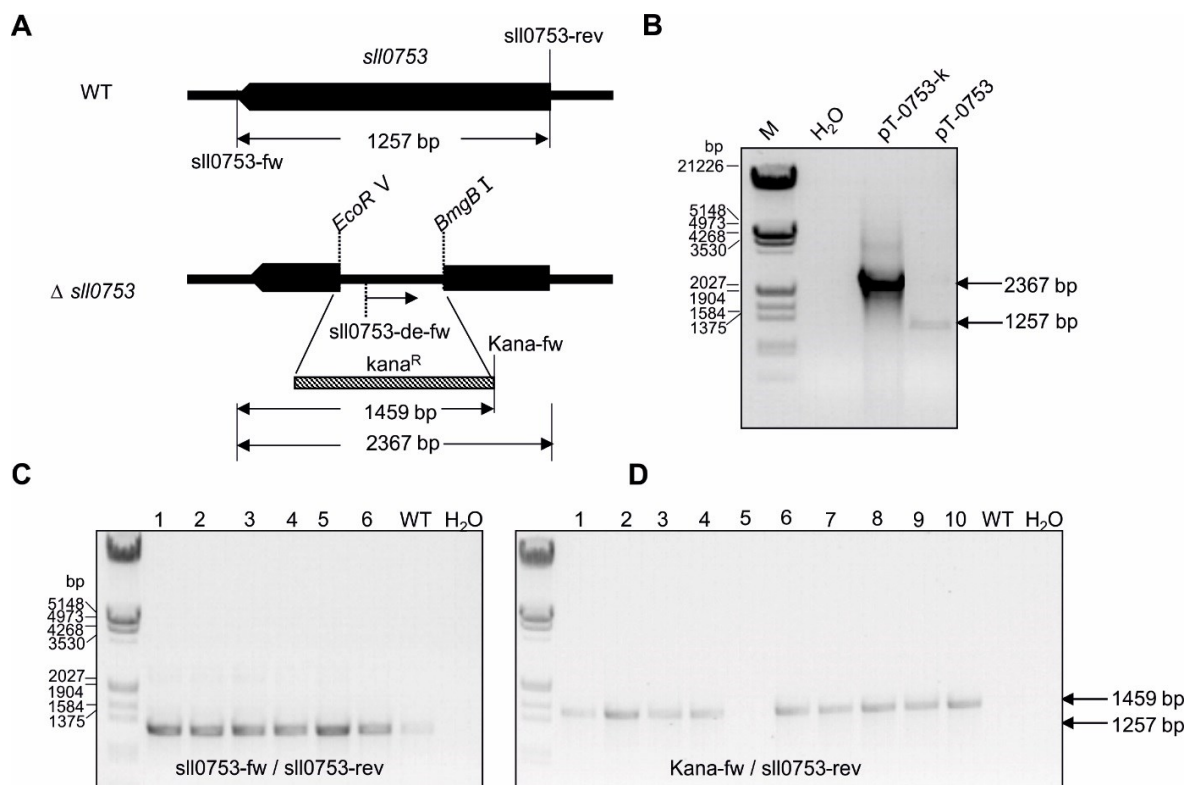


Figure 21: Attempts to delete gene *sll0753* in *Synechocystis* wild-type.

A. Construct for deletion of gene *sll0753* in *Synechocystis*. The *aphII* gene was inserted into gene *sll0753*. **B.** The completed plasmids named pT-0753-K were characterized by the primer *sll0753-fw/sll0753-rev*. M: marker; pT-0753: plasmid containing the entire gene *sll0753*. **C** and **D.** The genotypes of selected clones were characterized by the primer pair *sll0753-fw/sll0753-rev* and *Kana-fw/sll0753-rev*.

4.4.3 Attempts to generate mutant $\Delta foID$ in the presence of exogenous enzyme FTL

Theoretically the introduction of FTL should satisfy the demand of 10-formyl-THF for purine synthesis and enable the complete deletion of gene *foID*. Similar results were reported before with *Leishmania major*, which confirmed that the overexpression of its endogenous gene *ftl* enabled the complete loss in *foID* (Murta et al., 2009). We already obtained an FTL-expressing strain exFTL described in the previous chapters (see Fig. 7), which should satisfy the demand of 10-formyl-THF via formate assimilation. The *foID* deletion construct pT-0753-k was then introduced into the FTL-expressing strain exFTL. Analysis of 6 independent clones named exFTL/ $\Delta foID$ showed they possessed *ftl* gene except exFTL/ $\Delta foID$ -a-3 (Fig. 22A) and contained the *sII0753* mutant gene (Fig. 22B) in the genome. But all of the 15 selected clones still kept wild-type gene copies of *sII0753* (Fig. 22C). The further supplementation of formate aiming at enhancing the production of 10-formyl-THF did also not result in the complete segregation of *foID* in total 13 clones (Fig. 22D).

4.4.4 Attempts to generate mutant $\Delta foID$ using nutritional supplements

The unexpected difficulties to segregate the *foID* mutation are likely related to a limited rate for 10-formyl-THF synthesis via FTL in the absence of FoID in *Synechocystis*. To overcome this possible limitation, I performed metabolite complementation experiments. To this end, 0.3 mM IMP and inosine together with formate were supplied into the growth medium of non-segregated clones. After approximately 7 d incubation, the genotype of clones was checked by PCR with *sII0753*-specific primers. Among them, one non-segregated clone was selected for continuous acclimation with IMP or inosine and formate. These steps were repeated for three times. Albeit the copies of mutant gene with fragment at 2367 bp increased to some extent with time, the wild-type gene (1257 bp) was still detected in total 90 clones by PCR analysis (Fig. 23).

Results

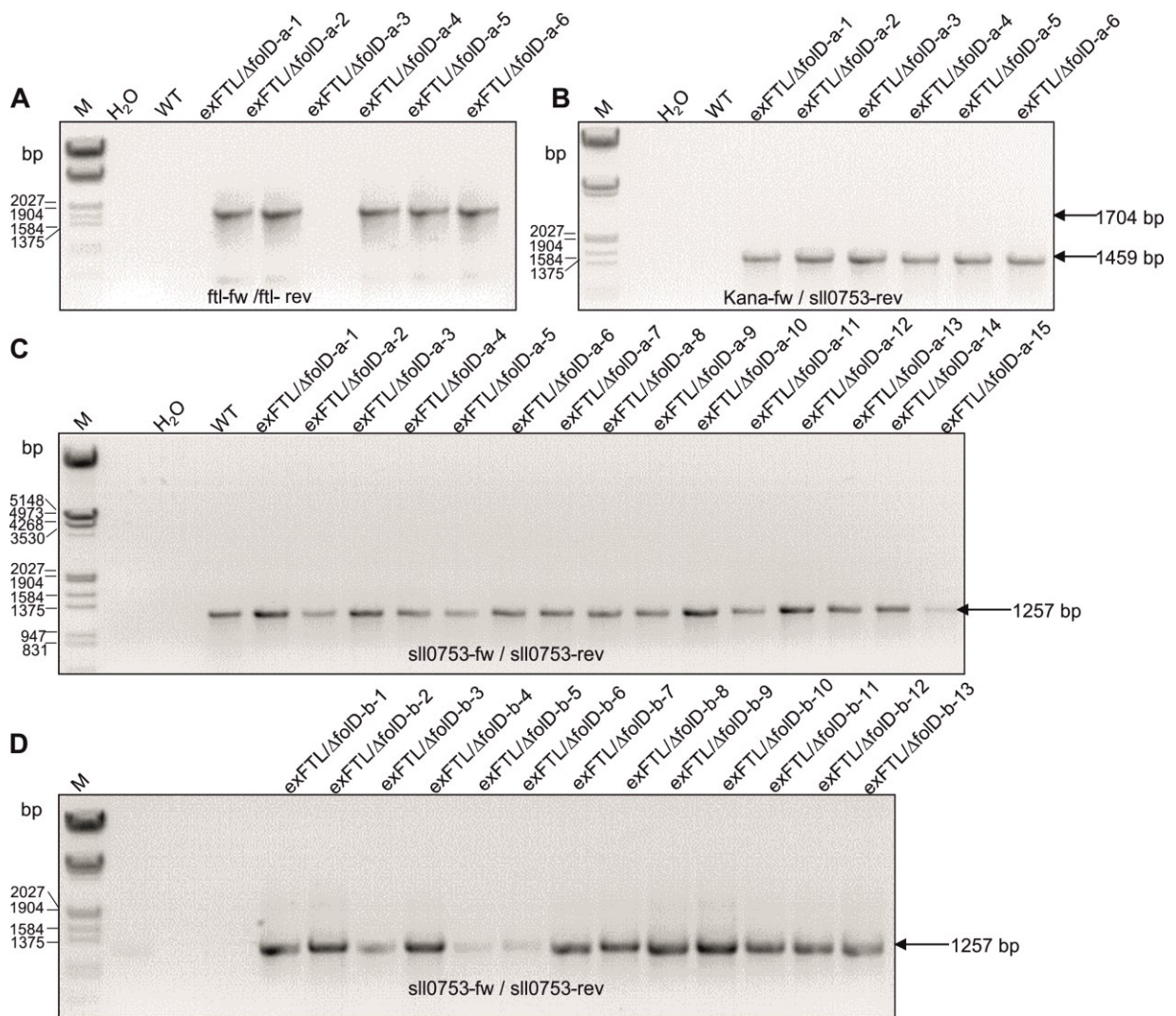


Figure 22: Attempts to delete gene *sII0753* in the presence of exogenous FTL.

A. The genotypes of 6 selected clones (exFTL/ Δ foiD-a-1 – exFTL/ Δ foiD-a-6) were characterized by the primer pair ftl-fw/ftl-rev (as shown in Table 1). WT: wild-type cells; M: marker; H₂O: without DNA. **B.** The genotypes of 6 selected clones were characterized by the primer pair Kana-fw/sII0753/rev. **C and D.** The genotypes of 28 selected clones were characterized by the primer pair sII0753-fw/sII0753-rev. One non-segregated clone exFTL/ Δ foiD-a was selected and further inoculated with formate for 7 d. After that, 13 clones named exFTL/ Δ foiD-b-n were selected and their genotypes were characterized by PCR. exFTL/ Δ foiD-1 – exFTL/ Δ foiD-n: different selected clones.

Results

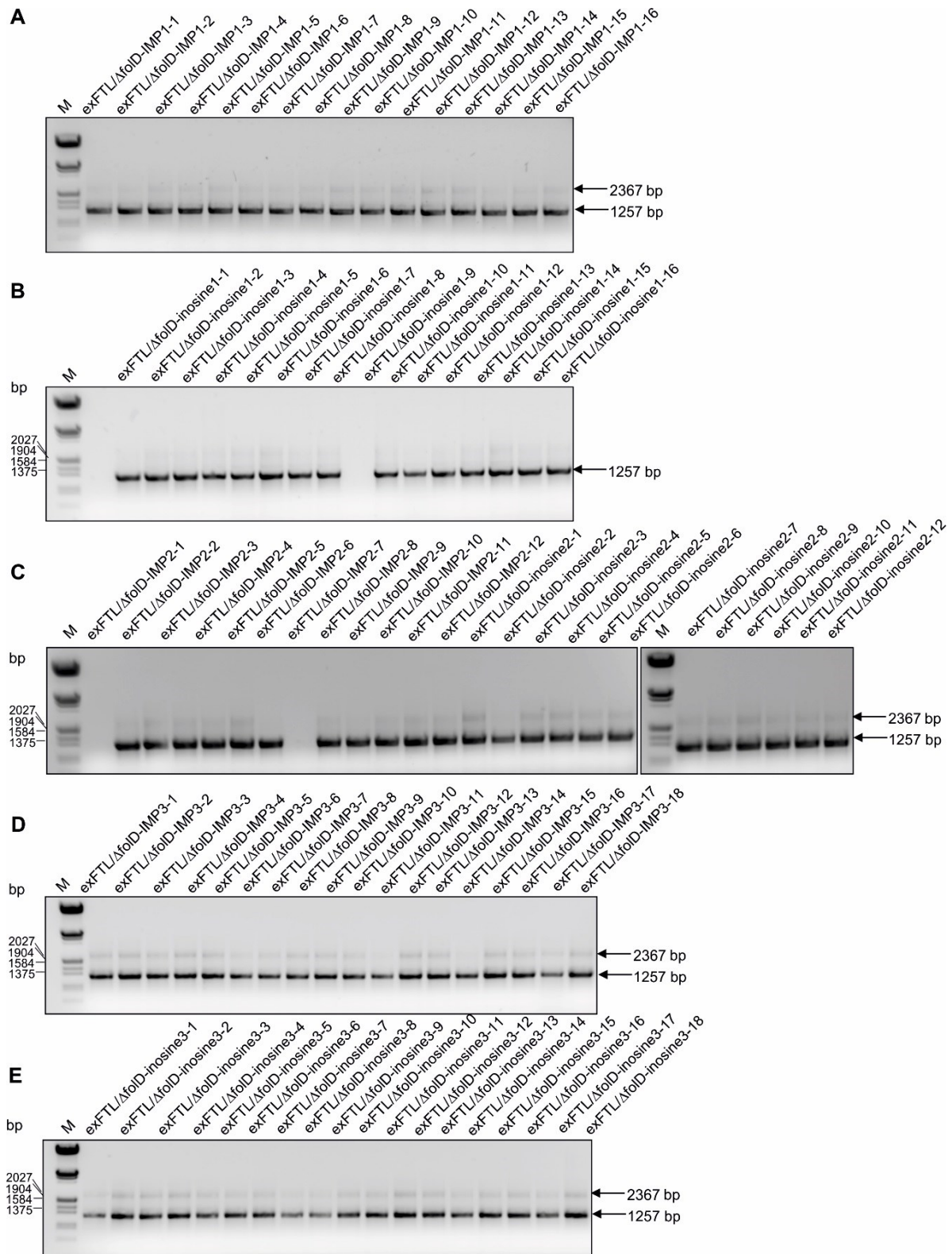


Figure 23: Attempts to delete gene *slI0753* after supplementation with IMP or inosine.

A-E. The genotypes of selected clones were characterized by the primer pair *slI0753-fw/slI0753-rev*. M: marker; exFTL/ Δ foiD-inosine/IMP-n: different selected clones; WT: wild-type cells. Some lanes did not show bands because of insufficient DNA quality.

Results

4.4.5 The deletion of *foiD* in the presence of exogenous enzymes FTL and MtdA

The expression of FTL and nutritional supplement did not bypass the essential requirement of *FoID*, which might indicate that *FoID* is probably also playing important roles in other metabolic processes. To guarantee the complete deletion of *foiD*, we assumed that the strain exF-C-M expressing proteins FTL and MtdA should satisfy the demand of endogenous *FoID* in *Synechocystis*. The deletion construct pT-0753-k was introduced into the exF-C-M strain supplemented with formate on the transformation plates. To verify the complete loss of gene *foiD*, an internal primer located in the deletion fragment was designed. This new approach finally resulted in the complete segregation of mutant $\Delta foID$, because in contrast with previous results all wild-type-sized fragments of *sll0753* disappeared (Fig. 24).

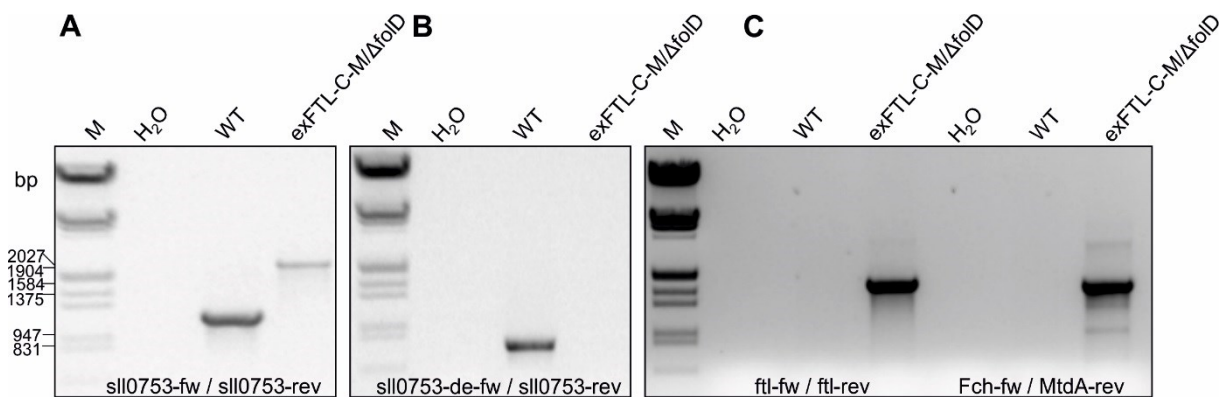


Figure 24: The completely deletion of *sll0753*.

A. The genotype of exF-C-M/ $\Delta foID$ was characterized by the specific primer pair sll0753-fw/sll0753-rev. **B.** The complete segregation of *foiD* was examined by primer pair sll0753-de-fw/sll0753-rev. **C.** The introduction of gene *ftl*, *fchA* and *mtdA* in exF-C-M/ $\Delta foID$ was confirmed by PCR amplified with the specific primer pair ftl-fw/ ftl-rev and Fch-fw/MtdA-rev.

5 Discussion

5.1 Impact of external formate on *Synechocystis*

There are several reports describing positive but also negative effects after addition of external formate on photoautotrophic organisms mostly plants. The growth of rice in terms of the length of aerial part and fresh weight was reported to be stimulated by low external sodium formate amounts of 1.8 mM, while it was suppressed when incubated with 18 mM formate (Shiraishi et al., 2000). The growth stimulation probably resulted from an increased CO₂ concentration in the rice leaves due to formate oxidation by FDH. Formate (Different formate salt were tested) above 4 mM delayed the seed germination and reduced primary root elongation, while lower concentration of formate caused no obvious effect in *Arabidopsis thaliana* (Li et al., 2002). Formic acid treatments below 1 mM had also no obvious influence on seed germination and the length of seedlings of garden cress and ryegrass, but higher concentration severely reduced their germination and growth (Himanen et al., 2012). According to these reports, it can be concluded that higher concentrations of formate are toxic to plants and different plant species exhibit different sensitivity toward formate.

Why is formate toxic? Formate is broadly known to significantly inhibit the electron transfer and proton release at PSII, which can be reversed by the addition of bicarbonate (Xiong et al., 1998). Bicarbonate is bound to specific sites in the PS II and stimulates its activity (e.g., Shevela et al., 2007), whereas the analog formate is supposed to remove bicarbonate from its position and thus inhibiting PSII activity.

Similar to the situation in plants, I observed concentration-dependent effects of formate on *Synechocystis*. Low concentrations of formate are tolerated and are not affecting growth and photosynthetic activity. Only concentrations exceeding 20 mM have negative impact on photosynthesis and growth of wild-type cells (Fig. 5A and B). These results showed that formate up to 20 mM can be added externally to *Synechocystis* to test its assimilation in wild-type and different transgenic strains.

Discussion

Furthermore, the negative effects of high formate concentrations also imply that formate can be taken up possibly via diffusion into the *Synechocystis* cells, since no homologs to known formate transport systems are encoded in its chromosome. In contrast, a formate transporter FocA as an integral membrane protein was identified in *E. coli* (Suppmann and Sawers, 1994; Wang et al., 2009). It belongs to formate/nitrite transporter family widely distributed most among enterobacteria (Wei et al., 2013). Formate is a major product under anaerobic fermentation via the pyruvate formate lyase (PFL) pathway in many enterobacteria (Wang et al., 2009; Roger et al., 2017). The accumulation of formate might cause cytoplasmic acidification. Therefore, formate must be exported from cytoplasm to periplasm to be metabolized to CO₂ by FDHs (Wang et al., 2009). In addition, FocA from *Salmonella typhimurium* was recognized to switch its mode from a passive exporter at high external pH to an active formate/H⁺ importer at low pH (Lü et al., 2011). Different to *E. coli*, the preliminary ¹⁴C-formate uptake assay (Fig. 25) provided a proof that formate could be taken up in *Synechocystis* and most likely via diffusion due to its lower rate. Further repeats and optimization of the formate uptake assay needs to be done to rule out the reason for the initial decrease in radioactivity. Nevertheless, FA pathway can be investigated with supplementation of external formate before the introduction of a suitable FDH synthesizing formate directly from CO₂.

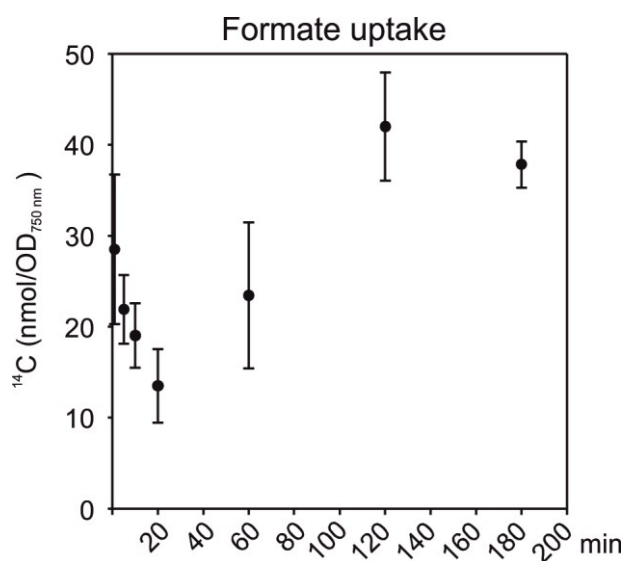


Figure 25: Formate uptake assay.

Pre-cultures were grown under ambient air in liquid BG11. Cells were adjusted to OD_{750 nm}=1

Discussion

supplemented with 10 mM unlabeled-sodium formate containing 0.1% ^{14}C labeled-sodium formate. 1 mL Samples were taken at given time points (0, 5, 10, 20, 60, 120 and 180 min), filtered and washed with 10 mL pre-cooled BG11 containing 10 mM formate. Uptake of radioactive formate was measured on the filters by liquid scintillation counter.

5.2 Investigation of candidate gene *sII1359* encoding FDH

Our aim is to establish a FA pathway in photoautotrophic organisms. Therefore, their endogenous cellular metabolism should not negatively interfere with formate assimilation. The protein FDH is the first enzyme of formate metabolism, which can be found in many organisms. FDH is capable of oxidizing formate into CO_2 or reducing CO_2 into formate. Plant FDHs mostly work in the oxidizing direction and regulate the intracellular content of formate in response to stress (Ambard-Bretteville et al., 2003). The addition of external formate strongly induced the expression of FDH in potato (Hourton-Cabassa et al., 1998) and *Arabidopsis* (Olson et al., 2000). Overexpression of FDH protected *Arabidopsis* against toxic effects of excess formate (Li et al., 2002). Additionally, formate oxidation is coupled to the reduction of diverse terminal electron acceptors to supply energy in prokaryotes (Maia et al., 2017).

FDHs are also found in diverse prokaryotes such as *E. coli* (Jormakka et al., 2002; Raaijmakers and Romão, 2006), and was detected with some nitrogen-fixing cyanobacteria (Heyer et al., 1989; Norman and Colman, 1992). There are reports on the excretion of several fermentation products including formate, which further imply the existence of FDH in cyanobacterial phylum (Heyer and Krumbein, 1991). For example, *Synechocystis* was reported to possess a photorespiratory branch that degrades glyoxylate through oxalate and formate into two molecules of CO_2 including an FDH as last enzyme. Due to weak sequence similarities it was predicted that the protein SII1359 could represent the FDH (Eisenhut et al., 2008b). To verify the FDH function of this protein, the gene *sII1359* was expressed in *E. coli* to obtain recombinant protein for biochemical studies (Fig. 6D) and a corresponding mutant was generated and investigated (Fig. 6C). Many completely segregated mutant clones were obtained, which indicated that protein SII1359 is not functionally important under laboratory conditions. Moreover, the mutant $\Delta sII1359$ did not show the expected increased sensitivity

Discussion

toward formate compared with wild-type, which made an involvement in SII1359 as formate degradation unlikely. Consistently, we did not observe formate oxidizing activity with recombinant protein SII1359. In contrast, potato plants whose FDH was suppressed accumulated more internal formate due to the decreased consumption of formate (Ambard-Bretteville et al., 2003). Hence, we can conclude that gene *sII1359* most probably does not encode FDH in *Synechocystis*. Variable FDH expression was reported in *E. coli*, where it was found that formate was required for the expression of FDH-N and FDH-H (Birkmann et al., 1987; Leonhartsberger et al., 2002). Hence, we tried to measure FDH activity in total lysates from wild-type cells inoculated either with or without formate, but without success. Together with the missing growth stimulation of external formate, these results imply that *Synechocystis* does not express FDH, or, FDH activity is quite low in cells grown under our specific lab condition.

Collectively, we concluded from these experiments that the establishment of a FA pathway will be not interfered by significant formate degradation via an endogenous FDH in *Synechocystis*. Hence, in the absence of a suitable FDH for formate production via CO₂ reduction inside *Synechocystis*, we can establish the FA pathway on the expense of externally supplied formate.

5.3 Expression of FTL in wild-type

The second step in the FA pathway is the insertion of formate into the C1 unit pool bound to THF, which is initially done by the action of FTL. The single introduction of a heterologous FTL enabled *E. coli* to assimilate external formate into serine through the FA pathway (Bang and Lee, 2018). Approximately 10% of carbon atoms in the entire serine pool were labeled in the FTL-expressing *E. coli* strain supplemented with ¹³C-labeled sodium formate, which was close to theoretical consideration (Bang and Lee, 2018).

The success in *E. coli* encouraged us to establish the same formate metabolizing pathway in photosynthetic organism *Synechocystis* by expression of FTL. For this purpose we used the FTL protein from *M. extorquens*, which was shown before to perform high enzyme activity and

Discussion

enabled *E. coli* to incorporate formate (Marx et al., 2003). Although, it was successfully expressed in *Synechocystis*, our FTL-expressing strain exFTL did not grow faster with formate compared to wild-type (Fig. 8A). If external formate was assimilated by FA pathway, an increased organic carbon flux into serine would be predicted. According to our pathway depicted in Fig. 4, the expression of FTL enables cells to incorporate formate into 10-formyl-THF, which then might be converted to 5, 10-methylene-THF by the endogenous FdD and further to serine via the endogenous SHMT. As expected, the serine pool increased about 3-fold in exFTL strain upon addition of formate (Fig. 8B). Meanwhile, the glycine level in exFTL was approximately 3-fold reduced in the presence of formate (Fig. 8C). These changes of serine and glycine are consistent with the close relationship of these metabolites in the GDC/SHMT catalyzed serine-glycine cycling and the associated C1 metabolism.

In addition, exFTL exhibited higher resistance toward external glycine and formate compared to wild-type, which is consistent with the significantly reduced glycine and the supposed increased formate assimilation into serine. Hence, these two critical intermediates are detoxified in higher rates, formate via FTL alleviating toxic effects on PSII caused from excess formate (Sah et al., 2015), whereas the toxic effect of glycine via its Mg^{2+} -chelating effect (Eisenhut et al., 2007) is reduced due to increased usage of glycine for serine synthesis via SHMT. Our results also imply that glycine and formate supplementation have an additive toxic effect to *Synechocystis* cells (Fig. 8D). There are two possible explanations for this observation. First, the supplementation of formate could result in the accumulation of glycine, for example the higher amount of methyl-THF might reduce glycine oxidation via GDC. In addition, formate could also inhibit the glyoxylate degradation through the decarboxylation branch of the 2-PG metabolism producing more glycine. Accordingly, the addition of formate probably stimulated the concentration of glycolate and further glycine. However, glycine contents decreased after formate incubation in exFTL cells (Table 4) making this scenario unlikely. Second, formate and glycine might have a joint negative effect on photosynthesis and carbon fixation rate due to the block in photosynthetic electron transfer and the inactivation of Rubisco, respectively. Thus, high external concentration of formate and glycine caused severely inhibition to cells than

Discussion

either of them alone.

Many other cellular metabolites also showed alteration after formate addition to strain exFTL (Table 4) suggesting that a massive metabolic reprogramming occurred. Consistent with the changes of serine and glycine, a slightly elevated amount of 3-PGA and a decrease in 2-PG were measured, which could indicate less photorespiration and better CBBC activity. Moreover, 2-OG and other organic acids involved in the TCA cycle exhibited significantly reduced level, indicating the introduction of FTL reduced TCA cycle flux. The meta-analysis of metabolic data showed that the intermediates of TCA cycle/GABA shunt were affected in a wide range of plant photorespiratory mutants, implying a close connection between the two pathways (Bauwe et al., 2010; Florian et al., 2013; Florian et al., 2016). For example, the *Arabidopsis* mutants defective in GGAT displayed a slight photorespiratory phenotype and reduced TCA cycle-related organic acids including pyruvate, fumarate and succinate (Dellero et al., 2015). In contrast, most amino acids increased to different extent in exFTL when supplemented with formate (Table 4), the exceptions were glutamate, asparagine, arginine and isoleucine indicating a modification in amino acids metabolisms. The aminotransferases involved in the photorespiratory pathway could affect the specific composition and total amount of amino acids (Florian et al., 2013). GGAT and SGAT mediate the transamination of glyoxylate to form glycine functionally importantly in the regulation of major amino acids level in plants (e.g. glutamate and glutamine) (Fahnenstich et al., 2008). GGAT converts glutamate and glyoxylate to glycine and 2-OG, while SGAT uses serine and glyoxylate to produce glycine and hydroxypyruvate. Glutamine synthase (GS) combines glutamate and free ammonia to synthesize glutamine, which is subsequently used to produce glutamate from 2-OG by glutamate synthase (GOGAT) (Bauwe et al., 2010). Hence, photorespiratory pathway closely interacts with nitrogen assimilation and has an important role in maintaining a steady state equilibrium of glutamate, glutamine and 2-OG in plants, which is most likely the same in cyanobacteria. Although we could not detailed explain why specific amino acids increase or decrease in exFTL strain supplied with formate, the intervention into photorespiration and C1 metabolism obviously did affect overall amino acids metabolism.

Discussion

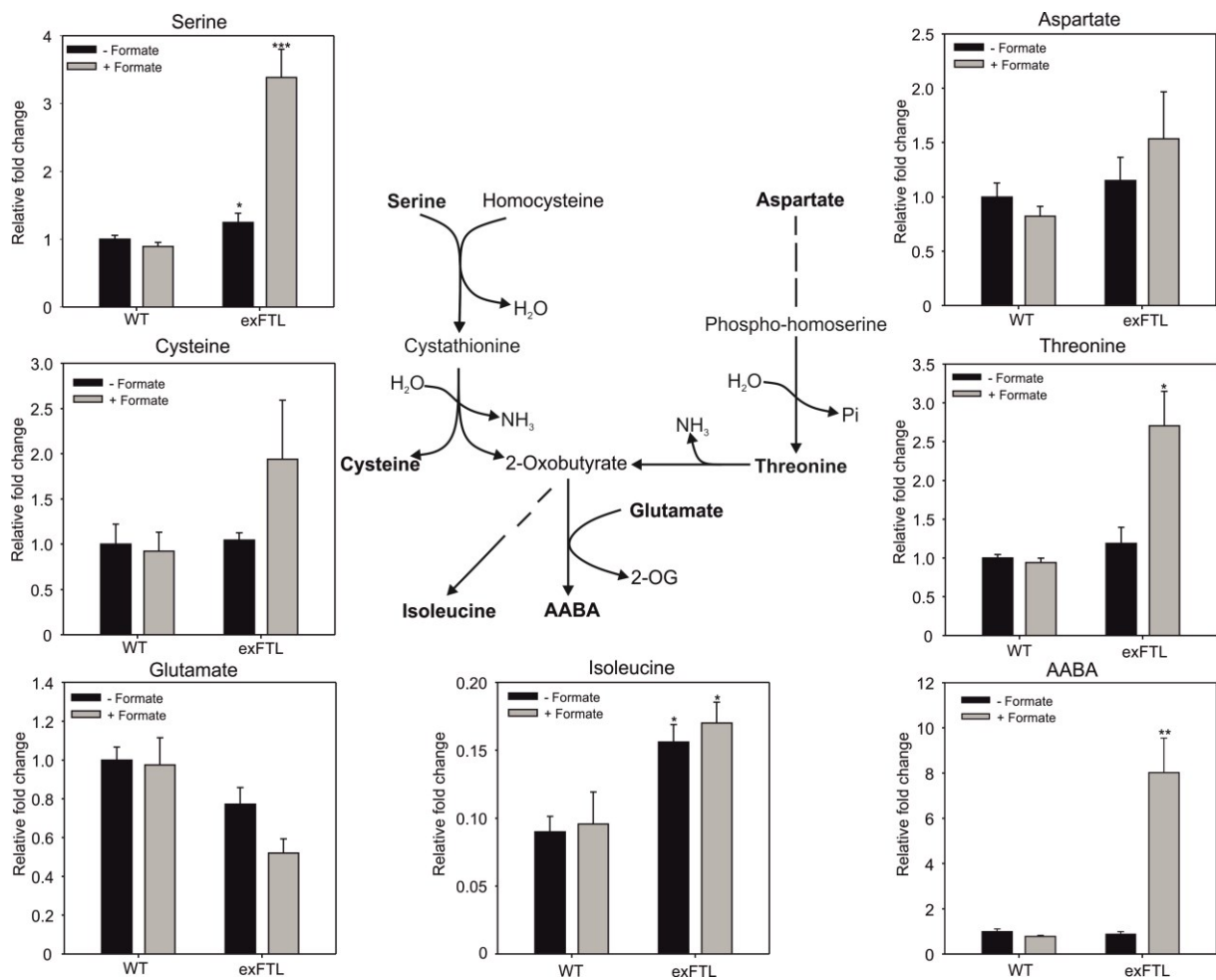


Figure 26: Changes of metabolites related to AABA metabolism.

The relative fold changes in metabolites related to AABA metabolism in cells of FTL-expressing strain (exFTL) compared to wild-type (WT). Samples were collected 24 h either with or without formate, respectively. Cells were cultivated under ambient air at $100 \mu\text{mol photons m}^{-2} \text{s}^{-1}$. Given are mean values and SE of at least three independent replicates. *: $P < 0.05$; **: $P < 0.01$; ***: $P < 0.001$.

Surprisingly, the highest increase (9-fold) of AABA was observed in the formate supplemented exFTL strain. AABA is a non-proteinogenic amino acid, which is of pharmacological significance (Zhang et al. 2009; Seo et al., 2012). Up to now, the natural pathway for the *de novo* biosynthesis of AABA is scarcely understood. According to the KEGG pathway database, AABA might appear as side-product from serine cleavage or branched amino acids synthesis as shown in Fig. 26. AABA could be produced from 2-oxobutyrate by amination (Weber et al., 2017), and 2-oxobutyrate is mainly synthesized from threonine that acts as precursor for the branched amino acid isoleucine biosynthesis in *E. coli* (Guillouet et al., 1999). In addition, this

Discussion

intermediate is also one product of cystathionine cleavage by cystathionine γ -lyase (Nagasawa et al., 1984), and cystathionine could be formed from serine by cystathionine β -synthase (Jhee et al., 2000). As shown in Fig. 26, serine, cysteine, aspartate and threonine increased to different extents, while glutamate declined slightly in the formate inoculated exFTL strain in comparison to wild-type. But the increase of isoleucine in exFTL strain was independent of formate. Thus, the increased AABA was most likely related to increased serine and threonine pools in exFTL strain.

In addition, the high accumulation of AABA indicates that serine is not sufficiently fast converted into 3-PGA in the photorespiratory cycle as expected in our designed pathway. Thus, enzyme SGAT from *Arabidopsis thaliana* was expressed in the above generated strain exFTL aiming to improve serine-to-hydroxypyruvate conversion rate. To investigate the role of enhanced SGAT activities in FA pathway, gene *SGAT* is translationally fused to the promoter of the *petJ* gene encoding cytochrome c553 that is repressed by copper (Kuchmina et al., 2012) (Fig. 12A). No stimulation on growth (Fig. 12D) was observed with the exFTL-SGAT strain when supplemented with formate, which might be due to the low expression level of protein SGAT indicated from the faint signal band in western-blotting (Fig. 12C). Hence, the expression of SGAT needs to be further improved as well as analysis of the according metabolites changes.

5.4 Attempts to enhance FA rate by increasing glycine level

According to the metabolic data of exFTL strain, the significantly declined glycine might be also limiting factor. Hence, to increase the FA rate, enhancing the pool of the precursor glycine might be an option. Consistent with this assumption, growth of strain exFTL was best stimulated by the combined addition of 10 mM formate and 3 mM glycine, while this treatment did not influence growth of the wild-type (Fig. 9). Hence, we aimed to express *ftl* in a strain with defective photorespiration ($\Delta 3pr$) and enhanced glycine concentration (Eisenhut et al. 2008) to obtain better FA. Moreover, the GDC is inactivated in this strain, which also should minimize photorespiratory CO₂ losses and NH₃ production and could further enhance the efficiency of FA route. As expected, the expression of FTL enhanced the growth of exFTL/ $\Delta 3pr$ compared to

Discussion

mutant $\Delta 3pr$. But the stimulation did not depend on the supplementation of formate, which is an interesting and surprising observation (Fig. 10D). This result could suggest that mutant $\Delta 3pr$ might produce formate internally, which was not expected since all the three photorespiratory pathways to detoxify glycolate were blocked in mutant $\Delta 3pr$. However, it has been shown that formate can appear due to decarboxylation of glyoxylate to formate via non-enzymatic oxidation (Igamberdiev and Eprintsev, 2016). Besides, formate is also reported as a co-product in conversion of fatty aldehydes to alkanes by aldehyde decarbonylase in cyanobacteria (Warui et al., 2011).

Despite the growth stimulation, the content of serine did not significantly change in $exFTL/\Delta 3pr$ compared to wild-type either with or without formate (Fig. 11A). This observation implied that external formate did not stimulate serine formation rate in $exFTL/\Delta 3pr$ cells, which was contrary to the enhanced serine production observed with $exFTL$. A possible explanation of this observation might be related to the fact that mutant $\Delta 3pr$ was defective in GDC and the production of 5,10-methylene-THF could be affected. Hence, to meet the demand of C1 units, SHMT probably catalyzed the breakdown of serine to synthesize glycine and 5,10-methylene-THF in mutant $\Delta 3pr$. Photorespiration was considered as an important pathway via SHMT/GDC to produce serine from glycine in photosynthetic organisms including *Synechocystis* (Ros et al., 2014; Knoop et al. 2010). However, it has been shown that SHMTs from *Synechocystis* (Eisenhut et al., 2006) and halotolerant cyanobacterium *A. halophytica* (Waditee-Sirisattha et al., 2012) catalyze the conversion of serine and THF to glycine and 5, 10-methylene-THF, which could provide all the necessary glycine and C1 units for the cell from serine produced via the phosphoserine pathway (Klemke et al. 2015). This scenario is supported by the findings that GDC could be mutated whereas it was not possible to completely knock out gene *shmt* in *Synechocystis* (Hagemann et al., 2005). Furthermore, *Synechocystis* as all other cyanobacteria employs the CCM to increase CO₂ concentration at the site of Rubisco diminishing photorespiration to a large extent, only approximately 1% oxygenation relative to carboxylation of Rubisco was observed (Orf et al., 2016) leading to a very small photorespiratory flux in *Synechocystis* (Young et al., 2011). These results indicate that

photorespiration might contribute only marginal to the serine pool. Due to the essential nature of the phosphoserine pathway for serine biosynthesis, for example the deletion of *serA* failed even when fed with external serine, this assumption could not be yet proven experimentally (Klemke et al., 2015). I also tried to mutate *serA* in this thesis but again with no success. These observations make it likely that SHMT could produce 5,10-methylene-THF and glycine from serine explaining unchanged serine and slightly decreased glycine pools in exFTL/ $\Delta 3pr$ after formate incubation. Theoretically, 5,10-methylene-THF should be synthesized via FTL and endogenous FOLD in the strain exFTL/ $\Delta 3pr$, which is then used to synthesize serine from the enhanced glycine pool. Obviously, the expressed FTL only provided an alternative way for the synthesis of 10-formyl-THF, the precursor for purine synthesis, which could also explain the general stimulation of growth in the strain exFTL/ $\Delta 3pr$ compared to $\Delta 3pr$. In order to improve the conversion of 10-formyl-THF into 5,10-methylene-THF we later on considered replacing endogenous FOLD by another enzyme as has been done before in *E. coli* strains engineered to assimilate formate_ (Yishai et al., 2017; Bang and Lee, 2018; Tashiro et al., 2018).

5.5 Labeling pattern of proteinogenic amino acid

Nowadays, application of ^{13}C isotope analysis of proteinogenic amino acids provides a straight way to verify the detailed metabolic flux (Azizan et al., 2017). Therefore, we fed strain exFTL with ^{13}C -labeled formate and analyzed the isotopic signature of proteinogenic amino acids. Glycine was completely unlabeled in strain exFTL (Fig. 13A), which is in agreement with our hypothesis. However, serine was also unlabeled (Fig. 13B) disproving our assumption that increased serine was synthesized from external formate in exFTL. Approximately 1.5% of methionine and histidine were labeled. This weak label could originate from FTL-dependent formate assimilation into 10-formyl-THF and its conversion into 5-methyl-THF (Fig. 13C and D), which serve as precursors for these amino acids. Obviously, the subsequent conversion of 10-formyl-THF up to serine was inhibited by the addition of formate in exFTL strain. A likely candidate is endogenous FOLD, since it has been shown that the Mtd activity of FOLD could be allosterically inhibited by 10-formyl-THF, the product of this enzyme, as a feedback regulation

Discussion

mechanism in C1 metabolism (Dev and Harvey, 1978). The attempts to establish the FA pathway in *E. coli* confirmed this speculation. The expression of only FTL from *M. extorquens* AM1 did not enable the *E. coli* serine-auxotrophic mutant $\Delta serA\Delta gcvTHP$ to synthesize enough serine from formate and glycine (Yishai et al., 2017). Only the overexpression of endogenous FoID alongside with FTL rescued the growth of this mutant in serine-free medium (Yishai et al., 2017). Another study showed that single overexpression of FTL in *E. coli* had only a rather weak effect on carbon assimilation, less than 10% carbon of proteinogenic methionine and serine became once labeled but the labeling increased to 70% with additional expression of endogenous FoID (Bang and Lee, 2018). Interestingly, over 90% carbon of methionine and serine was labeled in a strain, which overexpressed FTL and the two proteins FchA and MtdA from *M. extorquens* AM1 that form FoID activity. Furthermore, this strain consumed about half of the externally supplied formate within 50 h cultivation, while the *ftl*-expressing strains with endogenous *E. coli* FoID only consumed low formate amounts (Bang and Lee, 2018). Expression FTL and FoID from *Moorella thermoacetica* were also shown to be sufficient to rescue mutant $\Delta serA\Delta gcvP$ with formate and displayed much higher activities than endogenous FoID (Yu and Liao, 2018). The similar result was obtained due to overexpression of the enzymes FTL, Fch and Mtd from *C. ljungdahlii* but not with those from *Acetobacterium woodii* (Tashiro et al., 2018). Therefore, the absence of ^{13}C incorporation into serine from labeled formate was most likely due to the reduced activity of FoID in the *Synechocystis* exFTL strain.

After obtaining these results the question appeared, why did the steady state contents of serine increase and glycine decrease after formate incubation in exFTL? Probably, the enzyme SHMT was inhibited in exFTL in addition to FoID (as shown in Fig. 27). It has been shown that 10-formyl-THF may strongly inhibit Mtd activity of FoID (Dev and Harvey, 1978), which might result in the accumulation of the reaction intermediate 5,10-methenyl-THF converted from 10-formyl-THF in the formate inoculated exFTL strain. Hence, the accumulation of 10-formyl-THF produced in exFTL cells affects the equilibrium state between the C1 units 5,10-methylene-THF and 5,10-methenyl-THF. The latter intermediate can be also used by SHMT to form 5-

Discussion

formyl-THF, which is a strong inhibitor of SHMT (Stover and Schirchs., 1990; Goyer et al., 2005; Collakova et al., 2008). Hence, most likely the serine accumulation in the *Synechocystis* strain exFTL results from the inhibition of SHMT via 5-formyl-THF. This regulatory effect results in the accumulation of serine produced via the phosphoserine pathway and also explains why the product glycine decreased. Cancer cells with suppressed activity in mitochondrial FoID also exhibited increased serine and decreased glycine amounts, which was explained by a regulatory effect on SHMT (Koufaris et al., 2016).

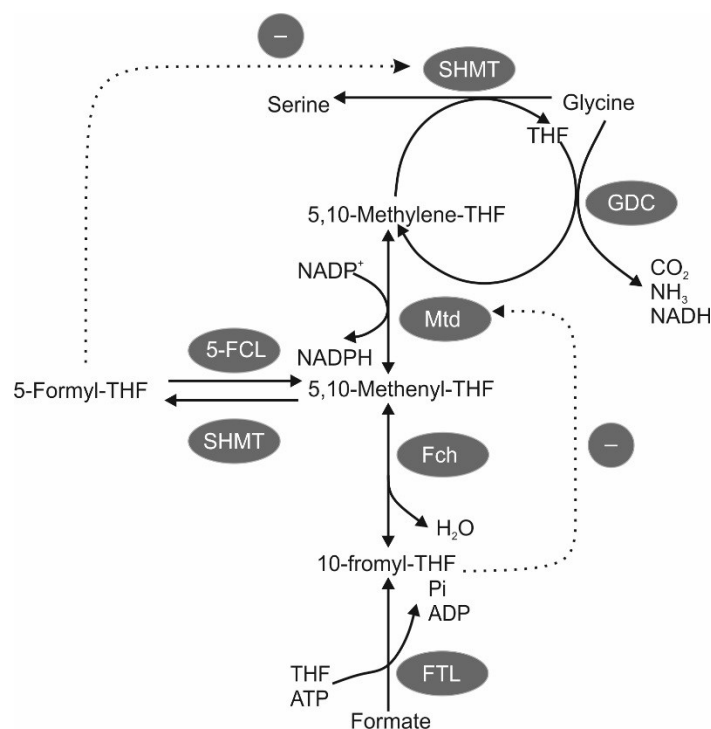


Figure 27: A Scheme displaying the probable interaction of photorespiration and one-carbon metabolism in *Synechocystis*.

5-FCL, 5-formyl-THF cycloligase. Possible SHMT inhibition by 5-formyl-THF as well as Mtd activity inhibition by 10-formyl-THF are shown by a dashed line.

5.6 Attempts to improve FA rate by overexpression of an alternative FoID in wild-type

The above discussed issues clearly indicate that an efficient solution to enhance formate assimilation flux is to express an additional better suited FoID to enhance the serine-forming flux from formate. As discussed, instead of the bifunctional FoID from *Synechocystis*, FoIDs from *M. extorquens* AM1, *M. thermoacetica* and *C. ljungdahlii*, which use two separate

Discussion

enzymes to catalyze the two-step conversion of formyl-THF into 5,10-methylene-THF, are suitable candidates. Considering that gene *ftl* we used originates from *M. extorquens* AM1, genes *fchA* and *mtdA* from the same organism were chosen and expressed in this study to keep consistency. The two genes were synthesized in an artificial operon and successively transferred into the strain exFTL.

To investigate the role of their activities in FA pathway, a synthetic theophylline-dependent riboswitch (Ma et al., 2014) was used to control the expression of *fchA* (Fig. 14A). The available data indicated that probably only the *M. extorquens mtdA* gene was successively expressed in strain exF-C-M (Fig. 14B), because a protein with correct molecular mass was detected in cells of this strain independent from the addition of theophylline (Fig. 15B). The gene *fchA* was also successively transferred into exF-C-M (Fig. 14B). However, the expression of the FchA protein could not be verified, since the His-tag antibody did not detect a protein around 21 kDa in crude extracts of exF-C-M. Most likely the synthetic riboswitch fused to the coding sequence of gene *fchA* could prevent its unsuccessful expression, because the successful expression of the downstream gene *mtdA* showed that the constitutive promoter was active. Here, we used exactly the same riboswitch E published by Ma et al. (2014), which was proven to permit highest levels of expression after induction with theophylline in different cyanobacteria species. However, it has been shown that the expression of only FTL and endogenous FOLD was sufficient to rescue the growth of the *E. coli* serine-auxotrophic mutant $\Delta serA\Delta gcvP$ in serine-free medium after formate addition (Bang and Lee, 2018). Since the accumulated 10-formyl-THF might inhibit the Mtd activity of the bifunctional FOLD as discussed, we hope that the successful expression of FTL and MtdA in this study might also build FA pathway without additional expression of FchA in *Synechocystis*.

We observed retarded growth of the strain exF-C-M in the absence of additional formate but growth was recovered similarly to exFTL in the presence of formate in the medium under ambient air (Fig. 16). A prolonged lag phase was also observed for *E. coli* strains equipped with *M. extorquens* FTL, FchA and MtdA, whereby cells only expressing FTL grew normally

Discussion

(Bang and Lee, 2018). These results suggested that such a rewiring of C1 metabolism made cells more dependent on formate. To test if the FA pathway stimulated cell growth under very low carbon condition, the CO₂ amount in ambient air was reduced using barium hydroxide (Radmer et al., 1978) (Fig. 17). Cells grew very slowly under this condition suggesting the successful depletion of CO₂ in the air. Unfortunately, we did not observe any stimulation of growth with formate in both exFTL and exF-C-M strain. In exF-C-M, the levels of most amino acids increased except glutamate and histidine implying that folate-dependent C1 metabolism affected amino acids homeostasis (Table 5). The most intriguingly observation was the increased glutamate and decreased glutamine in exF-C-M inoculated with formate, the opposite trend with those in exFTL. The increased glutamate/glutamine ratio along with accumulated 2-OG might be a sign of nitrogen depletion (Zhang et al., 2018). A reasonable explanation could be that ammonia release by glycine decarboxylation reaction was inhibited in strain exF-C-M, because an active FA pathway will provide additional carbon fixation from formate via 5,10-methylene-THF. This intermediate, as a product of GDC, inhibits glycine decarboxylation and reduces the release of CO₂ and ammonia. Theoretically, the FA pathway might then contribute to serine synthesis.

The question arises, if higher production of serine could theoretically improve cyanobacterial cell growth. This possibility was tested by serine supplementation in growth experiments with wild-type cells, because *Synechocystis* expresses transport systems for amino acids (Quintero et al., 2001; Eisenhut et al., 2007; Bualuang et al., 2015). Serine supplementation at 10 mM did not stimulate growth of cyanobacterium *Anabaena cylindrica* PCC 7122 compared to cells without serine (Rawson, 1985). Here, we added serine at 10 mM and 20 mM to the *Synechocystis* wild-type. The preliminary growth assay indicated that serine higher than 10 mM rather caused a slight inhibitory effect on growth of *Synechocystis* (Fig. 28). Further growth experiments need to be done with serine at concentration lower than 10 mM also including ¹³C-labeled serine to estimate the potential of increased serine availability on growth of *Synechocystis*. We can at least conclude from this experiment that it will be quite hard to observe a significant growth stimulation from the FA pathway in the wild-type background,

Discussion

since 10 mM of formate can maximal form 10 mM of serine. Therefore, another background is necessary to test FA efficiency. For the alterations of other amino acids, it is hard to explain only with the current data due to the complexity in their regulation mechanisms. For example, the increase of lysine and threonine level in exF-C-M compared to exFTL is still an open question and needs further investigation.

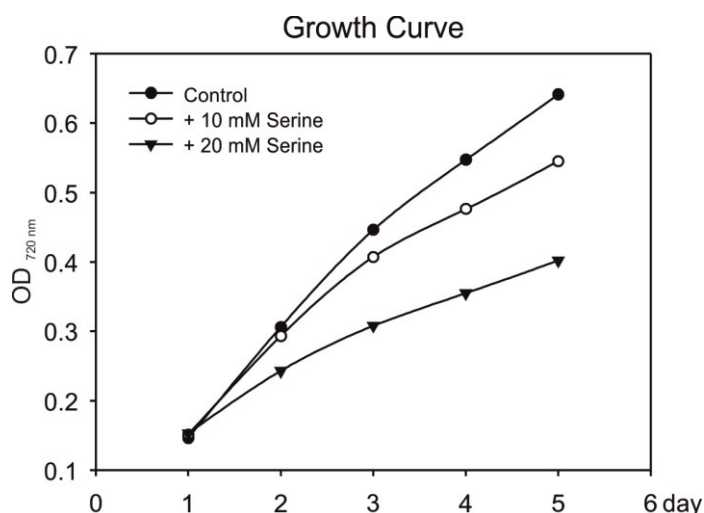


Figure 28: Growth of wild-type feed with different concentration of serine.

Growth of cells was measured in BG11 supplemented with different amount of serine (0 mM (solid circle), 10 mM (open circle) and 20 mM (triangle)). Cells were grown in liquid BG11 in the multi-cultivator at ambient air and $100 \mu\text{mol photons m}^{-2} \text{s}^{-1}$.

5.7 Establishing the FA pathway in ΔcmmM mutant

As discussed above in great detail, it was not possible to observe positive effects of the FA pathway on growth and serine assimilation in the *Synechocystis* wild-type. This is most likely based on the situation that the CCM enables cyanobacteria such as *Synechocystis* to perform efficient carbon fixation even at very low CO_2 levels and it also suppresses photorespiration to much smaller amount than in plants (Orf et al., 2016). Therefore, we assumed that FA pathways may bring higher benefits in a cell background with less efficient CO_2 assimilation and higher photorespiratory flux. For this purpose, we used subsequently the ΔcmmM mutant, where the mutation of the CcmM protein abolishes the formation of carboxysomes thereby disrupting the CCM and stimulating photorespiration (Hackenberg et al. 2012). To test if the

Discussion

establishment of FA pathway reduces the CO₂ dependence of $\Delta ccmM$ mutant, an independent gas mixing system was used to connect with multi-cultivator regulating the concentration of CO₂, allowing to do the growth experiment in a stepwise decreasing CO₂ condition. The expression of FTL in $\Delta ccmM$ mutant initially extended the lag phase. However, during the stepwise reduced CO₂ condition, the FTL-expressing mutant cells still showed growth at 0.4 and even 0.3% CO₂, where the parental mutant already stopped growth. Unfortunately, this effect was found in the presence but also the absence of formate supplementation (Fig. 18C). No huge changes in metabolites were observed with $\Delta ccmM$ when inoculated with formate (Table 6), while most amino acids and intermediates of TCA cycle displayed alterations in $\Delta ccmM$ /exFTL compared to $\Delta ccmM$ representing the introduction of FTL did affect the endogenous metabolisms. Interestingly, the accumulation of serine observed in exFTL was not found with $\Delta ccmM$ /exFTL supplied with formate. A possible explanation is that the photorespiratory flux of $\Delta ccmM$ /exFTL under the provided CO₂ concentration might be higher than that in exFTL accelerating serine-to-hydroxypyruvate conversion. When FTL and MtdA were simultaneously expressed in $\Delta ccmM$ mutant, similar effects observed before with strain exF-C-M appeared. The new strain $\Delta ccmM$ /exF-C-M showed retarded growth in the absence of formate compared to $\Delta ccmM$ /exFTL. However, the growth retardation was relieved when supplied with formate (Fig. 19B). In the presence of formate, similar growth was observed in the strains $\Delta ccmM$ /exF-C-M and $\Delta ccmM$ /exFTL indicating no further reduction of CO₂ requirement after expression of *fchA* and *mtdA*. However, significant changes were detected in the metabolite profiles (Table 7). The content of glutamine and glutamate decreased nearly by 60% and increased 65%-100%, respectively, in $\Delta ccmM$ /exF-C-M with time. This change resembles the alterations of glutamine and glutamate in strain exF-C-M. Meanwhile, TCA cycle associated intermediates increased approximately 65 - 90%. Accordingly, these changes were most likely related to the reduction of glycine decarboxylation activity as discussed above for the strains with wild-type background. Although FA did not reduce the CO₂ dependence, the FA pathway might be established in the new constructed strain $\Delta ccmM$ /exF-C-M. Further improvement on the FA flux could be done in the $\Delta ccmM$ background, easily validating its

efficiency supporting carbon fixation.

5.8 Attempts to generate a formate-dependent strain on the basis of $\Delta foID$

For the future selection of suitable FDHs as entrance enzyme of the FA pathway, we aimed to generate a formate-dependent *Synechocystis* strain. As shown before in other bacteria (Sah et al., 2015), we assumed that a knockout of *foID* could result in a formate-dependent C1-auxotrophy strain, since supplementation with formate and expression of *ftl* should sustain the synthesis of formyl-THF as precursor for purine synthesis. In the beginning, we verified that the gene encoding FoID was correctly annotated in the *Synechocystis* genome (Fig. 20). Attempts to generate completely segregated mutant $\Delta foID$ by standard interposon-mutagenesis were unsuccessful, despite analysis of a large amount of independent clones (Fig. 21). In all cases, these clones contained both wild-type and mutant gene copies in their genome, which excluded the possibility of failure in transformation. Hence, we are confident in concluding that gene *foID* plays an essential role in *Synechocystis* under our lab condition.

As mentioned above, organism dependent on FoID activity because of its essential product 10-formyl-THF. Hence, FoID could be dispensable when an additional pathway for 10-formyl-THF synthesis or enough external nutrients substituting 10-formyl-THF are provided. The ectopic expression of FTL provides an alternative route for 10-formyl-THF synthesis from formate, which enabled the complete deletion of *foID* in *Leishmania major* (Murta et al., 2009). Similar results were obtained in *E. coli* by expression of heterologous FTL from *Clostridium perfringens* but the mutant depended on formate and glycine (Sah et al., 2015). In this study, plasmid pT-0753-k to generate mutant $\Delta foID$ was transformed into the previously obtained FTL-expressing strain exFTL. But mutation in *foID* was still not segregated even after long-term formate supplementation (Fig. 22). We doubted that the production of 10-formyl-THF synthesized through FTL was insufficient to meet the requirement for purine biosynthesis. The lower rate of formate uptake (Fig. 25) might not satisfy the demand on formate of FTL which was reported with K_m 22 mM for formate (Marx et al., 2003). It has been shown that the introduction of FTL enabled *E. coli* to lose gene *foID*, but 10-formyl-THF in this mutant displayed significantly lower level compared to the control strain (Sah et al., 2015). Thus,

Discussion

inosine or IMP, the important intermediates in the purine synthesis together with formate was supplied to inoculate the non-segregated mutant *exFTL/ΔfoID*. After several rounds of selections, 90 clones were investigated with PCR (Fig. 23). The mutant gene copies seemed to become enriched with the inoculation time, but none of the clones completely lost gene *foID*. Our result suggested that except the synthesis of 10-formyl-THF as purine synthesis precursor, FoID might also have important function in other metabolisms in *Synechocystis*. For example, as one product of FoID, 5,10-methenyl-THF acts as a cofactor of photolyase in algae (Heijde et al., 2010).

Theoretically, an alternative FoID should be able to compensate the absence of the endogenous FoID. Accordingly, plasmid pT-0753-k was transformed into the *exF-C-M* strain generated in this study, which expresses in addition to FTL the FoID from *M. extorquens*. Indeed, with supplementation of formate during the transformation process, a segregated null mutant $\Delta foID$ was obtained with additional expression of FTL and MtdA (Fig. 24). Although the null mutant can survive without formate, it grew very slowly and formate clearly rescued its growth as shown in the preliminary growth assay (Fig. 29). These results implied that formate-dependent FA pathway might be established in mutant $\Delta foID$ with the expression of FTL and MtdA providing C1 units from formate. The result also shows that the new constructed mutant has the potent for screening suitable FDHs for the further research.

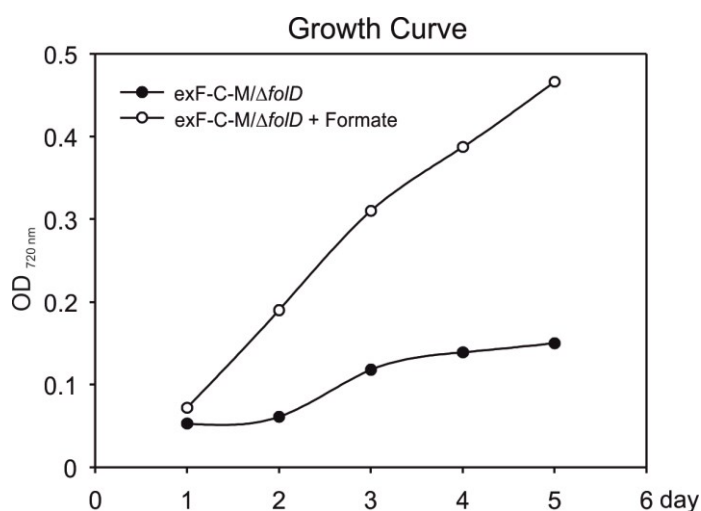


Figure 29: Growth of *exF-C-M/ΔfoID* in the presence or in the absence of external formate.

Growth of cells was measured supplied either with (open circle) or without (solid circle) 10 mM formate. Cells were grown in liquid BG11 in the multi-cultivator at ambient air under 100 $\mu\text{mol photons m}^{-2} \text{s}^{-1}$.

5.9 Future perspectives

Although we are not able to show whether the FA pathway stimulates the growth of *Synechocystis*, the mutant $\Delta foID$ dependent on formate was developed. Its use paves the way to test suitable FDHs in the *Synechocystis*. Moreover, this strain should be also used to analyze whether serine could improve cell growth. The effect of lower concentration of serine on growth is needed to be investigated. In our study, we could only test to improve FA efficiency by enhancing FoID activity via the expression of MtdA, indicating from that the overexpression of FTL and MtdA stimulate the growth of transgenic strains in the presence of formate. Future studies are needed to further improve FoID through the introduction of both enzyme activities Fch and Mtd. Besides, our study shows that high CO₂-requiring mutant $\Delta ccmM$ is more suitable background to test FA efficiency. With the free adjusted CO₂ concentration cultivator, the CO₂ dependence of $\Delta ccmM$ engineered with FA pathway could be easily monitored. Additionally, formate assimilation through reverse glycine pathway to synthesize glycine from CO₂ was already constructed in *E. coli* (Bang and Lee, 2018; Yishai et al., 2018), which could also be tested in $\Delta ccmM$. ¹³C isotope analysis is also required to verify ¹³C-labeling serine in the newly designed strain fed with ¹³C-formate. Attempts to obtain an absolute serine auxotroph strain $\Delta serA$ can be tried on this basis.

In addition, one intriguingly point is the unexpected accumulation of AABA in FTL-expressing strain. AABA is used as an important chiral intermediate for the production of several important drugs including the anticonvulsant brivaracetam, levetiracetam and ethambutol (Zhang et al. 2009; Seo et al., 2012). But it is still a huge challenge to achieve the high-level production in commercial systems. Our study might provide a good vision in investigating the synthetic mechanism of AABA. Furthermore, we observed many more unexpected changes in the primary metabolism of *Synechocystis*, which probably are connected to imbalances in the C1 homeostasis, which is generally not well understood. Possibly, some of the strains generated here could be also used in future studies to analyze regulatory impact of formyl-THF and related compounds in more detail.

6 Reference

- Raven JA, Cockell CS, De La Rocha CL (2008) The Evolution of Inorganic Carbon Concentrating Mechanisms in Photosynthesis. *Philos Trans R Soc B Biol Sci* **363**: 2641–2650
- Alissandratos A, Kim H-K, Easton CJ (2013) Formate Production Through Biocatalysis. *Bioengineered* **4**: 348–350
- Ambard-Bretteville F, Sorin C, Rébeillé F, Hourton-Cabassa C, Colas Des Francs-Small C (2003) Repression of Formate Dehydrogenase in *Solanum Tuberosum* Increases Steady-state Levels of Formate and Accelerates the Accumulation of Proline in Response to Osmotic Stress. *Plant Mol Bio* **52**: 1153–1168
- Azizan KA, Resson HW, Mendoza ER, Baharum SN (2017) ¹³C Based Proteinogenic Amino Acid (PAA) and Metabolic Flux Ratio Analysis of *Lactococcus Lactis* Reveals Changes in Pentose Phosphate (PP) Pathway in Response to Agitation and Temperature Related Stresses. *PeerJ* **5**: 3451–3451
- Bang J, Lee SY (2018) Assimilation of Formic Acid and CO₂ by Engineered *Escherichia Coli* Equipped with Reconstructed One-carbon Assimilation Pathways. *Proc Natl Acad Sci* **115**: 9271–9279
- Bar-Even A (2018) Daring Metabolic Designs for Enhanced Plant Carbon Fixation. *Plant Sci* **273**: 71–83
- Bar-Even A, Noor E, Lewis NE, Milo R (2010) Design and Analysis of Synthetic Carbon Fixation Pathways. *Proc Natl Acad Sci* **107**: 8889–8894
- Bauwe H, Hagemann M, Fernie AR (2010) Photorespiration: Players, Partners and Origin. *Trends Plant Sci* **15**: 330–336
- Berg IA, Kockelkorn D, Buckel W, Fuchs G (2007) A 3-Hydroxypropionate/4-Hydroxybutyrate Autotrophic Carbon Dioxide Assimilation Pathway in Archaea. *Science* **318**: 1782-1786.
- Birkmann A, Zinoni F, Sawers G, Böck A (1987) Factors Affecting Transcriptional Regulation of the Formate-hydrogen-lyase Pathway of *Escherichia Coli*. *Arch Microbiol* **148**: 44–51
- Blankenship RE, Tiede DM, Barber J, Brudvig GW, Fleming G, Ghirardi M, Gunner MR, Junge W, Kramer DM, Melis A, et al (2011) Comparing Photosynthetic and Photovoltaic Efficiencies and Recognizing the Potential for Improvement Downloaded from. *Science* **332**: 805–809
- Blume C, Behrens C, Eubel H, Braun H-P, Peterhansel C (2013) A Possible Role for the Chloroplast Pyruvate Dehydrogenase Complex in Plant Glycolate and Glyoxylate Metabolism. *Phytochemistry* **95**: 168–176
- Bonacci W, Teng PK, Afonso B, Niederholtmeyer H, Grob P, Silver PA, Savage DF (2012) Modularity of a Carbon-fixing Protein Organelle. *Proc Natl Acad Sci* **109**: 478–483
- Bräutigam A, Hoffmann-Benning S, Weber APM (2008) Comparative Proteomics of Chloroplast Envelopes from C₃ and C₄ Plants Reveals Specific Adaptations of the Plastid Envelope to C₄ Photosynthesis and Candidate Proteins Required for Maintaining C₄ Metabolite Fluxes. *Plant Physiol* **148**: 568–579

Reference

- Bualuang A, Incharoensakdi A** (2015) Growth Enhancing Effect of Exogenous Glycine and Characterization of its Uptake in Halotolerant Cyanobacterium *Aphanothece halophytica*. *World J Microb Biot* **31**: 379–384
- Bualuang A, Kageyama H, Tanaka Y, Incharoensakdi A, Takabe T** (2015) Functional Characterization of a Member of Alanine or Glycine: Cation Symporter Family in Halotolerant Cyanobacterium *Aphanothece halophytica*. *Biosci Biotechnol Biochem* **79**: 230–235
- von Caemmerer S, Evans JR** (2010) Enhancing C₃ Photosynthesis. *Plant Physiol* **154**: 589–592
- von Caemmerer S, Farquhar GD** (1981) Some Relationships Between the Biochemistry of Photosynthesis and the Gas Exchange of Leaves. *Planta* **153**: 376–387
- von Caemmerer S, Quick WP, Furbank RT** (2012) The Development of C₄ Rice: Current Progress and Future Challenges. *Science* **336**: 1671–1672
- Cai F, Bernstein SL, Wilson SC, Kerfeld CA** (2016) Production and Characterization of Synthetic Carboxysome Shells with Incorporated Luminal Proteins. *Plant Physiol* **170**: 1868–1877
- Cameron JC, Wilson SC, Bernstein SL, Kerfeld CA** (2013) Biogenesis of a Bacterial Organelle: The Carboxysome Assembly Pathway. *Cell* **155**: 1131–1140
- Carreras CW, Santi D V** (1995) The Catalytic Mechanism and Structure of Thymidylate Synthase. *Annu Rev Biochem* **64**: 721–762
- Carvalho J de FC, Madgwick PJ, Powers SJ, Keys AJ, Lea PJ, Parry MAJ** (2011) An Engineered Pathway for Glyoxylate Metabolism in Tobacco Plants Aimed to Avoid the Release of Ammonia in Photorespiration. *BMC Biotechnol* **11**: 1–17
- Chatterjee A, Basu A** (2011) Rubisco: Limitations and Re-engineering for a Better Enzyme. *Int Res J Plant Sci* **2**: 22–24
- Choe H, Joo JC, Cho DH, Kim MH, Lee SH, Jung KD, Kim YH** (2014) Efficient CO₂-reducing Activity of NAD-dependent Formate Dehydrogenase from *Thiobacillus* sp. KNK65MA for Formate Production from CO₂ Gas. *PLoS One* **9**: 103111
- Christensen KE, MacKenzie RE** (2006) Mitochondrial One-carbon Metabolism is Adapted to the Specific Needs of Yeast, Plants and Mammals. *BioEssays* **28**: 595–605
- Clark JE, Ljungdahl LG** (1984) Purification and Properties of 5,10-Methylenetetrahydrofolate Reductase, an Iron-sulfur Flavoprotein from *Clostridium formicoaceticum*. *J Biol Chem* **259**: 10845–10849
- Collakova E, Goyer A, Naponelli V, Krassovskaya I, Gregory JF, Hanson AD, Shachar-Hill Y** (2008) *Arabidopsis* 10-Formyl Tetrahydrofolate Deformylases Are Essential for Photorespiration. *Plant Cell* **20**: 1818–1832
- Cotton CA, Edlich-Muth C, Bar-Even A** (2018) Reinforcing Carbon Fixation: CO₂ Reduction Replacing and Supporting Carboxylation. *Curr Opin Biotechnol* **49**: 49–56
- Dalal J, Lopez H, Vasani NB, Hu Z, Swift JE, Yalmanchili R, Dvora M, Lin X, Xie D, Qu R, et al** (2015) A Photorespiratory Bypass Increases Plant Growth and Seed Yield in Biofuel Crop *Camelina sativa*. *Biotechnol Biofuels* **8**: 175
- Dartois V, Liu J, Hoch JA** (2003) Alterations in the Flow of One-carbon Units Affect KinB-

Reference

- dependent Sporulation in *Bacillus Subtilis*. *Mol Microbiol* **25**: 39–51
- Dellero Y, Lamothe-Sibold M, Jossier M, Hodges M** (2015). *Arabidopsis thaliana ggt1* Photorespiratory Mutants Maintain Leaf Carbon/Nitrogen Balance by Reducing RuBisCO Content and Plant Growth. *Plant J* **83**: 1005-1018.
- Denton AK, Simon R, Weber AP** (2013) C₄ Photosynthesis: from Evolutionary Analyses to Strategies for Synthetic Reconstruction of the Trait. *Curr Opin Plant Biol* **16**: 315–321
- Dev IK, Harvey RJ** (1978) A Complex of N⁵,N¹⁰-Methylenetetrahydrofolate Dehydrogenase and N⁵,N¹⁰-Methenyltetrahydrofolate Cyclohydrolase in *Escherichia Coli*. Purification, Subunit Structure, and Allosteric Inhibition by N¹⁰-Formyltetrahydrofolate. *J Biol Chem* **253**: 4245–4253
- Drake HL, Gößner AS, Daniel SL** (2008) Old Acetogens, New Light. *Ann N Y Acad Sci* **1125**: 100–128
- Durall C, Lindblad P** (2015) Mechanisms of Carbon Fixation and Engineering for Increased Carbon Fixation in Cyanobacteria. *Algal Res* **11**: 263–270
- Eisenhut M, Bauwe H, Hagemann M** (2007) Glycine Accumulation is Toxic for the Cyanobacterium *Synechocystis* sp. strain PCC 6803, but Can Be Compensated by Supplementation with Magnesium Ions. *FEMS Microbiol Lett* **277**: 232–237
- Eisenhut M, Kahlon S, Hasse D, Ewald R, Lieman-Hurwitz J, Ogawa T, Ruth W, Bauwe H, Kaplan A, Hagemann M** (2006) The Plant-like C₂ Glycolate Cycle and the Bacterial-Like Glycerate Pathway Cooperate in Phosphoglycolate Metabolism in Cyanobacteria. *Plant Physiol* **142**: 333–342
- Eisenhut M, Matthijs HCP, Bauwe H, Hagemann M** (2008a) Oxalate Decarboxylase is Involved in Turnover of 2-Phosphoglycolate in *Synechocystis* sp. Strain PCC 6803. *Photosynth. Energy from Sun*. Springer Netherlands, Dordrecht, 815–818
- Eisenhut M, Ruth W, Haimovich M, Bauwe H, Kaplan A, Hagemann M** (2008b) The Photorespiratory Glycolate Metabolism is Essential for Cyanobacteria and Might Have Been Conveyed Endosymbiotically to Plants. *Proc Natl Acad Sci* **105**: 17199–17204
- Erb TJ, Jones PR, Bar-Even A** (2017) Synthetic Metabolism: Metabolic Engineering Meets Enzyme Design. *Curr Opin Chem Biol* **37**: 56–62
- Erb TJ, Zarzycki J** (2016) Biochemical and Synthetic Biology Approaches to Improve Photosynthetic CO₂-fixation. *Curr Opin Chem Biol* **34**: 72–79
- Evans LT** (1997) Adapting and Improving Crops: The Endless Task. *Philos Trans R Soc B Biol Sci* **352**: 901–906
- Fahnenstich H, Scarpeci TE, Valle EM, Flügge U-I, Maurino VG** (2008) Generation of Hydrogen Peroxide in Chloroplasts of *Arabidopsis* Overexpressing Glycolate Oxidase as an Inducible System to Study Oxidative Stress. *Plant Physiol* **148**: 719–729
- Fan M, Shen J, Yuan L, Jiang R, Chen X, Davies WJ, Zhang F** (2012) Improving Crop Productivity and Resource Use Efficiency to Ensure Food Security and Environmental Quality in China. *J Exp Bot* **63**: 13–24
- Feller U, Anders I, Mae T** (2008) Rubiscolytics: Fate of Rubisco after its Enzymatic Function in a Cell is Terminated. *J Exp Bot* **59**: 1615–1624
- Feng L, Wang K, Li Y, Tan Y, Kong J, Li H, Li Y, Zhu Y** (2007) Overexpression of SBPase

Reference

- Enhances Photosynthesis Against High Temperature Stress in Transgenic Rice Plants. *Plant Cell Rep* **26**: 1635–1646
- Ferla MP, Patrick WM** (2014) Bacterial Methionine Biosynthesis. *Microbiol* **160**: 1571–1584
- Fischer RA, Edmeades GO** (2010) Breeding and Cereal Yield Progress. *Crop Sci* **50**: 85–98
- Florian A, Araújo Jo WL, Fernie & AR, Fernie CAR, Weber EA** (2013) New Insights into Photorespiration Obtained from Metabolomics. *Plant Biol* **15**: 656–666
- Florian A, Obata T, Fernie AR, Bauwe H, Timm S** (2016) On the Metabolic Interactions of (Photo)respiration. *J Exp Bot* **67**: 3003–3014
- Fuchs G** (2011) Alternative Pathways of Carbon Dioxide Fixation: Insights into the Early Evolution of Life? *Annu Rev Microbiol* **65**: 631–658
- Gowik U, Bräutigam A, Weber KL, Weber APM, Westhoff P** (2011) Evolution of C₄ Photosynthesis in the Genus *Flaveria*: How Many and Which Genes Does It Take to Make C₄? *Plant Cell* **23**: 2087–2105
- Goyer A, Collakova E, Díaz De La Garza R, Quinlivan EP, Williamson J, Iii JFG, Shachar-Hill Y, Hanson AD** (2005) 5-Formyltetrahydrofolate Is an Inhibitory but Well Tolerated Metabolite in *Arabidopsis* Leaves. *J Biol Chem* **280**: 26137–26142
- Grigorieva G, Shestakov S** (1982) Transformation in the Cyanobacterium *Synechocystis* sp. 6803. *FEMS Microbiol Lett* **13**: 367–370
- Guillouet S, Rodal AA, An G-H, Lessard PA, Sinskey AJ** (1999) Expression of the *Escherichia Coli* Catabolic Threonine Dehydratase in *Corynebacterium Glutamicum* and Its Effect on Isoleucine Production. *Appl Environ Microbiol* **65**: 3100–3107
- Haake V, Geiger M, Walch-Liu P, Engels C, Zrenner R, Stitt M** (1999) Changes in Aldolase Activity in Wild-type Potato Plants are Important for Acclimation to Growth Irradiance and Carbon Dioxide Concentration, Because Plastid Aldolase Exerts Control over the Ambient Rate of Photosynthesis Across a Range of Growth Condition. *Plant J* **17**: 479–489
- Hackenberg C, Huege J, Engelhardt A, Wittink F, Laue M, Matthijs HCP, Kopka J, Bauwe H, Hagemann M** (2012) Low-Carbon Acclimation in Carboxysome-less and Photorespiratory Mutants of the Cyanobacterium *Synechocystis* sp. Strain PCC 6803. *Microbiology* **158**: 398–413
- Hagemann M, Bauwe H** (2016) Photorespiration and the Potential to Improve Photosynthesis What is Photorespiration? *Curr Opin Chem Biol* **35**: 109–116
- Hagemann M, Oberpichler I, Bauwe H, Boldt R, Vinnemeier J** (2005) The Glycine Decarboxylase Complex is not Essential for the Cyanobacterium *Synechocystis* sp. Strain PCC 6803. *Plant Biol* **7**: 15–22
- Hall, T** (2011). BioEdit: an Important Software for Molecular Biology. *GERF Bull Biosci* **2**: 60–61
- Hanson AD, Roje S** (2001) One-carbon Metabolism in Higher Plants. *Annu Rev Plant Physiol Plant Mol Biol* **52**: 119–137
- Harrison EP, Willingham NM, Lloyd JC, Raines CA** (1998) Reduced Sedoheptulose-1,7-bisphosphatase Levels in Transgenic Tobacco Lead to Decreased Photosynthetic Capacity and Altered Carbohydrate Accumulation. *Planta* **204**: 27–36
- Häusler RE, Hirsch H-J, Kreuzaler F, Peterhä Nsel C** (2002) Overexpression of C₄-cycle

Reference

- Enzymes in Transgenic C₃ Plants: a Biotechnological Approach to Improve C₃-Photosynthesis. *J Exp Bot* **53**: 591–607
- Häusler RE, Rademacher T, Li J, Lipka V, Fischer KL, Schubert S, Kreuzaler F, Hirsch H-J** (2001) Single and Double Overexpression of C₄-cycle Genes Had Differential Effects on the Pattern of Endogenous Enzymes, Attenuation of Photorespiration and on Contents of UV Protectants in Transgenic Potato and Tobacco Plants. *J Exp Bot* **52**: 1785–1803
- Heijde M, Zabulon G, Corellou F, Ishikawa T, Brazard J, Usman A, Sanchez F, Plaza P, Martin M, Falciatore A, et al** (2010) Characterization of Two Members of the Cryptochrome/Photolyase family from *Ostreococcus Tauri* Provides Insights into the Origin and Evolution of Cryptochromes. *Plant, Cell Environ* **33**: 1614–1626
- Henkes S** (2001) A Small Decrease of Plastid Transketolase Activity in Antisense Tobacco Transformants Has Dramatic Effects on Photosynthesis and Phenylpropanoid Metabolism. *Plant Cell Online* **13**: 535–551
- Heyer H, Krumbein WE** (1991) Excretion of Fermentation Products in Dark and Anaerobically Incubated Cyanobacteria. *Arch Microbiol* **155**: 284–287
- Heyer H, Stal L, Krumbein WE** (1989) Simultaneous Heterolactic and Acetate Fermentation in the Marine Cyanobacterium *Oscillatoria Limosa* Incubated Anaerobically in the Dark. *Arch Microbiol* **151**: 558–564
- Hibberd JM, Sheehy JE, Langdale JA** (2008) Using C₄ Photosynthesis to Increase the Yield of Rice—rationale and Feasibility. *Curr Opin Plant Biol* **11**: 228–231
- Himanen M, Prochazka P, Hänninen K, Oikari A** (2012) Phytotoxicity of Low-weight Carboxylic Acids. *Chemosphere* **88**: 426–431
- Ho Lee W, Woo Sung M, Hee Kim J, Kwan Kim Y, Han A, Yeon Hwang K** (2011) Crystal Structure of Bifunctional 5,10-Methylenetetrahydrofolate Dehydrogenase/Cyclohydrolase from *Thermoplasma Acidophilum*. *Biochem Biophys Res Commun* **406**: 459–463
- Hourton-Cabassa C, Ambard-Bretteville F, Moreau F, de Virville JD, Rémy R, Colas des Francs-Small C** (1998) Stress Induction of Mitochondrial Formate Dehydrogenase in Potato Leaves. *Plant Physiol* **116**: 627–635
- Igamberdiev AU, Eprintsev AT** (2016) Organic Acids: The Pools of Fixed Carbon Involved in Redox Regulation and Energy Balance in Higher Plants. *Front Plant Sci* **7**: 1042
- Ikeuchi M, Tabata S** (2001) *Synechocystis* sp. PCC 6803 - a Useful Tool in the Study of the Genetics of Cyanobacteria. *Photosynth Res* **70**: 73–83
- Jabrin S, Ravanel S, Gambonnet B, Douce R, Rébeillé F** (2003) One-carbon Metabolism in Plants. Regulation of Tetrahydrofolate Synthesis during Germination and Seedling Development. *Plant Physiol* **131**: 1431–1439
- Jhee K-H, McPhie P, Miles EW** (2000) Domain Architecture of the Heme-Independent Yeast Cystathionine β -Synthase Provides Insights into Mechanisms of Catalysis and Regulation. *Biochemistry* **39**: 10548–10556
- Jormakka M, Byrne B, Iwata S** (2003) Formate Dehydrogenase - A Versatile Enzyme in Changing Environments. *Curr Opin Struct Biol* **13**: 418–423
- Jormakka M, Törnroth S, Byrne B, Iwata S** (2002) Molecular Basis of Proton Motive Force Generation: Structure of Formate Dehydrogenase-N. *Science* **295**: 1863–1868

Reference

- Kamennaya NA, Ahn S, Park H, Bartal R, Sasaki KA, Holman H-Y, Jansson C** (2015) Installing Extra Bicarbonate Transporters in the Cyanobacterium *Synechocystis* sp. PCC6803 Enhances Biomass Production. *Metab Eng* **29**: 76–85
- Kang RJ, Shi DJ, Cong W, Ma WM, Cai ZL, Ouyang F** (2005) Effects of Co-expression of Two Higher Plants Genes ALD and TPI in *Anabaena* sp. PCC7120 on Photosynthetic CO₂ Fixation. *Enzyme Microb Technol* **36**: 600–604
- Kebeish R, Niessen M, Thiruveedhi K, Bari R, Hirsch H-J, Rosenkranz R, Stähler N, Schönfeld B, Kreuzaler F, Peterhänsel C** (2007) Chloroplastic Photorespiratory Bypass Increases Photosynthesis and Biomass Production in *Arabidopsis Thaliana*. *Nat Biotechnol*. **5**: 593-599
- Kerfeld CA, Melnicki MR** (2016) Assembly, Function and Evolution of Cyanobacterial Carboxysomes. *Curr Opin Plant Biol* **31**: 66–75
- Khozaei M, Fisk S, Lawson T, Gibon Y, Sulpice R, Stitt M, Lefebvre SC, Raines CA** (2015) Overexpression of Plastid Transketolase in Tobacco Results in a Thiamine Auxotrophic Phenotype. *Plant Cell* **27**: 432–447
- Klemke F, Baier A, Knoop H, Kern R, Jablonsky J, Beyer G, Volkmer T, Steuer R, Lockau W, Hagemann M** (2015) Identification of the Light-independent Phosphoserine Pathway as an Additional Source of Serine in the Cyanobacterium *Synechocystis* sp. PCC 6803. *Microbiol*, **161**: 1050–1060
- Koufaris C, Gallage S, Yang T, Lau C-H, Valbuena GN, Keun HC** (2016) Suppression of MTHFD2 in MCF-7 Breast Cancer Cells Increases Glycolysis, Dependency on Exogenous Glycine, and Sensitivity to Folate Depletion. *J Proteome Res* **15**: 16
- Ku MSB, Agarie S, Nomura M, Fukayama H, Tsuchida H, Ono K, Hirose S, Toki S, Miyao M, Matsuoka M** (1999) High-level Expression of Maize Phosphoenolpyruvate Carboxylase in Transgenic Rice Plants. *Nat Biotechnol* **17**: 76–80
- Kuchmina E, Wallner T, Kryazhov S, Zinchenko VV, Wilde A** (2012) An Expression System for Regulated Protein Production in *Synechocystis* sp. PCC 6803 and its Application for Construction of a Conditional Knockout of the Ferrochelatase Enzyme. *J Biotechnol* **162**: 75–80
- Lefebvre S** (2005) Increased Sedoheptulose-1,7-Bisphosphatase Activity in Transgenic Tobacco Plants Stimulates Photosynthesis and Growth from an Early Stage in Development. *Plant Physiol* **138**: 451–460
- Leonhartsberger S, Korsa I, Böck A** (2002) The Molecular Biology of Formate Metabolism in Enterobacteria. *J Mol Microbiol Biotechnol* **4**: 269–276
- Li P, Ponnala L, Gandotra N, Wang L, Si Y, Lori Tausta S, Kebrom TH, Provart N, Patel R, Myers CR, et al** (2010) The Developmental Dynamics of the Maize Leaf Transcriptome. *Nat Genet* **42**: 1060–1067
- Li R, Moore M, Bonham-Smith PC, King J** (2002) Overexpression of Formate Dehydrogenase in *Arabidopsis Thaliana* Resulted in Plants Tolerant to High Concentrations of Formate. *J Plant Physiol* **10**: 1069
- Lin MT, Occhialini A, Andralojc PJ, Parry MAJ, Hanson MR** (2014) A Faster Rubisco with Potential to Increase photosynthesis in Crops. *Nature* **513**: 547–550

Reference

- Lindahl PA, Münck E, Ragsdale SW** (1990) CO Dehydrogenase from *Clostridium Thermoaceticum*. EPR and Electrochemical Studies in CO₂ and Argon Atmospheres. *J Biol Chem* **265**: 3873–3879
- Ljungdahl LG** (1986) The Autotrophic Pathway of Acetate Synthesis in Acetogenic Bacteria. *Appl Microbiol Biotechnol* **40**: 415–450
- Ljungdahl LG, O'Brien WE, Moore MR, Liu M-T** (1980) Methylenetetrahydrofolate Dehydrogenase from *Clostridium Formicoaceticum* and Methylenetetrahydrofolate Dehydrogenase, Methenyltetrahydrofolate Cyclohydrolase (combined) from *Clostridium Thermoaceticum*. *Methods Enzymol* **66**: 599–609
- Long BM, Yih Hee W, Sharwood RE, Rae BD, Kaines S, Lim Y-L, Nguyen ND, Massey B, Bala S, Von Caemmerer S, et al** (2018) Carboxysome Encapsulation of the CO₂-fixing Enzyme Rubisco in Tobacco Chloroplasts. *Nat Commun* **1**: 3570–3584
- Long SP, Zhu XG, Naidu SL, Ort DR** (2006) Can Improvement in Photosynthesis Increase Crop Yields? *Plant, Cell Environ* **29**: 315–330
- Lovell CR, Przybyla A, Ljungdahl LG** (1988) Cloning and Expression in *Escherichia Coli* of the *Clostridium Thermoaceticum* Gene Encoding Thermostable Formyltetrahydrofolate Synthetase. *Arch Microbiol* **149**: 280–285
- Lu SC** (2000) S-Adenosylmethionine. *Int J Biochem Cell Biol* **32**: 391–395
- Lü W, Du J, Wacker T, Gerbig-Smentek E, Andrade SLA, Einsle O** (2011) pH-Dependent Gating in a FocA Formate Channel. *Science* **332**: 352–354
- Ma AT, Schmidt CM, Golden JW** (2014) Regulation of Gene Expression in Diverse Cyanobacterial Species by Using Theophylline-responsive Riboswitches. *Appl Environ Microbiol* **80**: 6704–6713
- Ma W, Wei L, Wang Q, Shi D, Chen H** (2008) Increased Activity of the Tandem Fructose-1,6-bisphosphate Aldolase, Triosephosphate Isomerase and Fructose-1,6-bisphosphatase Enzymes in *Anabaena* sp. Strain PCC 7120 Stimulates Photosynthetic Yield. *J Appl Phycol* **20**: 437–443
- Maia LB, Moura I, Moura JJG** (2017) Molybdenum and Tungsten-containing Formate Dehydrogenases: Aiming to Inspire a Catalyst for Carbon Dioxide Utilization. *Inorganica Chim Acta* **455**: 350–363
- Maia LB, Moura JJG, Moura I** (2015) Molybdenum and Tungsten-dependent Formate Dehydrogenases. *J Biol Inorg Chem* **20**: 287–309
- Maier A, Fahnenstich H, von Caemmerer S, Engqvist MKM, Weber APM, Flügge U-I, Maurino VG** (2012) Transgenic Introduction of a Glycolate Oxidative Cycle into *A. Thaliana* Chloroplasts Leads to Growth Improvement. *Front Plant Sci* **3**: 38
- Majeran W, Cai Y, Sun Q, van Wijk KJ** (2005) Functional Differentiation of Bundle Sheath and Mesophyll Maize Chloroplasts Determined by Comparative Proteomics. *Plant Cell* **17**: 3111–3140
- Majeran W, van Wijk KJ** (2009) Cell-type-specific Differentiation of Chloroplasts in C₄ plants. *Trends Plant Sci* **14**: 100–109
- Marx CJ, Laukel M, Vorholt JA, Lidstrom ME** (2003) Purification of the Formate-tetrahydrofolate Ligase from *Methylobacterium Exorquens* AM1 and Demonstration of Its

Reference

- Requirement for Methylotrophic Growth. *J Bacteriol* **185**: 7169–7175
- McGrath JM, Long SP** (2014) Can the Cyanobacterial Carbon-concentrating Mechanism Increase Photosynthesis in Crop Species? A Theoretical Analysis. *Plant Physiol* **164**: 2247–2261
- Miyagawa Y, Tamoi M, Shigeoka S** (2001) Overexpression of a Cyanobacterial Fructose-1,6-/sedoheptulose-1,7-bisphosphatase in Tobacco Enhances Photosynthesis and Growth. *Nat. Biotechnol* **19**: 965–969
- Murta SMF, Vickers TJ, Scott DA, Beverley SM** (2009) Methylene Tetrahydrofolate Dehydrogenase/Cyclohydrolase and the Synthesis of 10-CHO-THF Are Essential in *Leishmania Major*. *Mol Microbiol* **71**: 1386–1401
- Nagasawa T, Kanzaki H, Yamada H** (1984) Cystathionine Gamma-lyase of *Streptomyces Phaeochromogenes*. The Occurrence of Cystathionine Gamma-lyase in Filamentous Bacteria and its Purification and Characterization. *J Biol Chem* **259**: 10393–10403
- Nakamura Y, Kanakagiri S, Van K, He W, Spalding MH** (2005) Disruption of the Glycolate Dehydrogenase Gene in the High-CO₂-requiring Mutant HCR89 of *Chlamydomonas Reinhardtii*. *Can J Bot* **83**: 820–833
- Nakamura Y, Kaneko T, Hirose M, Miyajima N, Tabata S** (1998) CyanoBase, a www Database Containing the Complete Nucleotide Sequence of the Genome of *Synechocystis* sp. Strain PCC6803. *Nucleic Acids Res* **26**: 63–67
- Nguyen BT, Rittmann BE** (2016) Effects of Inorganic Carbon and pH on Growth Kinetics of *Synechocystis* sp. PCC 6803. *Algal Res* **19**: 363–369
- Nielsen BL, Misra BB, Mitsui T, Uehara S, Adachi F, Ito-Inaba Y, Inaba T** (2016) Specific and Efficient Targeting of Cyanobacterial Bicarbonate Transporters to the Inner Envelope Membrane of Chloroplasts in *Arabidopsis*. *Front Plant Sci* **7**: 115905
- Nölke G, Houdelet M, Kreuzaler F, Peterhänsel C, Schillberg S** (2014) The Expression of a Recombinant Glycolate Dehydrogenase Polyprotein in Potato (*Solanum Tuberosum*) Plastids Strongly Enhances Photosynthesis and Tuber Yield. *Plant Biotechnol J* **12**: 734–742
- Norman EG, Colman B** (1992) Formation and Metabolism of Glycolate in the Cyanobacterium *Coccochloris Penicystis*. *Archives of Microbiol* **157**: 375–380.
- Occhialini A, Lin MT, Andralojc PJ, Hanson MR, Parry MAJ** (2016) Transgenic Tobacco Plants with Improved Cyanobacterial Rubisco Expression but no Extra Assembly Factors Grow at Near Wild-type Rates if Provided with Elevated CO₂. *Plant J* **85**: 148–160
- Olcer H** (2001) Photosynthetic Capacity Is Differentially Affected by Reductions in Sedoheptulose-1,7-bisphosphatase Activity during Leaf Development in Transgenic Tobacco Plants. *Plant Physiol* **125**: 982–989
- Olson BJSC, Skavdahl M, Ramberg H, Osterman JC, Markwell J** (2000) Formate Dehydrogenase in *Arabidopsis Thaliana*: Characterization and Possible Targeting to the Chloroplast. *Plant Sci* **159**: 205–212
- Orf I, Timm S, Bauwe H, Fernie AR, Hagemann M, Kopka J, Nikoloski Z** (2016) Can Cyanobacteria Serve as a Model of Plant Photorespiration? – A Comparative Meta-analysis of Metabolite Profiles. *J Exp Bot* **67**: 2941–2952

Reference

- Orr DJ, Pereira AM, Da P, Pereira F, Pereira-Lima ÍA, Zsögön A, Araújo WL** (2017) Engineering Photosynthesis: Progress and Perspectives. *F1000Research* **6**
- Ort DR, Merchant SS, Alric J, Barkan A, Blankenship RE, Bock R, Croce R, Hanson MR, Hibberd JM, Long SP, et al** (2015) Redesigning Photosynthesis to Sustainably Meet Global Food and Bioenergy Demand. *PNAS* **112**: 8529–8536
- Pawełek PD, Allaire M, Cygler M, Mackenzie RE** (2000) Channeling Efficiency in the Bifunctional Methylene-tetrahydrofolate Dehydrogenase/cyclohydrolase Domain: the Effects of Site-directed Mutagenesis of NADP Binding Residues. *Biochimica et Biophysica Acta* **1479**: 59–68
- Pengelly J, Förster B, Von Caemmerer S, Badger MR, Price GD, Whitney SM** (2014) Transplastomic Integration of a Cyanobacterial Bicarbonate Transporter into Tobacco Chloroplasts. *J Exp Bot* **65**: 3071–3080
- Pete S** (2018) Managing the Global Land Resource. *Proc R Soc B Biol Sci* **285**: 20172798
- Peterhansel C, Krause K, Braun H-P, Espie GS, Fernie AR, Hanson DT, Keech O, Maurino VG, Mielewczik M, Sage RF** (2013) Engineering Photorespiration: Current State and Future Possibilities. *Plant Biol* **15**: 754–758
- Quintero MJ, Montesinos ML, Herrero A, Flores E** (2001) Identification of Genes Encoding Amino Acid Permeases by Inactivation of Selected ORFs from the *Synechocystis* Genomic Sequence. *Genome Res* **11**: 2034–2040
- Raaijmakers HCA, Romão MJ** (2006) Formate-reduced *E. Coli* Formate Dehydrogenase H: the Reinterpretation of the Crystal Structure Suggests a New Reaction Mechanism. *JBIC J Biol Inorg Chem* **11**: 849–854
- Radmer R, Kok B, Ollinger O** (1978) Kinetics and Apparent K_m of Oxygen Cycle under Conditions of Limiting Carbon Dioxide Fixation. *Plant Physiol* **61**: 915-917
- Ragsdale SW** (2008) Enzymology of the Wood-Ljungdahl Pathway of Acetogenesis. *Ann N Y Acad Sci* **1125**: 129–136
- Ravanel S** (2011) Metabolism of Foliates in Plants. *Adv Bot Res* **59**: 67–106
- RAWSON DM** (1985) The Effects of Exogenous Amino Acids on Growth and Nitrogenase Activity in the Cyanobacterium *Anabaena Cylindrica* PCC 7122. *Microbiology* **131**: 2549–2554
- Ray DK, Mueller ND, West PC, Foley JA** (2013) Yield Trends Are Insufficient to Double Global Crop Production by 2050. *PLoS One* **8**: 66428
- Roger M, Brown F, Gabrielli W, Sargent F** (2017) Efficient Hydrogen-dependent Carbon Dioxide Reduction by *Escherichia Coli*. *Curr Biol* **28**: 140–145
- Rolland V, Badger MR, Price GD** (2016) Redirecting the Cyanobacterial Bicarbonate Transporters BicA and SbtA to the Chloroplast Envelope: Soluble and Membrane Cargos Need Different Chloroplast Targeting Signals in Plants. *Front Plant Sci* **7**: 185
- Ros R, Muñoz-Bertomeu J, Krueger S** (2014) Serine in Plants: Biosynthesis, Metabolism, and Functions. *Trends Plant Sci* **19**: 564–569
- Rosenthal DM, Locke AM, Khozaei M, Raines CA, Long SP, Ort DR** (2011) Over-expressing the C_3 Photosynthesis Cycle Enzyme Sedoheptulose-1-7 Bisphosphatase Improves Photosynthetic Carbon Gain and Yield under Fully Open Air CO_2 Fumigation (FACE).

Reference

- BMC Plant Biol. **11**: 123
- Sah S, Aluri S, Rex K, Varshney U (2015)** One-carbon Metabolic Pathway Rewiring in *Escherichia Coli* Reveals an Evolutionary Advantage of 10-formyltetrahydrofolate Synthetase (Fhs) in Survival under Hypoxia. *J Bacteriol* **197**: 717–726
- Sah S, Varshney U (2015)** Impact of Mutating the Key Residues of a Bifunctional 5,10-methylenetetrahydrofolate Dehydrogenase-cyclohydrolase from *Escherichia Coli* on Its Activities. *Biochemistry* **54**: 3504–3513
- Schuchmann K, Müller V (2016)** Energetics and Application of Heterotrophy in Acetogenic Bacteria. *Appl Environ Microbiol* **82**: 4056–4069
- Schuler ML, Mantegazza O, Weber APM (2016)** Engineering C₄ Photosynthesis into C₃ Chassis in the Synthetic Biology Age. *Plant J* **87**: 51–65
- Schulz J, Dettlaff S, Fritzsche U, Harms U, Schiebel H, Derer W, Fusenig NE, Hiilsen A, Shm MB (1994)** The Amido Black Assay: a Simple and Quantitative Multipurpose Test of Adhesion, Proliferation, and Cytotoxicity in Microplate Cultures of Keratinocytes (HaCaT) and Other Cell Types Growing Adherently or in Suspension. *J Immunol Methods* **167**: 1–13
- Schwander T, Schada von Borzyskowski L, Burgener S, Cortina NS, Erb TJ (2016)** A Synthetic Pathway for the Fixation of Carbon Dioxide *in vitro*. *Science* **354**: 900–904
- Sedelnikova O V., Hughes TE, Langdale JA (2018)** Understanding the Genetic Basis of C₄ Kranz Anatomy with a View to Engineering C₃ Crops. *Annu Rev Genet* **52**: 249–270
- Selim ASM, Greenberg DM (1959)** An Enzyme that Synthesizes Cystathionine and Deaminates L-Serine. *J Biol Chem* **234**: 1474–1480
- Semin BK, Loviagina ER, Aleksandrov AY, Kaurov YN, Novakova AA (1990)** Effect of Formate on Mössbauer Parameters of the Non-heme Iron of PS II Particles of Cyanobacteria. *FEBS Lett* **270**: 184–186
- Seo Y-M, Mathew S, Bea H-S, Khang Y-H, Lee S-H, Kim B-G, Yun H (2012)** Deracemization of Unnatural Amino Acid: Homoalanine Using D-Amino Acid Oxidase and ω -transaminase. *Org Biomol Chem* **10**: 2482
- Sharwood RE (2017)** Engineering Chloroplasts to Improve Rubisco Catalysis: Prospects for Translating Improvements into Food and Fiber Crops. *New Phytol* **213**: 494–510
- Sheppard CA, Trimmer EE, Matthews RG (1999)** Purification and Properties of NADH-dependent 5,10-Methylenetetrahydrofolate Reductase (MetF) from *Escherichia Coli* *J Bacteriol* **181**: 718–725
- Shevela D, Vyacheslav AE, Ae K, Messinger J (2007)** Interactions of Photosystem II with Bicarbonate, Formate and Acetate. *Photosynth Res* **94**: 247–264
- Shih PM, Zarzycki J, Niyogi KK, Kerfeld CA (2014)** Introduction of a Synthetic CO₂-fixing Photorespiratory bypass into a Cyanobacterium. *J Biol Chem* **289**: 9493–9500
- Shiraishi T, Fukusaki E-I, Kobayashi A (2000)** Formate Dehydrogenase in Rice Plant: Growth Stimulation Effect of Formate in Rice Plant. *J Biosci Bioeng* **89**: 241–246
- Sievers F, Wilm A, Dineen D, Gibson TJ, Karplus K, Li W, Lopez R, McWilliam H, Remmert M, Sö Ding J, et al (2011)** Fast, Scalable Generation of High-quality Protein Multiple Sequence Alignments Using Clustal Omega. *Mol Syst Biol* **7**: 539

Reference

- South PF, Cavanagh AP, Liu HW, Ort DR** (2019) Synthetic Glycolate Metabolism Pathways Stimulate Crop Growth and Productivity in the Field. *Science* **363**: eaat9077
- Stemler BA, Radmer R** (1975) Source of Photosynthetic Oxygen in Bicarbonate-Stimulated Hill Reaction. *Science* **190**: 457–458
- STITT M, SCHULZE D** (1994) Does Rubisco Control the Rate of Photosynthesis and Plant Growth? An Exercise in Molecular Ecophysiology. *Plant Cell Environ* **17**: 465–487
- Stover P, Schirchs V** (1990) Serine Hydroxymethyltransferase Catalyzes the Hydrolysis of 5,10-Methenyltetrahydrofolate to 5-Formyltetrahydrofolate. *J. Biol Chem* **265**: 14227–14233
- Suppmann B, Sawers G** (1994) Isolation and Characterization of Hypophosphite-resistant Mutants of *Escherichia Coli*: Identification of the FocA Protein, Encoded by the *pfl* Operon, as a Putative Formate Transporter. *Mol Microbiol* **11**: 965–982
- Suzuki Y, Kondo E, Makino A** (2017) Effects of Co-overexpression of the Genes of Rubisco and Transketolase on Photosynthesis in Rice. *Photosynth Res* **131**: 281–289
- Svetlitchnaia T, Svetlitchnyi V, Meyer O, Dobbek H** (2006) Structural Insights into Methyltransfer Reactions of a Corrinoid Iron-sulfur Protein Involved in Acetyl-CoA Synthesis. *Proc Natl Acad Sci* **103**: 14331–14336
- Takeuchi Y, Akagi H, Kamasawa N, Osumi M, Honda H** (2000) Aberrant Chloroplasts in Transgenic Rice Plants Expressing a High Level of Maize NADP-dependent Malic Eenzyme. *Planta* **211**: 265–274
- Tamoi M, Nagaoka M, Miyagawa Y, Shigeoka S** (2006) Contribution of Fructose-1,6-bisphosphatase and Sedoheptulose-1,7-bisphosphatase to the Photosynthetic Rate and Carbon Flow in the Calvin Cycle in Transgenic Plants. *Plant Cell Physiol* **47**: 380–390
- Taniguchi Y, Ohkawa H, Masumoto C, Fukuda T, Tamai T, Lee K, Sudoh S, Tsuchida H, Sasaki H, Fukayama H, et al** (2008) Overproduction of C₄ Photosynthetic Enzymes in Transgenic Rice Plants: an Approach to Introduce the C₄-like Photosynthetic Pathway into Rice. *J Exp Bot* **59**: 1799–1809
- Tashiro Y, Hirano S, Matson MM, Atsumi S, Kondo A** (2018) Electrical-biological Hybrid System for CO₂ Reduction. *Metab Eng* **47**: 211–218
- Tcherkez GGB, Farquhar GD, Andrews TJ** (2006) Despite Slow Catalysis and Confused Substrate Specificity, All Ribulose Bisphosphate Carboxylases may be nearly perfectly optimized. *Proc Natl Acad Sci* **103**: 7246–7251
- Tilman D, Balzer C, Hill J, Befort BL** (2011) Global Food Demand and the Sustainable Intensification of Agriculture. *Proc Natl Acad Sci* **108**: 20260–20264
- Tishkov VI, Popov VO** (2006) Protein Engineering of Formate Dehydrogenase. *Biomol Eng* **23**: 89–110
- Tottey S, Waldron KJ, Firbank SJ, Reale B, Bessant C, Sato K, Cheek TR, Gray J, Banfield MJ, Dennison C, et al** (2008) Protein-folding Location Can Regulate Manganese-binding Versus Copper-or Zinc-binding. *Nature* **455**: 1138–1142
- Uematsu K, Suzuki N, Iwamae T, Inui M, Yukawa H** (2012) Increased Fructose 1,6-bisphosphate Aldolase in Plastids Enhances Growth and Photosynthesis of Tobacco Plants. *J Exp Bot* **63**: 3001–3009

Reference

- Vickers TJ, Murta SMF, Mandell MA, Beverley SM** (2006) The Enzymes of the 10-Formyl-Tetrahydrofolate Synthetic Pathway Are Found Exclusively in the Cytosol of the Trypanosomatid Parasite *Leishmania major*. *Mol Biochem Parasite* **166**: 142–152
- Vorholt JA, Chistoserdova L, Lidstrom ME, Thauer RK** (1998) The NADP-Dependent Methylene Tetrahydromethanopterin Dehydrogenase in *Methylobacterium Exorquens* AM1. *J Bacteriol* **180**: 5351–5356
- Waditee-Sirisattha R, Sittipol D, Tanaka Y, Takabe T** (2012) Overexpression of Serine Hydroxymethyltransferase from Halotolerant Cyanobacterium in *Escherichia Coli* Results in Increased Accumulation of Choline Precursors and Enhanced Salinity Tolerance. *FEMS Microbiol Lett* **333**: 46–53
- Wang P, Khoshravesh R, Karki S, Tapia R, Balahadia CP, Bandyopadhyay A, Quick WP, Furbank R, Sage TL, Langdale JA** (2017) Re-creation of a Key Step in the Evolutionary Switch from C₃ to C₄ Leaf Anatomy. *Curr Biol* **27**: 3278–3287
- Wang P, Vlad D, Langdale JA** (2016) Finding the Genes to Build C₄ Rice. *Curr Opin Plant Biol* **31**: 44–50
- Wang Y, Huang Y, Wang J, Cheng C, Huang W, Lu P, Xu Y-N, Wang P, Yan N, Shi Y** (2009) Structure of the Formate Transporter FocA Reveals a Pentameric Aquaporin-like Channel. *Nature* **462**: 467–472
- Warui DM, Li N, Nørgaard H, Krebs C, Bollinger Jr JM, Booker, SJ** (2011) Detection of Formate, rather than Carbon Monoxide, as the Stoichiometric Co-product in Conversion of Fatty Aldehydes to Alkanes by a Cyanobacterial Aldehyde Decarbonylase. *J Am Chem Soc* **133**: 3316-3319.
- Weber APM, Bar-Even A** (2019) Update: Improving the Efficiency of Photosynthetic Carbon Reactions. *Plant Physiol* **179**: 803–812
- Weber N, Hatsch A, Labagnere L, Heider H** (2017) Production of (S)-2-Aminobutyric Acid and (S)-2-Aminobutanol in *Saccharomyces Cerevisiae*. *Microb Cell Fact* **16**: 51
- Wei L, Juan D, J SN, Tobias W, A ASL, Oliver E** (2013) The Formate/Nitrite Transporter Family of Anion Channels. *Biol Chem* **394**: 715–727
- Westerholm M, Moestedt J, Schnürer A** (2016) Biogas Production Through Syntrophic Acetate Oxidation and Deliberate Operating Strategies for Improved Digester Performance. *Appl Energy* **179**: 124–135
- Whitney SM, Houtz RL, Alonso H** (2011) Advancing Our Understanding and Capacity to Engineer Nature's CO₂-sequestering Enzyme, Rubisco. *Plant Physiol* **155**: 27–35
- Wood HG** (1991) Life with CO or CO₂ and H₂ as a Source of Carbon and Energy. *FASEB J* **5**: 156–163
- Xiong J, Minagawa J, Crofts A, Govindjee** (1998) Loss of Inhibition by Formate in Newly Constructed Photosystem II D1 Mutants, D1-R257E and D1-R257M, of *Chlamydomonas Reinhardtii*. *Biochim Biophys Acta - Bioenerg* **1365**: 473–491
- Yishai O, Bouzon M, Dö V, Bar-Even A** (2018) In Vivo Assimilation of One-Carbon via a Synthetic Reductive Glycine Pathway in *Escherichia Coli*. *ACS Synth Biol* **7**: 2023–2028
- Yishai O, Goldbach L, Tenenboim H, Lindner SN, Bar-Even A** (2017) Engineered Assimilation of Exogenous and Endogenous Formate in *Escherichia Coli*. *ACS Synth Biol*

Reference

- 6: 1722–1731
- Young JD, Shastri AA, Stephanopoulos G, Morgan JA** (2011) Mapping Photoautotrophic Metabolism with Isotopically Nonstationary ^{13}C Flux Analysis. *Metab Eng* **13**: 656–665
- Yu H, Li X, Duchoud F, Chuang DS, Liao JC** (2018) Augmenting the Calvin–Benson–Bassham Cycle by a Synthetic Malyl-CoA-glycerate Carbon Fixation Pathway. *Nat Commun* **9**: 2008
- Yu H, Liao JC** (2018) A Modified Serine Cycle in *Escherichia Coli* Converts Methanol and CO_2 to Two-carbon Compounds. *Nat Commun* **9**: 3992
- Yu S, Zhu L, Zhou C, An T, Zhang T, Jiang B, Mu W** (2014) Promising Properties of a Formate Dehydrogenase from a Methanol- assimilating Yeast *Ogataea Parapolyomorpha* DL-1 in His-tagged form. *Appl Microbiol Biotechnol* **98**: 1621–1630
- Zang X, Liu B, Liu S, Arunakumara KKIU, Zhang X** (2007) Optimum Conditions for Transformation of *Synechocystis* sp. PCC 6803. *J Microbiol* **45**: 241–245
- Zarzycki J, Brecht V, Mü Ller M, Fuchs G, Bryant DA** (2009) Identifying the Missing Steps of the Autotrophic 3-hydroxypropionate CO_2 Fixation Cycle in *Chloroflexus Aurantiacus*. *Proc Natl Acad Sci* **106**: 21317–21322
- Zelitch I, Day PR** (1973) The Effect on Net Photosynthesis of Pedigree Selection for Low and High Rates of Photorespiration in Tobacco. *Plant Physiol* **52**: 33–37
- Zelitch I, Schultes NP, Peterson RB, Brown P, Brutnell TP** (2009) High Glycolate Oxidase Activity Is Required for Survival of Maize in Normal Air. *Plant Physiol* **149**: 195–204
- Zhang CC, Zhou CZ, Burnap RL, Peng L** (2018) Carbon/Nitrogen Metabolic Balance: Lessons from Cyanobacteria. *Trends Plant Sci* **23**: 1116–1130
- Zhang K, Li H, Cho KM, Liao JC** (2010) Expanding Metabolism for Total Biosynthesis of the Nonnatural Amino Acid L-homoalanine. *Proc Natl Acad Sci* **107**: 6234–6239
- Zhu X-G, Long SP, Ort DR** (2010) Improving Photosynthetic Efficiency for Greater Yield. *Annu Rev Plant Biol* **61**: 235–261
- Zou K, Ouyang Q, Li H, Zheng J** (2017) A Global Characterization of the Translational and Transcriptional Programs Induced by Methionine Restriction through Ribosome Profiling and RNA-seq. *BMC Genomics* **18**: 189

Acknowledgement

Acknowledgement

At the very beginning, I would like to take this opportunity to express my most sincere appreciation to my supervisor **Prof. Dr. Martin Hagemann** for giving me such a precious chance that I could study and work under his guidance. What I learn from him, during my doctoral period, is not just limited to knowledge in the academic field and an attitude towards research, but also local customs and practices where I live four years. The dissertation could not be finished if I do not get visionary and comprehensive advice and patient guidance from him. Apart from that, I am also indebted to him since I always get inspired encouragement from him and let me get rid of frustration in daily work. For his kindness and consideration, I believe I obtain chances to promote myself in the future.

I am also grateful to **Prof. Dr. Hermann Bauwe** for recruiting me working as a member in such an extraordinary institute and group and giving me useful advices on my study and experiments.

I do sincerely appreciate my ex-supervisor **Prof. Dr. Yong Wang**. If I have not got the chance studying in his group and encouragement from him, I would not have such a prospect to study abroad and broaden my horizon.

I am gracious to my colleague **Dr. Eva-Maria Brouwer**, who supplies lots of assistance not only in the research but also in my life. The discussion with her inspired me how to do when I met problems with assays. I also appreciate **Klaudia Michl** and **Dr. Stefan Timm** who help me a lot with samples analysis through LC-MS/MS.

I sincerely thank **Dr. Arren Bar-Even** and **Dr. Yishai Oren** for providing the codon-optimized genes *ftl*, *fchA* and *mtdA*. I also appreciate the help from **Dr. Steffen Lindner** for his precise analysis of labeling samples. The same gratitude goes to **Dr. Dominik Brillhaus**. I also thank **Dr. Arren Bar-Even**, **Prof. Dr. Andreas P.M. Weber** and **Prof. Dr. Tobias Erb** for giving useful suggestions in this study.

My gratitude goes to dear members of my group **Maria Wittmiß**, **Katrin Gärtner**, **Dr. Friedrich**

Acknowledgement

Kirsch, Katharina Modde, Luna Viggiano de Alvarenga, Stefan Lucius, Manja Henneberg, Kathrin Jahnke, Saskia Schwab, as well as former colleagues **Dr. Ramona Kern, Dr. Nadin Pade, Dr. Franziska Flügel, Kris-Raymond Hippler** for providing me kind and hospitable assistance and such a comfortable and pleasant research condition. Working with all of you is one of the most unforgettable periods in my life.

I am gracious to **Prof. Dr. Birgit Piechulla** and **Dörte Warber** for providing lyophilizer. Thanks to the **Microbiology** department for providing oxygen-free bench.

I would also want to sincerely convey my appreciations to all **my friends** accompanying me through such wonderful moments in Rostock that I could overcome the difficulties during writing the thesis.

Last but not least, I am sincerely grateful to **my family**. I am fortunate to gradually get familiar with my husband and finally become one family. His exist makes my life completely different from before. His encouragement and understanding support me to insist on my research. Besides, my parents, my brother and my parents-in-law encouraged me a lot when I was frustrated. Any word is not suitable enough to describe how important they are for me and how I love them.

Curriculum vitae

Personal Information

Name	SONG, SHANSHAN
Date of birth	18 th Feb 1991
Place of birth	Shandong, China, P. R. China
Nationality	Chinese
Address	Albert-Einstein-Str. 3, 18059 Rostock, Germany
Email	shanshan.song2@uni-rostock.de
Phone	+49(381)1281-6114

Academic Background

10/2015 -	PhD student at Rostock University in the department Plant Physiology, supervised by Prof. Dr. Martin Hagemann, research topic: Engineering formate assimilation in <i>Synechocystis</i> sp. PCC 6803
9/2012 – 7/2015	Graduate Student at Nankai University (P.R. China) under the guidance of Prof. Dr. Yong Wang, research topic: The genetic manipulation of photorespiration
9/2008 – 7/2012	Studied at Qufu Normal University (P.R. China) as undergraduate student

Awards and scholarships

1. Professorinnenprogramm II Förderlinie Scholarship
2. Full scholarship for PhD study from China Scholarship Council (CSC)
3. Scholarship funded by Qufu Normal University

Eidesstattliche versicherung

Eidesstattliche versicherung

Ich erkläre hiermit an Eides Statt, dass ich die vorgelegte Dissertation über

„ Engineering formate assimilation in *Synechocystis* sp. PCC 6803 ”

selbständig angefertigt und mich anderer Hilfsmittel als der in ihr angegebenen nicht bedient habe, insbesondere, dass alle Entlehnungen aus anderen Schriften mit Angabe der betreffenden Schrift gekennzeichnet sind.

Ich versichere, die Grundsätze der guten wissenschaftlichen Praxis beachtet, und nicht die Hilfe einer kommerziellen Promotionsvermittlung in Anspruch genommen zu haben.

Rostock, den